UNIVERSITY OF CALIFORNIA SAN DIEGO

Dynamic regulation of genome during cell division and at the nuclear periphery

A dissertation submitted in partial satisfaction of the
requirements for the degree Doctor of Philosophy

in

Biology

by

Hyeseon Kang

Committee in charge:

Professor Martin Hetzer, Chair
Professor Fred Gage
Professor Jens Lykke-Andersen
Professor Cornelis Murre
Professor Karen Oegema

2020

The Dissertation of Hyeseon Kang is approved, and it is acceptable in quality and form for publication on microfilm and electronically:

_____

_____

_____

_____

_____
Chair

University of California San Diego

2020

DEDICATION

I dedicate my thesis to my loving parents, who have always supported and encouraged me in all aspects of my life and have given me opportunities beyond anything I could have ever hoped for.

TABLE OF CONTENTS

LIST OF FIGURES

ACKNOWLEDGEMENTS

I would like to acknowledge Professor Martin Hetzer for his support as the chair of my committee. I would like to thank my committee members for their contribution to my academic development. I would also like to acknowledge the Hetzer lab members, without whom I would not have finished this work. Their support and intellectual input have been invaluable.

Chapter 1, in full, has been submitted for publication in *Genes & Development*. Hyeseon Kang, Maxim N. Shokhirev, Zhichao Xu, Sahaana Chandran, Jesse R. Dixon, Martin W. Hetzer. “Dynamic regulation of histone modifications and long-range chromosomal interactions during post-mitotic transcriptional reactivation.” The author of this dissertation was the primary investigator and author of this paper.

Chapter 2, in part, is being prepared for submission for publication. Swati Tyagi, Hyeseon Kang, Martin W. Hetzer. “Nucleoporins regulate super-enhancer-associated genes through mediating CTCF.” The author of this dissertation was the co-primary investigator with Swati Tyagi and will submit as the co-first author of this paper.

VITA

2020 Doctor of Philosophy in Biology, University of California San Diego

ABSTRACT OF THE DISSERTATION

Dynamic regulation of genome during cell division and at the nuclear periphery

by

Hyeseon Kang

Doctor of Philosophy in Biology

University of California San Diego, 2020

Professor Martin Hetzer, Chair

In eukaryotes, the genome is hierarchically packaged inside the nucleus. The 3D organization of chromatin regulates various biological processes such as transcription, DNA replication, and cell division. The accurate gene regulation depends on when and where chromosomal interactions take place in the nucleus. This dissertation focuses on how the genome maintains its function after passing through mitosis and how the nuclear architecture at the nuclear periphery modulates transcription regulation.

A long-standing question in the field is how cells maintain genome structure and function over multiple cell divisions, despite the loss of, for example, chromatin structure and gene expression during mitosis. In the first part of this dissertation, we determine that retention of histone modification binding contributes to accurate transcriptional programs and genome organization. We characterize the role of H3K27ac in the activation of post-mitotic transcription. An increase in H3K27ac binding in

anaphase/telophase also shows a positive association with the formation of domains in the genome. Together, these results clarify the mechanism through which the histone modification landscape establishes precise genome regulation across mitosis.

The genome is enclosed in the nuclear envelope membrane, which contains the nuclear pore complex (NPC) components as crucial players in the dynamic organization of the genome and gene regulation. The second part of this dissertation aims to understand how NPC components interact with genomic regions for gene regulation at the nuclear periphery and identify molecular players that participate in NPC-mediated regulation of genome structure and function. We find that a subset of architecture protein CTCF is localized at the NPC and show how it acts as an interacting partner with NPC components to influence transcription. This unexpected, but exciting link provides us insights into how the structures of the nuclear periphery impact genome function.

INTRODUCTION

The nucleus is the largest organelle in eukaryotic cells and protects our genome. The nucleus is enclosed by its outermost barrier, the nuclear envelope, which is composed of a double phospholipid bilayer. Multiple nuclear pores perforate the nuclear envelope and the nuclear lamina, a meshwork of intermediate filaments, underlines the nuclear envelope at the nuclear periphery. Individual chromosomes occupy non-random territories. In chromosome territories, chromosomal interactions occur within and between chromosomes as well as nuclear structures such as the nuclear pore complexes (NPCs). The NPCs bind enhancers at the nuclear periphery to facilitate enhancer-promoter looping, which is created by CTCF and cohesin, and influence the gene expression in interphase cells (Fig.1). Nuclear organization contributes to the spatio-temporal regulation of transcription. In order to maintain cellular identity, the cell transmits its spatial information to its progeny (Amendola and van Steensel 2014, Buchwalter, Kaneshiro and Hetzer 2019). However, the mechanisms to re-establish the same nuclear architecture from mother to daughter cells remain unanswered.

Many interphase nuclear structures and processes undergo global changes during mitosis. When the chromatin becomes extremely condensed, the nuclear envelope, including NPCs (Wandke and Kutay 2013), lamina-associated domains (Kind et al. 2013), chromosome territories (Walter et al. 2003), and long-range chromatin folding (Naumova et al. 2013) disassemble at the beginning of mitosis. These interphase features are faithfully re-established during mitotic exit, but the potential factors that mediate nuclear architecture after mitosis are largely unknown.

Interactions between chromatin and the components of the nuclear envelope regulate gene expression. However, which components mediate the formation of these interactions is still poorly understood. During open mitosis, the nuclear envelope breaks down at the end of prophase, which leads to separation of chromatin from the nuclear envelope proteins such as the NPC proteins, called nucleoporins (Nups), along with the lamin proteins (Wandke and Kutay 2013). The NPCs are composed of multiple copies of ~30 unique proteins. They can be characterized by (1) the scaffold Nups: the Nup107-160 complex, (2) the cytoplasmic Nups: Nup214, Nup98, and Nup358, (3) the nuclear basket Nups: Nup153, Nup50 and Tpr, and (4) the transmembrane Nup POM121 (D'Angelo and Hetzer 2008). Although some Nups partially associate with the mitotic spindle or kinetochores, most of the Nups are dispersed throughout the mitotic cytoplasm or mitotic ER during mitosis and reassemble during mitotic exit (Ellenberg et al. 1997). Then, during mitotic exit when the nuclear envelope is rebuilt around chromatin, some Nups are recruited in early anaphase before membrane association (Burke and Ellenberg 2002). These early re-associated Nups may facilitate the proper contacts to regulate the proper gene expression.

The nuclear envelope reassembly requires the re-association of all the nuclear envelope components in anaphase, telophase, and early G1 that were dissociated during early mitosis. Quantitative time-lapse confocal microscopy allows us to investigate the kinetics of mitotic NPC reassembly (Dultz et al. 2008). The NPC reassembly follows a sequential and timely fashion. Given that the Nup107-160 complex has an essential role in NPC assembly (D'Angelo et al. 2006), the Nup107-160 complex, such as Nup133, binds to chromatin first during the metaphase-anaphase

transition. The nuclear basket proteins exhibit dynamic kinetics. Nup153 and Nup50 reassemble in anaphase before membrane assembly, while Tpr reassembles only in early G1 (Fig. 2). Pom121 and Nup98 reassemble after membrane association (Dultz et al. 2008, de Castro, Gokhan and Vagnarelli 2016). Based on the previous observations and our results, the interactions in the newly formed nuclear envelope may be mediated by Nup153 and Nup50 that are recruited early and localized close to chromatin.

Genomic regions contacting the nuclear lamina are defined as lamina associated domains (LADs), which are large domain with a median size of 0.5 Mb and encompass up to 30-40% of the genome. Peripherally located LADs enrich with repressive heterochromatin (Buchwalter et al. 2019, Lochs, Kefalopoulou and Kind 2019, Amendola and van Steensel 2014). Multiple studies indicate that proper positioning LADs contribute to cell type-specific gene expression and cellular identity (Peric-Hupkes et al. 2010, Poleshko et al. 2017). It remains unclear how positional information of LADs is maintained through cell division. Although LADs are mainly composed of lamin proteins, depletion of lamin B1, B2, or lamin A/C does not alter the chromatin-lamina contacts in mouse ESCs (Amendola and van Steensel 2015). A recent study shows that the H3K9me2 modification marks the peripheral heterochromatin through multiple cell divisions and guides the spatial organization of the genome (Poleshko et al. 2019). It could be interesting to investigate whether H3K9me2 or its histone methyltransferase G9a is essential for the establishment and maintenance of LADs-mediated cell type-specific gene expression through cell division.

It is also unclear how the chromatin is organized in the daughter nucleus. Long-range genome folding, including compartments, topologically associating domains, and

DNA loops, are dissociated in early mitosis and reorganized in the G1 phase (Naumova et al. 2013). Reorganization of these chromosomal interactions after mitosis could be mediated by architecture proteins such as CTCF and cohesin that are recruited in anaphase (Cai et al. 2018, Abramo et al. 2019). How can CTCF or cohesin bind to the anaphase chromatin before the nuclear envelope assembly, while most of proteins are only recruited back after telophase? Given that some NPC proteins reassemble in early anaphase and one of early reassembled Nup, Nup153 is known to interact with CTCF and cohesin in drosophila and mouse (Pascual-Garcia et al. 2017, Kadota et al. 2020), Nup153 may provide a platform for CTCF/cohesin binding to chromatin after mitosis. This idea can be tested by super-resolution imaging on synchronized anaphase enriched cells to capture their colocalization on anaphase chromatin.

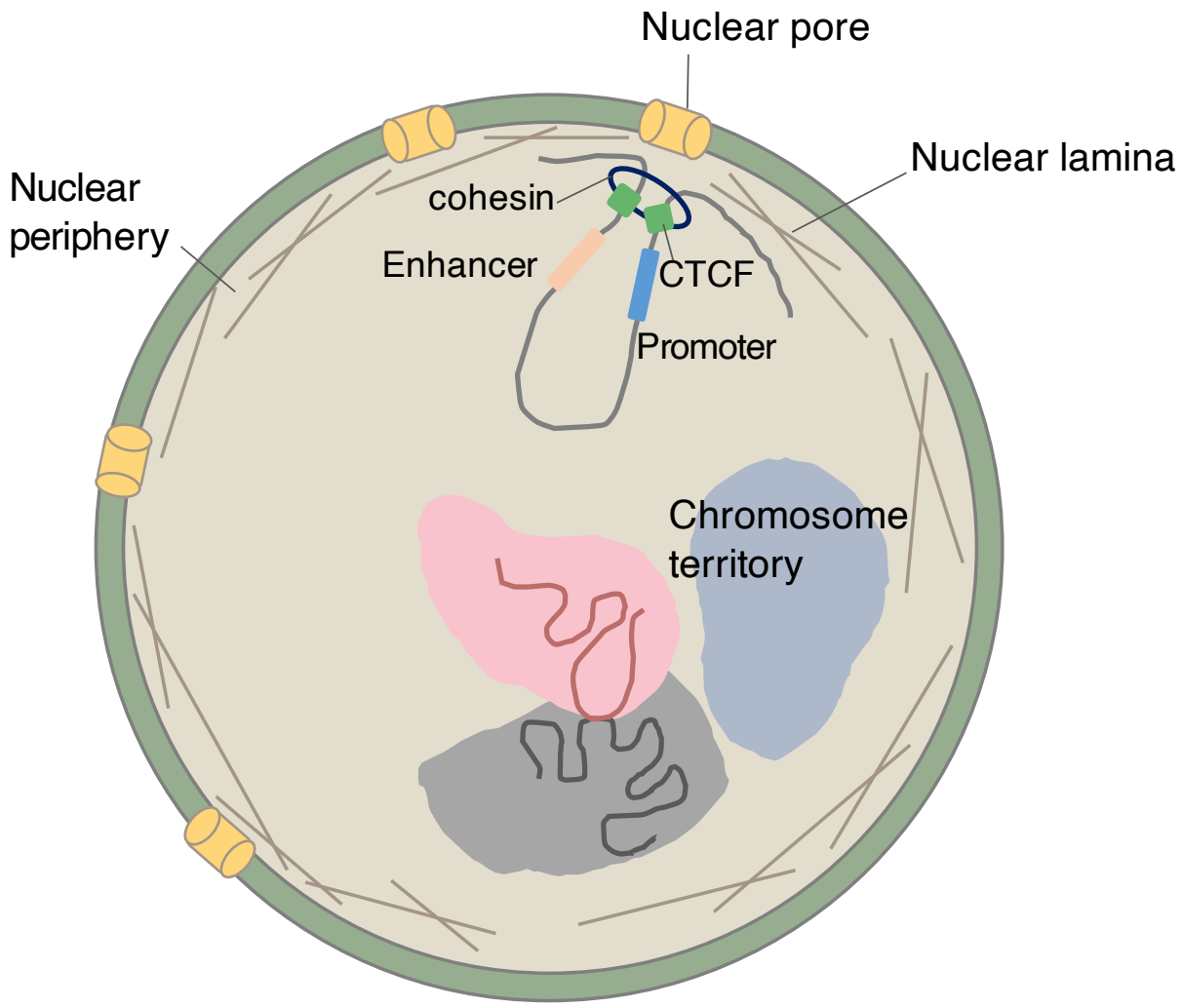

Figure I.1 Chromatin organization of the mammalian cell nucleus. The nuclear envelope contains nuclear pores and a meshwork of intermediate filaments, the nuclear lamina at the nuclear periphery. Chromosomes are organized in distinct chromosome territories. Chromosomal interactions occur within and between chromosomes. The enhancer–promoter looping, which is mediated by CTCF and cohesion, is underneath the NPCs.

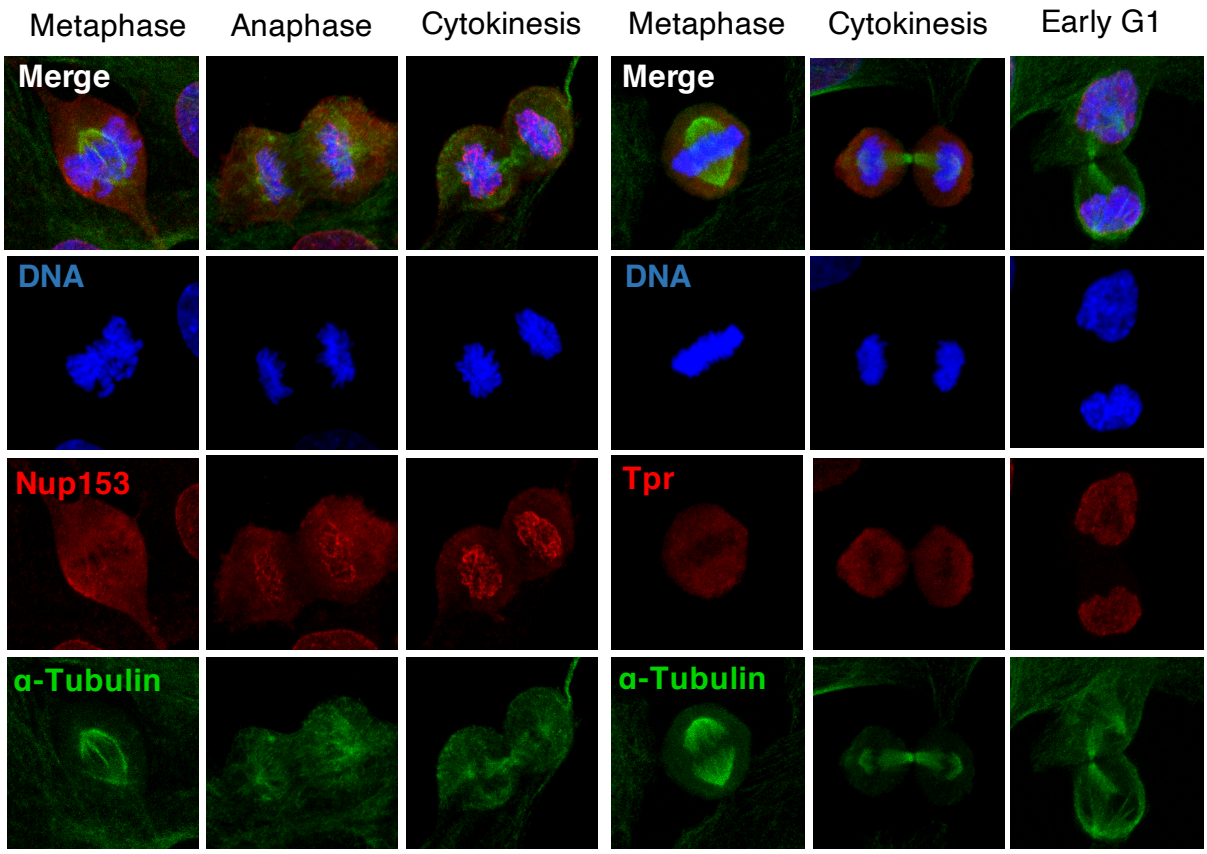

Figure I.2 The reassembly of the nuclear basket Nups. Immunofluorescence images show the recruitment of Nups after mitosis. U2OS cells were stained for DNA (blue), α-Tubulin (green) and either Nup153 or Tpr (red). Images were taken at mitotic cells naturally occurred.

Chapter 1. Dynamic regulation of histone modifications and long-range chromosomal interactions during post-mitotic transcriptional reactivation

1.1 Abstract

During mitosis, transcription of genomic DNA is dramatically reduced, before it is reactivated during nuclear reformation in anaphase/telophase. Many aspects of the underlying principles that mediate transcriptional memory and reactivation in the daughter cells remain unclear. Here, we used ChIP-seq on synchronized cells at different stages after mitosis to generate genome-wide maps of histone modifications. Combined with EU-RNA-seq and Hi-C analyses, we found that during prometaphase, promoters, enhancers, and insulators retain H3K4me3 and H3K4me1, while losing H3K27ac. Enhancers globally retaining mitotic H3K4me1 or locally retaining mitotic H3K27ac are associated with cell type-specific genes and their transcription factors for rapid transcriptional activation. As cells exit mitosis, promoters regain H3K27ac, which correlates with transcriptional reactivation. Insulators also gain H3K27ac and CCCTC-binding factor (CTCF) in anaphase/telophase. This increase of H3K27ac in anaphase/telophase is required for post-transcriptional activation and may play a role in the establishment of topologically associating domains (TADs). Together, our results suggest that the genome is reorganized in a sequential order, in which histone methylations occur first in prometaphase, histone acetylation and CTCF in anaphase/telophase, transcription in cytokinesis, and long-range chromatin interactions in early G1. We thus provide insights into the histone modification landscape that allows faithful reestablishment of the transcriptional program and TADs during cell division.

1.2 Introduction

Mitosis marks a dramatic transition during which cells move from a transcriptionally active to a largely repressed state in which most genes are transcriptionally inactive (Prescott and Bender 1962). This drastic reduction in transcriptional activity is associated with chromosome condensation (Vagnarelli 2013), loss of long-range DNA interactions (Naumova et al. 2013, Dileep et al. 2015, Gibcus et al. 2018), and exclusion of RNA polymerase II (Pol II) and most transcription factors (TFs) from chromatin (Gottesfeld and Forbes 1997). As cells exit mitosis and reform the nuclear envelope (NE), the transcriptional program is faithfully reactivated (Prasanth et al. 2003). This raises the important question of how the two daughter cells retain the memory of a defined gene expression program. Recent work has shown that a selective gene transcription program is maintained throughout mitosis (Palozola et al. 2017). However, how transcription is reactivated during mitotic exit and the underlying molecular mechanisms that control transcriptional memory remain poorly understood.

Several features of interphase chromatin landscapes remain associated with mitotic chromatin and have been proposed to function as 'bookmarks' of transcriptional programs during mitosis. These 'bookmarks' include retention of chromatin accessibility (Hsiung et al. 2015, Martínez-Balbás et al. 1995, Oomen et al. 2019, Teves et al. 2016), multiple general and lineage-specific TFs (Teves et al. 2016, Young et al. 2007, Kadauke et al. 2012, Caravaca et al. 2013, Deluz et al. 2016, Festuccia et al. 2016), and certain histone modifications (Kouskouti and Talianidis 2005, Valls, Sánchez-Molina and Martínez-Balbás 2005, Muramoto et al. 2010, Zhao et al. 2011). Specific histone modification patterns can define distinct chromatin states of *cis*-regulatory elements

(*cis*-REs), such as promoters and enhancers, and regulate gene expression via interaction with transcription factors. H3K4me3 and H3K27ac are highly enriched at active promoters near the transcription start site (TSS) and positively correlated with transcription. Enhancers play a crucial role in the activation and fine-tuning of their target promoters. Enhancer elements can exist in two major chromatin states, primed or active. Primed enhancers (PEs) are marked by H3K4me1/2 and their target genes are weakly or not expressed, whereas active enhancers (AEs) are additionally marked by the histone acetyltransferases CBP/p300-mediated H3K27ac and are associated with actively transcribed genes (Heintzman et al. 2007, Creyghton et al. 2010, Calo and Wysocka 2013). Recently, chromatin immunoprecipitation sequencing (ChIP-seq) studies revealed spatial genomic information of active histone marks, including H3K4me1/3, H3K9ac, or H3K27ac at prometaphase-arrested cells (Liu et al. 2017, Javasky et al. 2018, Liang et al. 2015). These studies allowed the comparison between mitotic and interphase histone marks and revealed specific modifications, dynamics of chromatin states at *cis*-REs, and estimation of TF binding that could serve as bookmarks. Although specific histone modifications remain associated with mitotic chromatin even at reduced levels, it remains unclear whether such association on mitotic chromatin has a regulatory role in transcriptional activation during or after mitosis. Further, it remains to be determined whether histone modifications, retained either at promoters or enhancers, contribute as bookmarks of transcriptional program during mitosis.

Genome-wide chromosome conformation capture data, such as that generated by the Hi-C method, can reveal that the structural features of interphase chromosomes,

such as A-and B-compartments, topologically associating domains (TADs), and DNA loops are lost during prometaphase and reestablished in G1 phase (Naumova et al. 2013, Abramo et al. 2019). TADs are thought of as important basic units of chromosome organization and are demarcated from each other by boundaries (Dixon et al. 2012, Nora et al. 2012). However, what mediates TAD formation after mitosis remains poorly understood. TAD boundaries in interphase have been shown to be enriched in active transcription, housekeeping genes, tRNA genes, and short interspersed nuclear elements (SINEs), as well as binding sites for the architectural proteins CCCTC-binding factor (CTCF) and cohesin complex (Dixon et al. 2012). Furthermore, targeted degradation of CTCF, using the auxin-induced rapid degradation system, resulted in the almost complete elimination of TADs, suggesting CTCF's essential role for the establishment of TADs (Nora et al. 2017). It is currently unclear whether CTCF or other features enriched at the boundaries in interphase chromatin are also involved in the reestablishment of TADs after mitosis.

In this study, we combined histone modification ChIP-seq, EU-RNA-seq, and Hi-C from prometaphase to G1 phase to comprehensively examine on a genome-wide level the temporal relationship between histone modification binding, nascent transcription, and long-range chromatin interactions during the mitosis-G1 transition. We found that H3K4me3 remains associated with almost all promoters and that H3K4me1 is highly retained at enhancers of cell type-specific genes during prometaphase. In contrast, H3K27ac is largely reduced during prometaphase, although a subset of H3K27ac remains at enhancers of cell type-specific genes and promotes early expression of these cell type-specific genes. During the anaphase/telophase transition,

most promoters gain H3K27ac, and this is essential for the accurate transmission of gene expression programs during cell division. Furthermore, TAD boundaries during prometaphase remain associated with H3K4me3 and H3K4me1 in the absence of CTCF, but CTCF is recruited and enriched at the boundaries during anaphase/telophase together with H3K27ac before the appearance of loops, TADs, and compartments. Altogether, the multilevel data of epigenetic landscape, nascent transcription, and TAD interaction shed light on not only the temporal order of genome organization after mitosis but also indicate a potential bookmarking role for histone modifications in accurate reestablishment of transcriptional activation pattern and long-range chromatin interactions.

1.3 Results

1.3.1 H3K27ac is lost in prometaphase and regained in anaphase/telophase.

Transcription is reactivated at the time of mitotic exit, as the NE starts reassembling and RNA Pol II globally rebinds to the chromatin (Prasanth et al. 2003). It is thus important to study this stage to fully understand genome organization during cell division. To determine the relationship between epigenetic dynamics, gene expression and long-range chromatin interactions at the mitosis-G1 transition, we used three independent methods: (a) ChIP-seq analysis to identify genome localization mapping of key histone modifications, (b) EU-RNA-seq to capture temporal nascent transcription expression, and (c) Hi-C to determine the timing of long-range chromatin interactions from prometaphase to G1 phase (Fig. 1A). In order to obtain cells at different cell cycle stages including mitotic exit, we synchronized two human cell lines, osteosarcoma

U2OS and retina pigment epithelia RPE1 cells using thymidine and nocodazole. The degree of synchrony at each cell cycle stage was monitored by fluorescence microscopy of Hoechst and α-Tubulin stained cells. Asynchronous populations (interphase) had less than 2% mitotic cells, nocodazole-arrested culture (prometaphase) contained more than 95% mitotic cells, and cells released from nocodazole-induced arrest for 35 min (anaphase/telophase) were about 70% enriched for anaphase/telophase (Supplemental Fig. S1A). Thus, our synchronization approach enables us to collect enriched populations of cells at prometaphase, anaphase/telophase, and interphase, respectively.

To determine the mitotic retention of histone modifications in our system, we focused on three histone modifications, H3K4me3, H3K4me1, and H3K27ac, which are associated with the activation of transcription in promoters (H3K4me3, H3K27ac) or active enhancers (H3K4me1, H3K27ac). We performed immunofluorescence in asynchronous cells and western blotting in histone extracts from interphase, prometaphase, and anaphase/telophase enriched cells. We observed that all three histone modifications (H3K4me3, H3K4me1, and H3K27ac) were detected in all phases of mitosis from both U2OS and RPE1 cells (Supplemental Fig. S1B,C). To comprehensively examine the extent and genomic localization of mitotic occupancy of histone modifications, we performed ChIP-seq for H3K4me3, H3K4me1, and H3K27ac in U2OS and RPE1 cell lines during interphase, prometaphase and anaphase/telophase. When there is a global signal change under different experimental conditions (e.g., interphase vs. mitosis), typical normalization by the total number of mapped reads can be misleading since similar distributions of positions are sampled

during sequencing. It is thus often challenging to quantitatively compare histone modification ChIP-seq data sets from different phases of the cell cycle. To overcome this, we used a spike-in based normalization strategy, whereby adding an equal amount of exogenous chromatin from a different species into each sample can be used as a more accurate normalization control (Orlando et al. 2014). We thus added spike-in chromatin from *Drosophila melanogaster* in each sample for global normalization and direct comparison of binding between interphase and mitotic sample (Egan et al. 2016). In accordance with previous observations (Liang et al. 2015, Javasky et al. 2018), our ChIP-seq analysis showed a significant overlap with binding sites of histone methylations between interphase and mitosis. We identified 26,276 H3K4me3 binding sites in interphase and 95% of those sites (25,038) were retained on chromatin during mitosis in U2OS and 92% of sites in RPE1. Similarly, 93% of interphase H3K4me1 binding sites in U2OS and 98% of H3K4me1 sites in RPE1 were detected in mitosis. In contrast, consistent with previous observations (Zhiteneva et al. 2017, Javasky et al. 2018, Ginno et al. 2018), H3K27ac showed a reduction in mitosis in both U2OS and RPE1. Only 18% of H3K27ac interphase binding sites in U2OS and 48% in RPE1 remained in mitosis (Fig. 1B). Therefore, our spike-in normalized ChIP-seq enables us to quantitatively compare the genomic localization of histone modifications during mitosis-G1.

We next asked whether the genomic distribution of histone modifications between interphase and mitosis appears to be uniform or different at active regulatory elements. We first classified promoter (H3K4me3+, proximity to TSS), PE (H3K4me1+, distal to TSS), and AE (H3K27ac+/H3K4me1+, distal to TSS) elements based on our

ChIP-seq data (Supplemental Fig. S1D) (Creyghton et al. 2010, Calo and Wysocka 2013). We then compared histone modification levels across the cell cycle at these elements. As has been shown before, interphase H3K4me3 peaks were preferentially bound at TSS (Supplemental Fig. S1E, left panel) and H3K4me1 peaks were depleted at TSS (Supplemental Fig. S1E, right panel) (Heintzman et al. 2009, Creyghton et al. 2010). During mitosis, H3K4me3 binding was significantly enriched, comparable to interphase at promoters (Fig. 1C). Mitotic H3K4me1 was also detected at a similar level in interphase, but with slightly higher levels at AEs and PEs (Fig. 1D). In contrast, we observed signal reduction in H3K27ac levels in the prometaphase cells at both promoters and AEs and its signals recovered in anaphase/telophase. The reduction of H3K27ac binding was observed in both promoters and AEs with similar levels, however the recovery of binding in anaphase/telophase was more pronounced at promoters (Fig. 1E), suggestive of the promoter-specific function of H3K27ac during anaphase/telophase. Altogether, these results demonstrate that, based on the number of binding sites and binding distribution at *cis*-REs of histone modifications, H3K4me3 and H3K4me1 are globally retained during mitosis, while H3K27ac is lost in prometaphase and regained as cells exit mitosis.

Figure 1.1 Cell cycle-dependent regulation of H3K27ac. (A) Schematic of the experimental strategy combining ChIP-seq, EU-RNA-seq, and Hi-C during prometaphase, anaphase/telophase, and various G1 phases. Mitotic cells were obtained by thymidine and nocodazole treatments. Anaphase/Telophase and G1 phase cells were obtained after release from mitotic arrest for indicated time. (B) Venn diagram showing the number of H3K4me3, H3K4me1, and H3K27ac binding sites that were found in interphase (Inter, orange), prometaphase (Prometa, gray), and anaphase/telophase (Ana/Telo, green) in U2OS (left panel) and RPE1 (right panel) cells. n represents the number of observed histone modification peaks in each cell cycle phase. Percentage of interphase peaks that were also detected in mitotic cells are shown. (C-E) Histogram showing ChIP-seq reads of H3K4me3 (C), H3K4me1 (D), and H3K27ac (E) ± 2 kb surrounding the peak center of sites at promoters, AEs, or PEs during interphase, prometaphase, and anaphase/telophase in U2OS (left panel) and RPE1 (right panel). In E, black arrow indicates reduced ChIP-seq reads of H3K27ac from interphase to prometaphase at promoters and AEs. Red arrow indicates gained ChIP-seq reads of H3K27ac from prometaphase to anaphase/telophase at promoters and AEs.

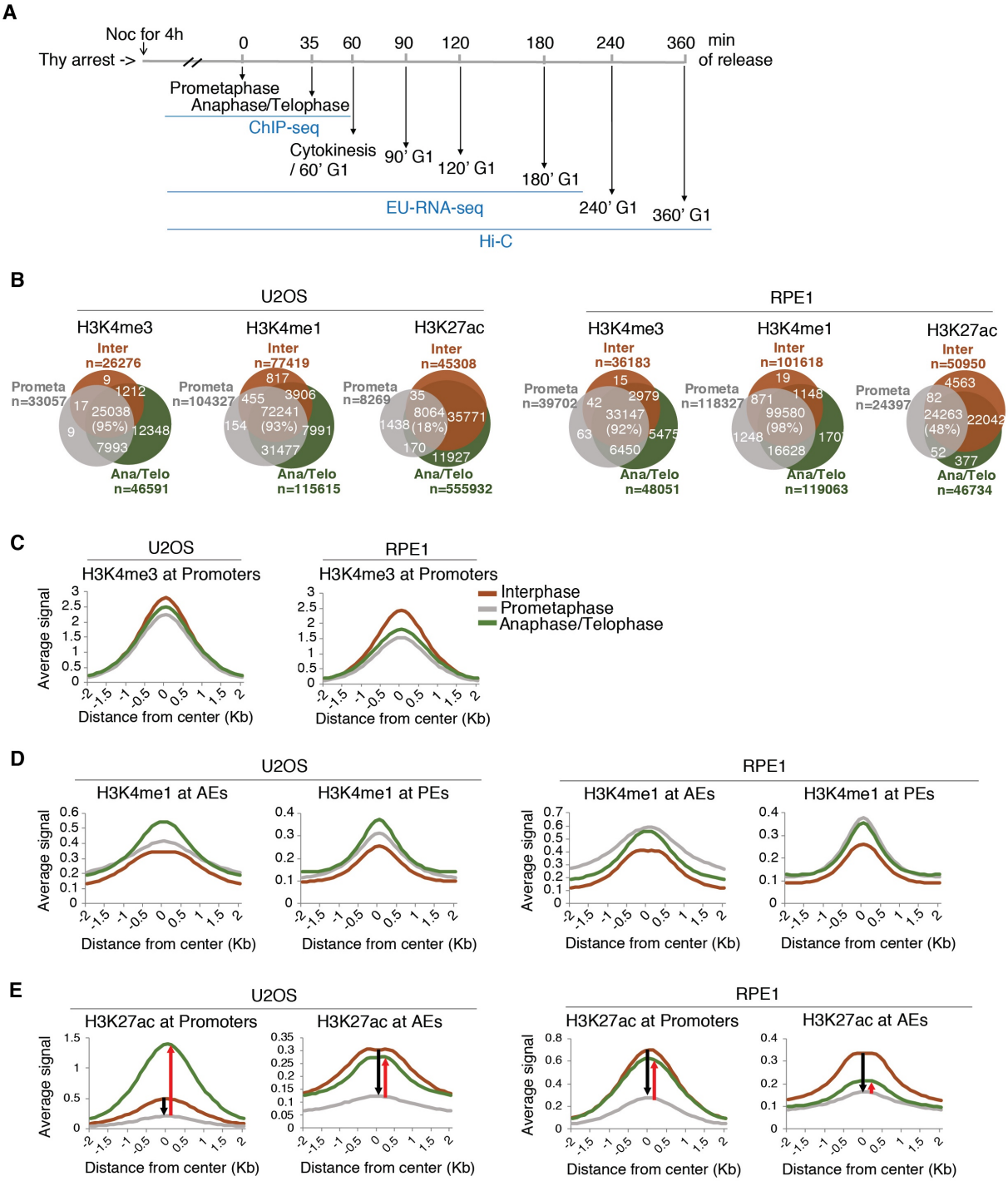
A
Noc for 4h
Thy arrest ->
0
35
60
90
120
180
240
360
min
of release
Prometaphase
Anaphase/Telophase
ChIP-seq
Cytokinesis
/ 60' G1
90' G1
120' G1
180' G1
EU-RNA-seq
240' G1
360' G1
Hi-C
B
U2OS
RPE1
H3K4me3
H3K4me1
H3K27ac
Inter
n=26276
Prometa
n=33057
Ana/Telo
n=46591
Inter
n=77419
Prometa
n=104327
Ana/Telo
n=115615
Inter
n=45308
Prometa
n=8269
Ana/Telo
n=555932
Inter
n=36183
Prometa
n=39702
Ana/Telo
n=48051
Inter
n=101618
Prometa
n=118327
Ana/Telo
n=119063
Inter
n=50950
Prometa
n=24397
Ana/Telo
n=46734
C
U2OS
RPE1
H3K4me3 at Promoters
Average signal
Distance from center (Kb)
Interphase
Prometaphase
Anaphase/Telophase
D
U2OS
RPE1
H3K4me1 at AEs
H3K4me1 at PEs
Average signal
Distance from center (Kb)
E
U2OS
RPE1
H3K27ac at Promoters
H3K27ac at AEs
Average signal
Distance from center (Kb)

1.3.2 Promoters maintain H3K4me3 and enhancers maintain H3K4me1 in the absence of H3K27ac during prometaphase.

We next wanted to determine how gene regulatory elements 'remember' their histone modification dynamics across mitosis. To answer this question, we selected all promoters and enhancers from interphase and compared the dynamics of each histone modification from interphase to prometaphase or to anaphase/telophase cells. Promoters can be marked by either H3K4me3 only or by both H3K27ac and H3K4me3. We found that the majority of H3K4me3+ promoters remained in prometaphase (98.3%). In contrast, only 1.1% of promoters remained associated with H3K27ac in prometaphase and 87% of H3K4me3+ promoters were able to regain H3K27ac in anaphase/telophase (Fig. 2A,B; Supplemental Fig. S2A,B). Only a small fraction of interphase AEs retained H3K27ac in prometaphase (18.0%). 69.2% of AEs lost H3K27ac, but retained H3K4me1 in prometaphase cells (Fig. 2C,D; Supplemental Fig. S2C,D). We found that the majority of PEs remained stable in prometaphase and anaphase/telophase (89.4% and 86.6%, respectively) similar to H3K4me3+ promoters (Fig. 2E,F; Supplemental Fig. S2E,F). These data suggest that promoters and enhancers continue to retain H3K4me3 and H3K4me1 respectively, as potential bookmarks, although they lose H3K27ac during prometaphase.

Figure 1.2 Histone methylations bookmark promoters and enhancers in the absence of H3K27ac during prometaphase. (A) Quantification of interphase promoters that are also detected in prometaphase or in anaphase/telophase. Promoters harboring both H3K27ac and H3K4me3 are shown in blue and H3K4me3 only in light blue. Promoters not containing any histone modification are shown in the lightest blue color. (B) ChIP-seq tracks at the promoter of the ITGB8 gene for H3K4me3, H3K27ac, and H3K4me1 during interphase, prometaphase, and anaphase/telophase. (C) Quantification of interphase AEs that are also detected in prometaphase or in anaphase/telophase. AEs harboring both H3K27ac and H3K4me1 are shown in orange and H3K4me1 only in gray. AEs not containing any histone modification are shown in light orange. (D) ChIP-seq tracks at AE of ABCC12 gene for H3K4me3, H3K27ac, and H3K4me1 during interphase, prometaphase, and anaphase/telophase. (E) Quantification of interphase PEs that are also detected in prometaphase or in anaphase/telophase. PEs harboring H3K4me1 are shown in gray. PEs not containing any histone modification are shown in light gray. (F) ChIP-seq tracks at PE of STEAP3 gene for H3K4me3, H3K27ac, and H3K4me1 during interphase, prometaphase, and anaphase/telophase. Peaks are highlighted by brown boxes. Abbreviations: interphase (Inter), prometaphase (Prometa), anaphase/telophase (Ana/telo), histone modification (HM).

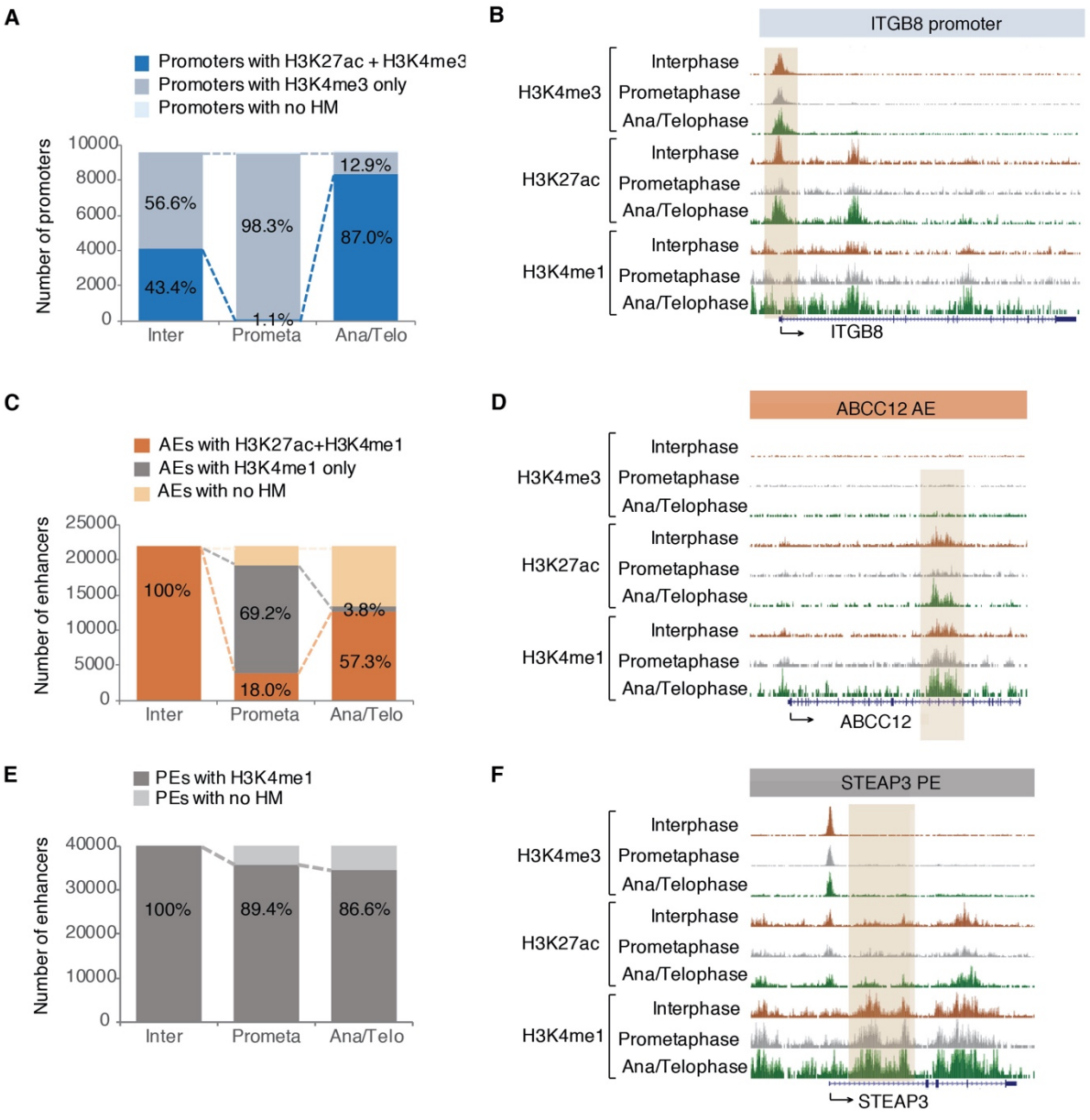
A
Promoters with H3K27ac + H3K4me3
Promoters with H3K4me3 only
Promoters with no HM
Number of promoters
10000
8000
6000
4000
2000
0
56.6%
43.4%
98.3%
1.1%
12.9%
87.0%
Inter
Prometa
Ana/Telo
B
ITGB8 promoter
H3K4me3
H3K27ac
H3K4me1
Interphase
Prometaphase
Ana/Telophase
ITGB8
C
AEs with H3K27ac+H3K4me1
AEs with H3K4me1 only
AEs with no HM
Number of enhancers
25000
20000
15000
10000
5000
0
100%
69.2%
18.0%
3.8%
57.3%
Inter
Prometa
Ana/Telo
D
ABCC12 AE
H3K4me3
H3K27ac
H3K4me1
Interphase
Prometaphase
Ana/Telophase
ABCC12
E
PEs with H3K4me1
PEs with no HM
Number of enhancers
40000
30000
20000
10000
0
100%
89.4%
86.6%
Inter
Prometa
Ana/Telo
F
STEAP3 PE
H3K4me3
H3K27ac
H3K4me1
Interphase
Prometaphase
Ana/Telophase
STEAP3

1.3.3 H3K4me1 remains at enhancers of cell type-specific genes during prometaphase.

Next, we asked whether continuous retention of H3K4me1 during prometaphase associates with a bookmark of cell type-specific genes. For this, we used U2OS cells, which are derived from cells of mesenchymal origin that differentiate to osteoblasts. There are several genes identified as essential for bone formation and differentiation to osteoblasts. These so-called osteoblast-specific genes include RUNX2, TNFRSF11B, DKK1, SP7, ALPL, MSX2, COL1A2, and SOST (GR and SH 2007, Chapurlat and Confavreux 2016, Kirkham and Cartmell 2007, Rutkovskiy, Stensløkken and Vaage 2016). Strikingly, all of these genes were associated with mitotic H3K4me1 at enhancers (RUNX2, TNFRSF11B, and ALPL shown in Figure 3A). Consistent with U2OS cells, RPE1 cells also showed that H3K4me1 during prometaphase was associated with RPE-specific genes (Zhang et al. 2012) such as ALDH1A3, EFEMP1, GJA1, TIMP3, AHR, TYRP1, LAMP2, SLC16A4, BMP4, VEGFA, and PRNP (ALDH1A3, EFEMP1, and GJA1 shown in Figure 3B). Next, we wanted to investigate whether mitotic histone modification binding sites are linked to genes with distinct biological functions. To do so, we performed Genomic Regions Enrichment of Annotations Tool (GREAT) (McLean et al. 2010) analysis on the promoters and enhancers in U2OS and RPE1 cells (Supplemental Fig. S3). Notably, promoters retaining H3K4me3 during prometaphase, were strongly enriched for genes involved in fundamental cellular processes, such as RNA and protein metabolism, whereas AEs either retaining or losing H3K27ac during prometaphase, were predominantly linked to differentiation or development-related genes in both cell lines. Specifically, we observed that AEs losing

H3K27ac, but retaining H3K4me1 were most strongly associated with genes involved in bone mineralization in U2OS (Supplemental Fig. S3A, bottom panel). Together, these results indicate that enhancers use H3K4me1 to maintain their cellular identity upon loss of H3K27ac throughout mitosis.

Previous studies demonstrated that although most TFs and co-factors are removed from mitotic chromatin, several tissue-specific or pathway-specific TFs such as RUNX2, GATA1, or FOXA1 remain bound on mitotic chromosomes to a subset of their interphase sites (Young et al. 2007, Caravaca et al. 2013, Kadauke et al. 2012). To determine the factors that associate with mitotic histone modifications at *cis*-REs, we performed *de novo* motif analysis of the bookmarked elements in U2OS cells. Our analysis showed that both AEs and PEs were preferentially enriched with motifs of the activator protein-1 (AP-1) family of TFs including Fosl2, Jun-AP1, Fra2, Fra1, and JunB (Fig. 3C), which has an essential role in osteoblast differentiation and collagen production by regulating osteoblast-lineage gene expression in bone cells (Bozec et al. 2010, Kveiborg et al. 2004, Sabatakos et al. 2000, Jochum et al. 2000). In addition to AP-1 TFs, we next sought to determine whether genomic regions harboring mitotic histone marks were enriched for TFs binding that has been known to regulate osteoblast differentiation such as RUNXs (Komori 2005), TEADs (Kegelman et al. 2018), and FOXOs (Rached et al. 2010, Teixeira et al. 2010). Our analysis revealed that these TFs regulating osteoblast-specific gene expression had preferential binding at PEs compared to AEs and promoters (Fig. 3D). A prior study shows that RUNX2, an essential TF for osteogenic cell fates, remains associated with mitotic chromosomes in multiple cell lines, including Saos-2 osteosarcomas and HeLa cells (Young et al. 2007).

Therefore, combined with previous observations, we conclude that retention of mitotic H3K4me1 peaks at enhancer regions provides a platform for interaction with a subset of cell type-specific TFs during and after mitosis.

Figure 1.3 H3K4me1 remains at enhancers of cell type-specific genes during prometaphase. (A) Representative genome browser tracks showing co-binding of osteoblast-specific genes (RUNX2, TNFRSF11B, and ALPL) with mitotic H3K4me1 at enhancers. (B) Representative genome browser tracks showing co-binding of RPE-specific genes (ALDH1A3, EFEMP1, and GJA1) with mitotic H3K4me1 at enhancers. Peaks are highlighted by brown boxes. (C) TF motif enrichments for bookmarked promoter (Pr, blue), AE (orange), and PE (gray) during mitosis. Sequence logos and P values are shown for the most highly enriched sequence motifs among the top 10. (D) Motif analysis of TFs-regulating osteoblast differentiation (RUNXs, TEADs, and FOXOs) for bookmarked promoter (Pr, blue), AE (orange), and PE (gray).

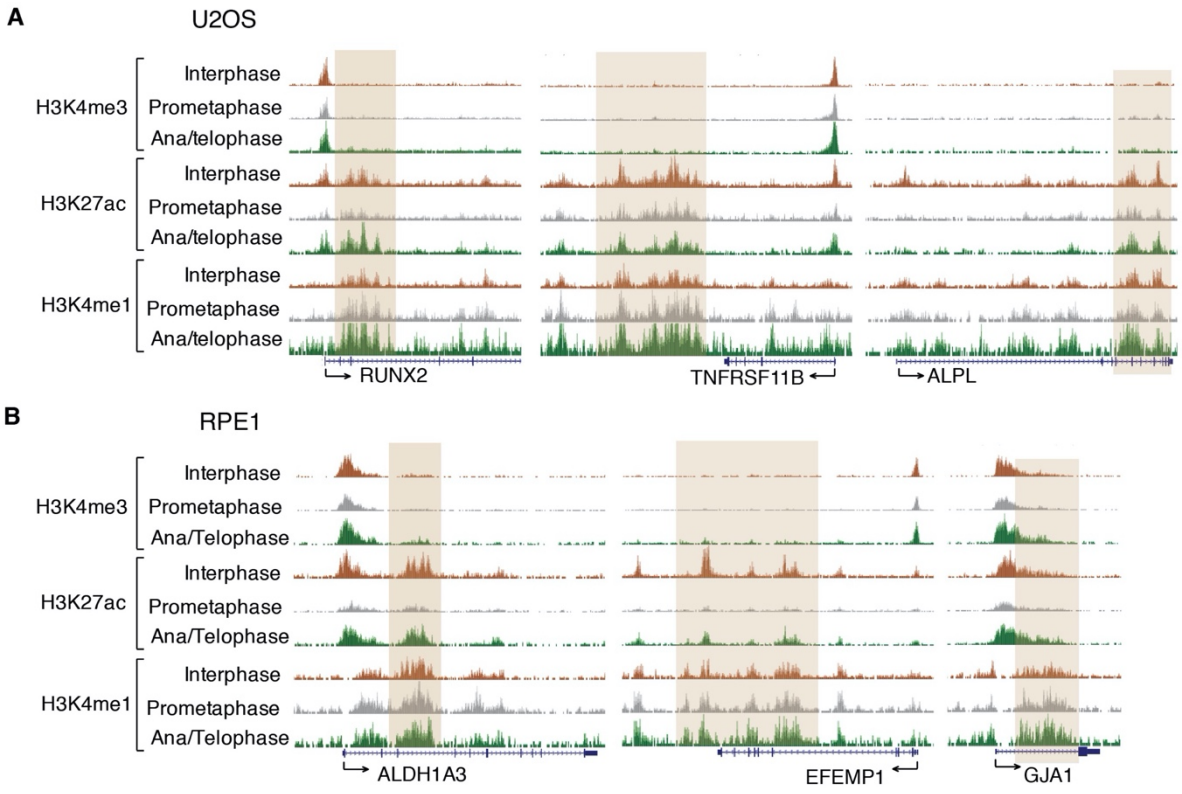

C

Transcription Factor	Motif	P-value Bookmarked elements Pr	AE	PE
Fosl2		$1e^{-0}$	$1e^{-75}$	$1e^{-819}$
Jun-AP1		$1e^{-0}$	$1e^{-66}$	$1e^{-772}$
Fra2		$1e^{-0}$	$1e^{-99}$	$1e^{-817}$
Fra1		$1e^{-0}$	$1e^{-94}$	$1e^{-817}$
JunB		$1e^{-0}$	$1e^{-84}$	$1e^{-779}$

D

Transcription Factor	Motif	P-value Bookmarked elements Pr	AE	PE
RUNX1		$1e^{-0}$	$1e^{-1}$	$1e^{-33}$
RUNX-AML		$1e^{-0}$	$1e^{-1}$	$1e^{-26}$
RUNX2		$1e^{-0}$	$1e^{-1}$	$1e^{-24}$
TEAD1		$1e^{-1}$	$1e^{-9}$	$1e^{-122}$
TEAD3		$1e^{-0}$	$1e^{-9}$	$1e^{-108}$
TEAD		$1e^{-0}$	$1e^{-7}$	$1e^{-107}$
FOXL2		$1e^{-1}$	$1e^{-1}$	$1e^{-11}$
FOXA1		$1e^{-0}$	$1e^{-0}$	$1e^{-7}$
FOXO3		$1e^{-1}$	$1e^{-0}$	$1e^{-6}$

1.3.4 Regained H3K27ac in anaphase/telophase is positively correlated with gene reactivation.

Histone modifications are found on mitotic chromatin with either a stable (H3K4me1/3) or reduced (H3K27ac) abundance when compared with interphase chromatin (Fig. 1). Together with an association with mitotic chromatin, it has been suggested that one feature of mitotic bookmarking is to enable activation of a defined transcriptional programs after mitosis (Zhao et al. 2011, Kouskouti and Talianidis 2005, Valls et al. 2005, Muramoto et al. 2010). To determine whether occupancy of mitotic histone modifications associates with post-mitotic transcriptional activation, we first examined temporal dynamics of gene expression during the mitosis-G1 transition. To do that, we labeled nascent transcripts with uridine analog, 5′-ethynyl uridine (EU) for 35 min, prior to isolation of RNA, during prometaphase, anaphase/telophase, cytokinesis, and various G1 phases (Supplemental Fig. S4A). Then, we captured nascent RNA by adding biotin-azide and generated cDNA libraries for sequencing. As there was a large difference in the amount of nascent RNA between interphase and mitotic cells, we used external controls that appropriately normalize the RNA-seq data (Supplemental Fig. S4B) (Palozola et al. 2017). Based on normalized FPKM, genes were divided into seven classes, first activated at 0 min, 35 min, 60 min, 90 min, 120 min, 180 min, and asynchronous. Consistent with the previous study, we found a hierarchy of gene reactivation at the mitosis to G1 transition (Fig. 4A) (Palozola et al. 2017). We also found a subset of genes expressed in mitosis (431 genes at 0 min and 2284 genes at 35 min) and the largest number of genes first activated at 60 min when most of the cells are at cytokinesis (Fig. 4B). Gene Ontology (GO) enrichment analysis showed that

genes first activated at 60 min are involved in basic cellular functions such as cellular organization, cell cycle progression, and RNA and protein metabolism. Conversely, genes expressed at later time points are linked to bone development (Fig. 4C). However, these cell type-specific genes may be expressed at all times but just overrepresented at the later time points, given that genes related to basic functions are first activated at the earlier time point by 60 min, when the majority of genes (88%) are expressed.

Next, we asked whether the presence of investigated histone modifications correlates with transcriptional activation during and after mitosis. To do that, we tested the Pearson correlation coefficient between transcription level of genes first activated at each time point and the read counts for histone modifications, at promoters versus AEs, and in each cell cycle phase. We found that at promoters, gene expression at 60 min was positively correlated with H3K4me3 or H3K27ac levels throughout all cell cycle phases. Notably, among the positive correlations, we found that genes whose promoters were associated with anaphase/telophase H3K27ac were most strongly correlated (R=0.60) (Fig. 4D). Further, we observed that all genes first activated at each time point showed the most positive correlation with anaphase/telophase H3K27ac at promoters (Supplementary Fig. 4C). AEs are associated with active transcription by bringing DNA loops physically close to gene promoters. However, for AEs, either H3K27ac or H3K4me1 level in mitosis was not positively correlated with gene expression (Fig. 4D). Altogether, these results indicate that recovery of H3K27ac at promoter regions in anaphase/telophase may be important for the reactivation of transcriptional programs in the daughter cells.

We observed that H3K4me1 at enhancers remains associated with cell type-specific genes during prometaphase (Fig. 3C; Supplemental Fig. S3). We thus asked whether H3K4me1 occupancy throughout mitosis associates with rapid transcriptional activation of cell type-specific genes. We obtained the list of 113 genes specifically expressed in bone or bone marrow which are also expressed in U2OS, using the Tissue-specific Gene Expression and Regulation (TiGER) database (Liu et al. 2008). This number was similar to the 149 liver-specific genes in HUH7 human hepatoma cells seen in a prior study (Palozola et al. 2017). We then analyzed the time when the 113 bone-specific genes are first activated across mitosis and found that bone-specific genes follow general gene expression pattern: most are reactivated at 60 min. Interestingly, however, there was a higher percentage of bone-specific genes first activated at 0 min, compared to EU-labelled total genes (Fig. 4E). To investigate whether bone-specific genes expressed at 0 min tend to contain mitotic histone marks at enhancers, the number of bone genes was counted at each time point based on its occupancy with either promoters retaining H3K4me3 or enhancers retaining H3K27ac/H3K4me1 during prometaphase. Strikingly, mitotic AEs and PEs showed higher enrichment for 0 min expressing bone-specific genes than EU-labelled total genes (Fig. 4G,H), while mitotic promoters did not show any particular enrichment for 0 min expressing bone-specific genes (Fig. 4F). This suggests that activation of early expressing bone-specific genes may involve association with mitotic H3K4me1 together with H3K27ac at enhancers.

Figure 1.4 Activation of transcriptional programs during mitosis-G1 is associated with histone modification binding. (A) EU-RNA-seq data heat map illustrating the relative expression of genes first activated at each time point during mitosis-G1. (B) Number of EU labeled genes first activated at each time point. (C) Representative GO terms at each time point. (D) Pearson correlation coefficient (R) was determined between 60 min transcriptional level and the ChIP-seq reads of H3K4me3, H3K27ac, and H3K4me1 in interphase (Inter), prometaphase (Prometa), and anaphase/telophase (Ana/Telo) at promoter and AE, defined in Figure S1D. (E-H) Barplot showing the percentage of genes first activated at each time point. Representative bone-specific genes are indicated at each time point (E). Percentage of genes containing mitotic promoters (F), mitotic AEs (G), and mitotic PEs (H) at each time point. Bone-specific genes are shown in yellow and EU genes in gray.

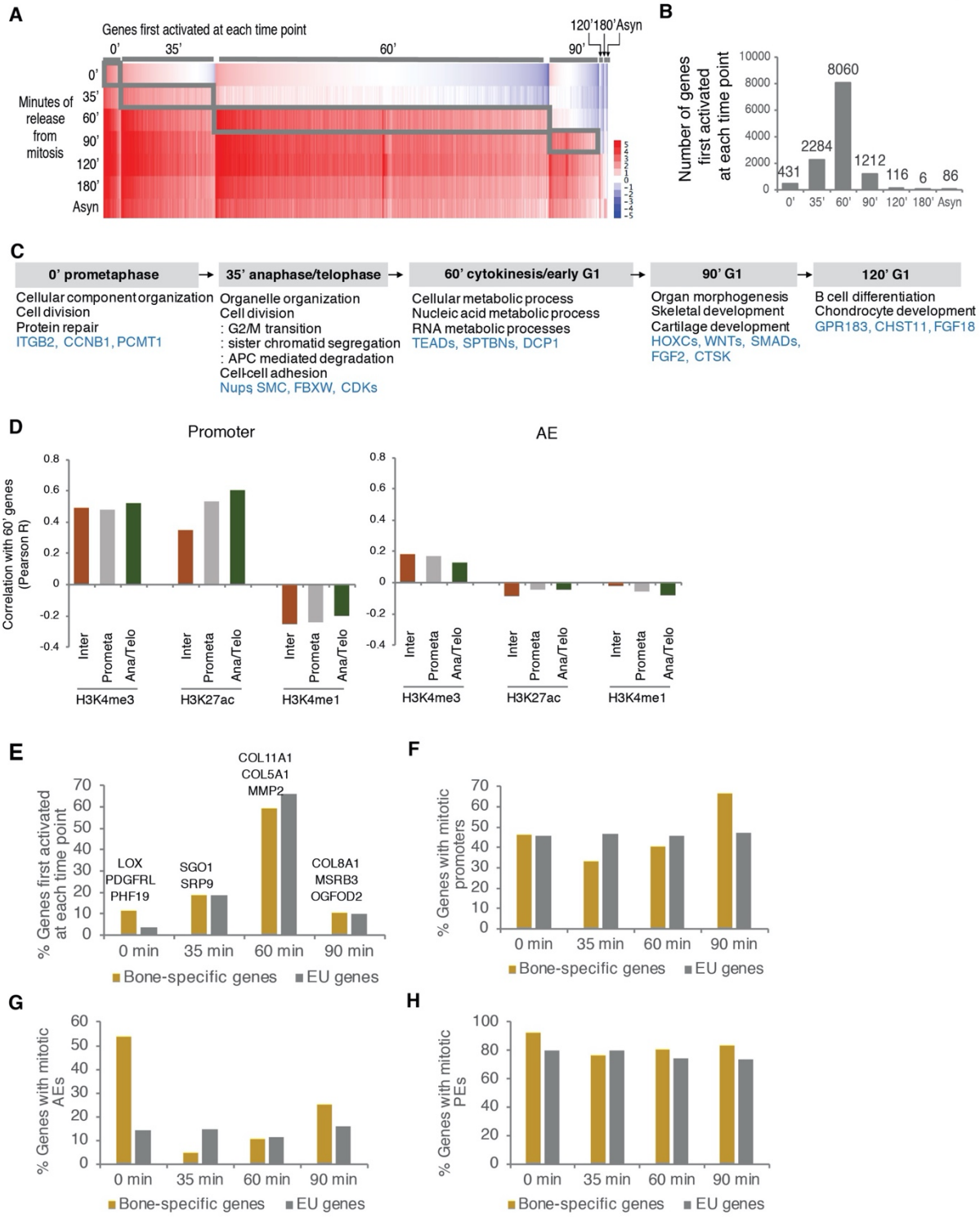
A
Genes first activated at each time point
0'
35'
60'
90'
120'
180'
Asyn
Minutes of release from mitosis
B
Number of genes first activated at each time point
431
2284
8060
1212
116
6
86
C
0' prometaphase
Cellular component organization
Cell division
Protein repair
ITGB2, CCNB1, PCMT1
35' anaphase/telophase
Organelle organization
Cell division
: G2/M transition
: sister chromatid segregation
: APC mediated degradation
Cell-cell adhesion
Nups, SMC, FBXW, CDKs
60' cytokinesis/early G1
Cellular metabolic process
Nucleic acid metabolic process
RNA metabolic processes
TEADs, SPTBNs, DCP1
90' G1
Organ morphogenesis
Skeletal development
Cartilage development
HOXCs, WNTs, SMADs, FGF2, CTSK
120' G1
B cell differentiation
Chondrocyte development
GPR183, CHST11, FGF18
D
Promoter
AE
Correlation with 60' genes (Pearson R)
Inter
Prometa
Ana/Telo
H3K4me3
H3K27ac
H3K4me1
E
% Genes first activated at each time point
LOX
PDGFRL
PHF19
SGO1
SRP9
COL11A1
COL5A1
MMP2
COL8A1
MSRB3
OGFOD2
0 min
35 min
60 min
90 min
Bone-specific genes
EU genes
F
% Genes with mitotic promoters
G
% Genes with mitotic AEs
H
% Genes with mitotic PEs

1.3.5 H3K27ac functions as a transcriptional bookmark.

Mitotic occupancy of histone modifications is associated with post-mitotic gene activation suggestive of mitotic bookmarking. However, a recent study showed that inhibition of mitotic BRD4 binding did not affect transcriptional activation, suggesting that mitotic occupancy can be passively bound to mitotic chromatin and dispensable for transcription (Behera et al. 2019). To test whether H3K27ac has a functional bookmarking role in post-mitotic activation of transcription, we examined how inhibition of H3K27ac affects gene expression. We utilized the p300/CBP catalytic inhibitor A-485 (Lasko et al. 2017) to inhibit (i) mitotic H3K27ac occupancy or (ii) recovery of H3K27ac from anaphase/telophase. First, we observed by western blot that 1h treatment of A-485 effectively reduced H3K27ac binding from nocodazole-arrested prometaphase cells (Fig. S5A, left panel). We then washed out both nocodazole and A-485 and released cells for 1h or 24h. Reduced H3K27ac binding from prometaphase chromatin was able to regain as cells exit mitosis to enter 1h cytokinesis or 24h next cell cycle (Fig. S5A, middle panel). Second, to inhibit H3K27ac regaining from anaphase/telophase, we released cells from mitotic arrest while treating with A-485 for 1h or 3h. The H3K27ac levels successfully decreased in both 1h and 3h treatment with A-485 (Fig. S5A, right panel). Next, nascent transcripts were pulse-labeled with the EU followed by sequencing and normalized by spike-in controls (Fig. 5A). We confirmed by EU-RNA-seq analysis that the biological replicates for each treatment were highly correlated (Supplemental Fig. S5B) and that A-485 treatment resulted in extensive transcriptional changes for all treatments (Supplemental Fig. S5C).

We first explored whether A-485 treatment alters post-mitotic transcriptional activation. Genes were clustered into three groups based on $\log_2$ fold change (down-regulated, up-regulated, and no change) upon A-485 treatment. When inhibiting mitotic H3K27ac, 56% (48% down and 8% up) of the genes in prometaphase and 45% (29% down and 16% up) of the genes in cytokinesis were dysregulated. Since the length of the cell cycle is approximately 24h for dividing mammalian cells, we let cells enter the next cell cycle upon mitotic inhibition of H3K27ac. Surprisingly, 45% (22% down and 23% up) of the genes in 24h release cells were dysregulated, suggesting that mitotic H3K27ac is required for maintaining transcriptional memory. H3K27ac begins to get regained from anaphase/telophase (Fig.1) and is the most predictive histone mark for gene reactivation (Fig. 4D), suggestive of a transcriptional bookmark. We thus investigated the functional role of H3K27ac recovery from anaphase/telophase in mitotic bookmarking. When inhibiting recovery of H3K27ac, 45% (23% down and 22% up) of the genes in cytokinesis were dysregulated and 50% (23% down and 27% up) of the genes in 3h G1 were also dysregulated (Fig. 5B). This suggests that post-mitotic transcriptional activation requires the recovery of H3K27ac. GO enrichment analysis showed that genes downregulated in all A-485 treated cells after cytokinesis were significantly enriched in gene sets involved in mRNA/protein metabolism and cell-cell adhesion (Fig. 5C), supporting the idea that faithful transmission of transcriptional programs requires both mitotic H3K27ac occupancy and H3K27ac recovery from anaphase/telophase.

Since transcription rate gradually increases as cells exit mitosis to enter the G1 phase (Fig. 4A), we hypothesized that perturbation of transcriptional activation by A-485

treatment would get recovered as cells get into late G1 (3h G1) from early G1 (cytokinesis). However, we noticed that the extent of down-regulated and up-regulated genes was consistent between cells in cytokinesis and 3h G1 upon A-485 treatment (Fig. 5D, right panel). The extent of down-regulated or up-regulated genes was also consistent between cells in cytokinesis and 24h release upon inhibition of mitotic H3K27ac (Fig. 5D, left panel). Therefore, the dysregulated genes by both inhibiting mitotic H3K27ac and H3K27ac recovery were not able to recover their own transcriptional activity in the daughter cells. These data suggest that H3K27ac during prometaphase and anaphase/telophase is essential for the activation of post-mitotic transcription, rather than regulates transcriptional rate.

Given that bone-specific genes expressed early tend to contain mitotic H3K27ac (Fig.4G), we hypothesized that removal of H3K27ac from mitotic chromatin would affect the early activation of bone-specific genes. Indeed, A-485 treatment during mitosis altered expression in bone-specific genes. Bone-specific genes at the 0 min timepoint were most noticeably down-regulated upon mitotic inhibition of H3K27ac (Fig. 5E). This indicates that mitotic H3K27ac is required for rapid transcriptional activation of cell type-specific genes.

Figure 1.5 H3K27ac serves as a mitotic bookmark. (A) Schematic of EU-RNA-seq strategy illustrating strategies to test bookmarking function. A-485 was used to inhibit H3K27ac binding during and after mitosis. (B) Proportion of genes down or up-regulated, or with no change due to A-485 treatment in each cell cycle phase. Number of each group of genes is indicated. Downregulated genes (green, log2 fold change < −1); Upregulated genes (red, log2 fold change > 1). (C) Top five GO enriched for downregulated genes in A-485 treated cells. Bar length represents the −log10 adjusted P-value. (D) Box and whisker plots of the log2 fold change in each cell cycle phase on treatment with A-485 across downregulated, upregulated and no change genes. Midline equals the median, top of box equals 75th percentile, and bottom of box equals 25th percentile. Upper and lower whisker equal the maximum and the minimum, respectively. (E) Box plot displaying the log2 fold change in expression of bone genes containing mitotic AEs at each time point upon A-485 treatment. Each gene was indicated with a dot (gray).

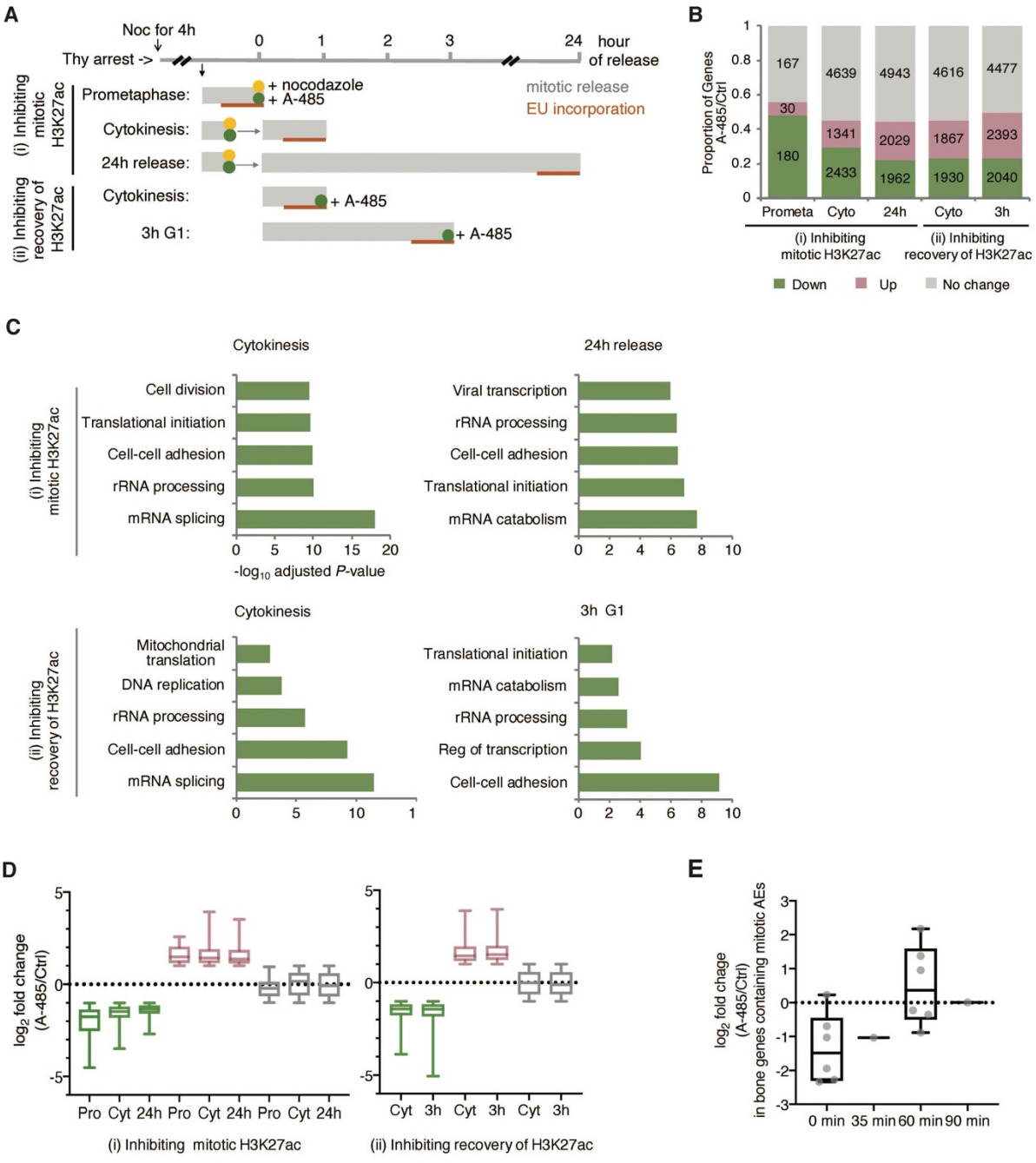
A
Noc for 4h
Thy arrest ->
0
1
2
3
24
hour of release
(i) Inhibiting mitotic H3K27ac
Prometaphase:
+ nocodazole
+ A-485
mitotic release
EU incorporation
Cytokinesis:
24h release:
(ii) Inhibiting recovery of H3K27ac
Cytokinesis:
+ A-485
3h G1:
+ A-485
B
Proportion of Genes A-485/Ctrl
167
30
180
4639
1341
2433
4943
2029
1962
4616
1867
1930
4477
2393
2040
Prometa
Cyto
24h
Cyto
3h
(i) Inhibiting mitotic H3K27ac
(ii) Inhibiting recovery of H3K27ac
Down
Up
No change
C
Cytokinesis
24h release
(i) Inhibiting mitotic H3K27ac
Cell division
Translational initiation
Cell-cell adhesion
rRNA processing
mRNA splicing
Viral transcription
rRNA processing
Cell-cell adhesion
Translational initiation
mRNA catabolism
-log10 adjusted P-value
Cytokinesis
3h G1
(ii) Inhibiting recovery of H3K27ac
Mitochondrial translation
DNA replication
rRNA processing
Cell-cell adhesion
mRNA splicing
Translational initiation
mRNA catabolism
rRNA processing
Reg of transcription
Cell-cell adhesion
D
log2 fold change (A-485/Ctrl)
Pro Cyt 24h Pro Cyt 24h Pro Cyt 24h
Cyt 3h Cyt 3h Cyt 3h
(i) Inhibiting mitotic H3K27ac
(ii) Inhibiting recovery of H3K27ac
E
log2 fold chage (A-485/Ctrl) in bone genes containing mitotic AEs
0 min
35 min
60 min
90 min

1.3.6 Long-range chromatin interactions are established between 90-120 min after release from mitotic arrest.

Long-range chromatin interactions are lost in prometaphase and reformed in early G1 (Naumova et al. 2013, Abramo et al. 2019). However, the role of TADs interactions during anaphase/telophase and whether they are already reestablished during anaphase/telophase to enable gene reactivation at cytokinesis remain unclear. To investigate when long-range interactions are reformed, we performed Hi-C to detect physical interactions between distant genomic elements, from prometaphase to 360 min G1. We assessed the reproducibility of Hi-C data between two biological replicates and observed a strong Pearson correlation coefficient at all time points (Supplemental Fig. S6). In agreement with previous observations, Hi-C contact maps showed that chromosomal interactions were no longer observed in mitotic cells (Naumova et al. 2013, Gibcus et al. 2018, Oomen et al. 2019, Nagano et al. 2017) including 0 min (prometaphase) and 35 min (anaphase/telophase) chromatin and appeared after 60 min (cytokinesis) (Abramo et al. 2019) (Fig. 6A). We observed that A-A and B-B compartments, TADs, and DNA loops between promoters and enhancers were no longer detected in prometaphase and started to reveal interactions from 60 min and completed between 90-120 min (Fig. 6B-D). Because long-range interactions are reformed after 60 min when the transcriptional program is reestablished, we reasoned that the formation of long-range interactions does not appear to be necessary for the majority of gene reactivation.

Figure 1.6 Long-range chromatin interactions are reformed between 90-120 min after release from mitotic arrest. (A) Hi-C contact maps of chromosome 6 : 70,000,000-76,000,000 showing TADs for each time point. (B) Saddle plots showing global A-A, B-B, and A-B compartment signals for each time point. A/B compartment score derived from first principle components were sorted and divided into 30 quantiles. Saddle plots show the average observed/expected interaction frequency between regions according to the eigen vector values of both ends. (C) Average insulation score near TAD boundaries for each time point. (D) Average DNA loop intensity for each time point. Loop annotations were firstly identified for the 360 min time point using hiccups. The loop intensity is the average observed/expected interaction frequency. (E-H) ChIP-seq signals of CTCF (E), H3K27ac (F), H3K4me3 (G), and H3K4me1 (H) in interphase (orange), prometaphase (gray), and anaphase/telophase (green) at TAD boundary regions. (I-L) Interphase and anaphase/telophase peaks were categorized into either interphase specific (Inter Specific, orange), anaphase/telophase specific (A/T Specific, green), or shared between interphase and anaphase/telophase (Inter+A/T Shared, black). CTCF (I), H3K27ac (J), H3K4me3 (K), and H3K4me1 (L) peaks in each category were aligned at TAD boundary regions. In K, no H3K4me3 interphase specific peaks were observed at TAD boundary regions.

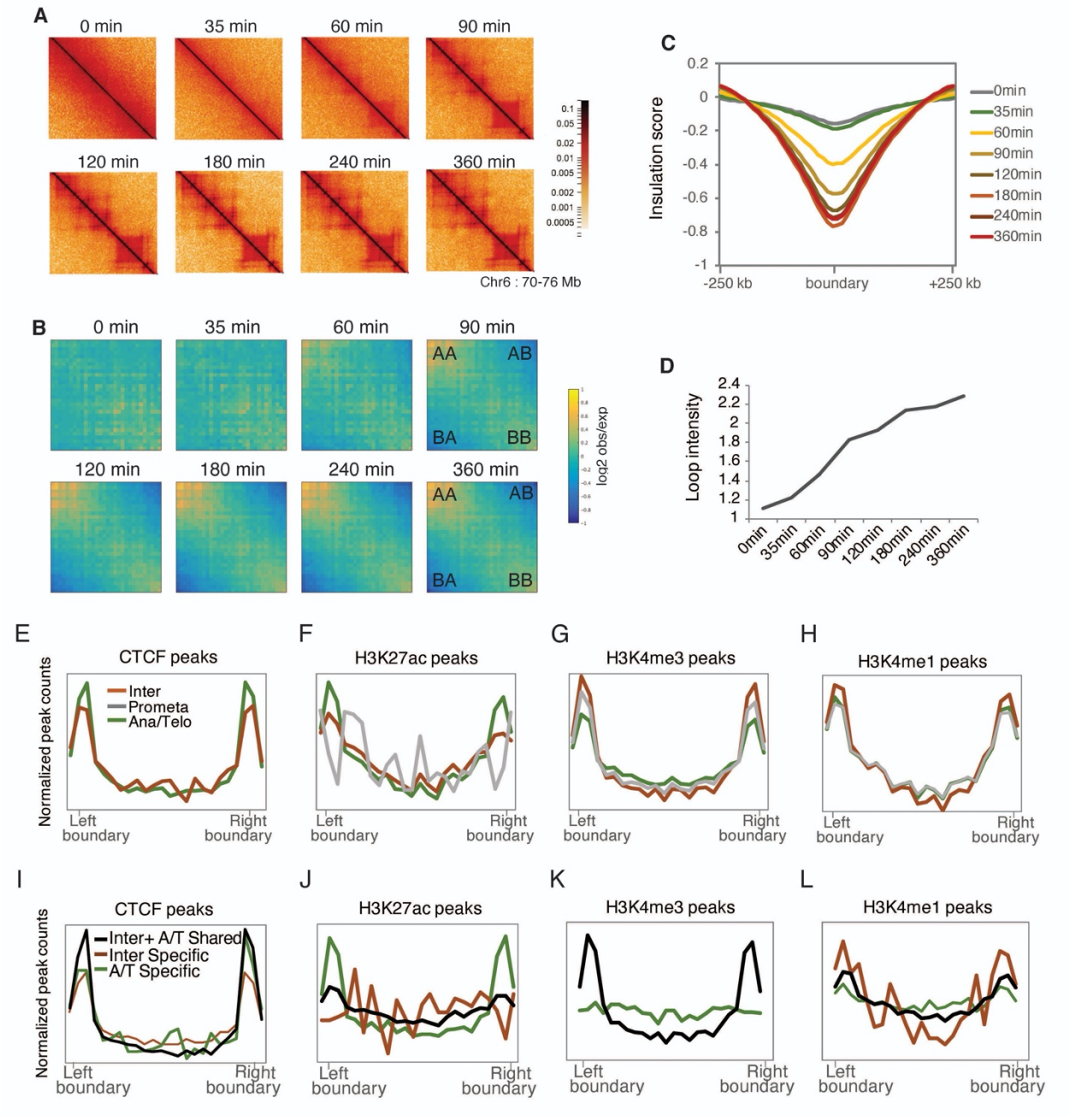
A
0 min
35 min
60 min
90 min
120 min
180 min
240 min
360 min
Chr6 : 70-76 Mb
B
AA
AB
BA
BB
log2 obs/exp
C
Insulation score
-250 kb
boundary
+250 kb
0min
35min
60min
90min
120min
180min
240min
360min
D
Loop intensity
E
CTCF peaks
Inter
Prometa
Ana/Telo
Normalized peak counts
Left boundary
Right boundary
F
H3K27ac peaks
G
H3K4me3 peaks
H
H3K4me1 peaks
I
CTCF peaks
Inter+ A/T Shared
Inter Specific
A/T Specific
J
H3K27ac peaks
K
H3K4me3 peaks
L
H3K4me1 peaks

1.3.7 CTCF and active histone modifications bookmark the TAD boundaries across mitosis.

It has been previously shown that the TAD boundaries are enriched in CTCF binding (Dixon et al. 2012, Rao et al. 2014, Vietri Rudan et al. 2015) and imaging analysis detects CTCF on mitotic chromatin, yet with reduced levels (Burke et al. 2005). To investigate how properly TADs are formed after mitosis, we asked whether a subset of CTCF is retained at the TAD boundaries across mitosis and acts as a bookmark for TAD formation. To do that, we first performed ChIP-seq for CTCF in prometaphase, anaphase/telophase, and interphase and analyzed retention of CTCF binding and its genome-wide distribution during mitosis. In accordance with a recent study, CTCF is largely depleted from mitotic chromatin (Oomen et al. 2019). We identified less than 3% of the total binding peaks in prometaphase (Supplemental Fig. S7C). In concordance with our ChIP-seq analysis, immunofluorescence and western blot analyses showed that CTCF is largely dispersed to the cytoplasm in prometaphase, then recruited on chromatin in anaphase/telophase (Supplemental Fig. S7A,B). We then analyzed the distribution of CTCF binding peaks at the TAD boundaries in each cell cycle phase. As previously suggested, interphase CTCF binding was enriched at the TAD boundaries. We did not observe any enrichment at the boundaries in prometaphase, possibly due to the limited numbers of binding sites during this stage. Strikingly, anaphase/telophase CTCF binding was strongly enriched at the boundaries even higher than that seen in interphase (Fig. 6E). These data indicate that although CTCF is not responsible for ‘memory’ of insulator elements during prometaphase, it may play a role in TAD reformation during anaphase/telophase, particularly by relocalizing at the boundaries.

Given that active histone marks are enriched at the TAD boundaries in the interphase chromatin (Dixon et al. 2012) and H3K4me3 and H3K4me1 are well retained throughout mitosis at *cis*-REs (Fig. 2), we hypothesized that H3K4me3 and H3K4me1 may bookmark the TAD boundaries in prometaphase when CTCF is absent. We examined the distribution of histone modification binding sites at the TAD boundaries in interphase, prometaphase, and anaphase/telophase. As expected, mitotic H3K27ac was depleted at the boundaries as reduced in prometaphase (Fig. 6F). Strikingly, however, H3K4me3 and H3K4me1 were enriched at the boundaries in all cell cycle phases including prometaphase and anaphase/telophase (Fig. 6G,H), suggesting that H3K4me3 and H3K4me1 act as a bookmark of insulator elements to allow cells to remember where TADs need to be formed after mitosis.

Although CTCF and H3K27ac binding were significantly decreased in prometaphase, 56% of CTCF (17,004 peaks) and 79% of H3K27ac (35,771 peaks) interphase binding sites were recovered in anaphase/telophase (Supplemental Fig. S7C; Fig.1B). Interestingly, we found new binding sites on anaphase/telophase chromatin for CTCF (1,728 peaks) and H3K27ac (11,927 peaks). In addition, both CTCF and H3K27ac were strongly enriched at the TAD boundaries, especially in anaphase/telophase (Fig. 6E,F). Thus, we investigated whether CTCF or H3K27ac may have anaphase/telophase specific function on insulator elements. To this end, peaks were divided into three categories: (a) ‘Shared’ observed in both interphase and anaphase/telophase, (b) ‘Interphase Specific’ observed only in interphase, and (c) ‘Anaphase/Telophase Specific’ observed only in anaphase/telophase. When characterizing the distribution of binding peaks in each category at the boundaries, we

observed that CTCF ‘Shared’ peaks were highest at the boundaries (Fig. 6I), indicating that CTCF is recruited at the boundaries in anaphase/telophase and remains there in the next G1 phase. Conversely, H3K27ac ‘Anaphase/Telophase Specific’ peaks were greatly enriched at the boundaries, stronger than ‘Shared’ peaks, while ‘Interphase Specific’ peaks were depleted (Fig. 6J), indicating that enrichment of H3K27ac binding at insulators is mostly either newly bound to anaphase/telophase or recovery of interphase binding after prometaphase. We did not observe noticeable enrichment in either H3K4me3 or H3K4me1 ‘Anaphase/Telophase Specific’ binding (Fig. 6K,L). Together, these results suggest that the increase in H3K27ac binding during anaphase/telophase may contribute to TAD reformation.

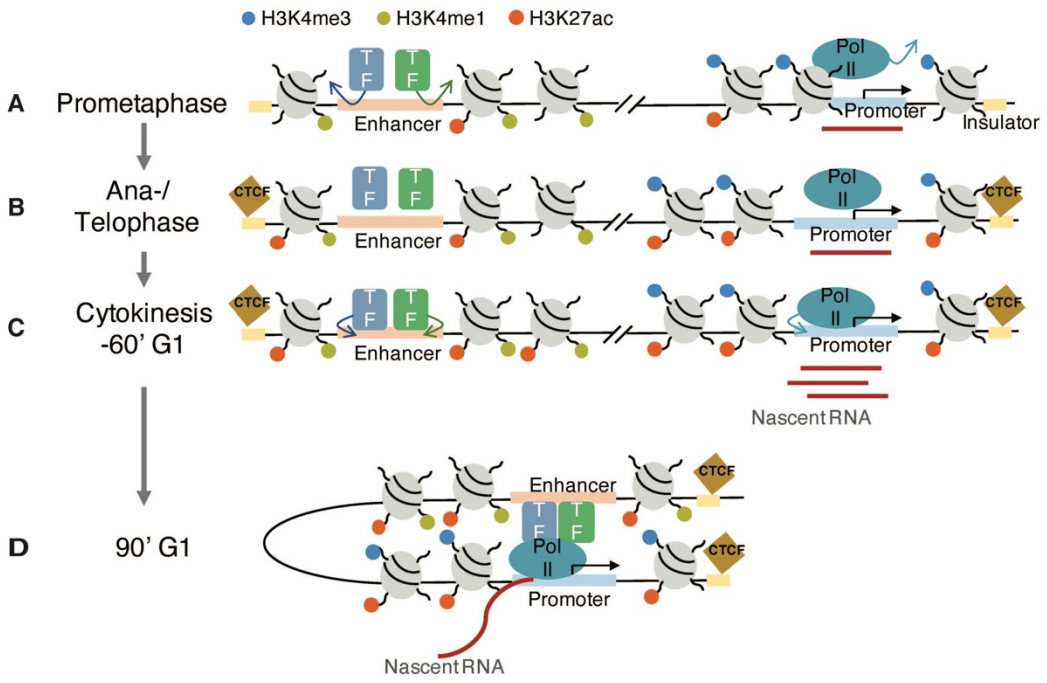

Figure 1.7 Temporal regulation of genome reorganization by histone modifications, nascent transcription, and long-range chromatin interactions during mitosis-G1. (A) In prometaphase, Pol II and TF, including CTCF, dissociate, although some genes are actively transcribed. H3K27ac is globally lost except for a subset of enhancers of cell type-specific genes and limited promoters of housekeeping genes, while H3K4me3 and H3K4me1 are stably bound at promoter and enhancer respectively, and both at insulator. (B) In anaphase/telophase, H3K27ac is recruited back at promoter, enhancer, and insulator. CTCF is also recruited at insulator. (C) In cytokinesis/60' G1, Pol II and TF reassociate and most genes are reactivated. (D) In 90' G1, long-range chromosomal interactions appear to be reestablished.

1.4 Discussion

Here, we provide a temporal order of genome organization during and after mitosis. During prometaphase, histone methylation binding is largely retained, however only low levels of transcription occur and no long-range chromatin interactions are detected. Because histone modifications are established first, we investigated whether mitotic histone modification binding contributes to gene reactivation or to the formation of long-range chromatin interactions. We observed that levels of H3K4me3 and H3K4me1 are stable throughout mitosis at promoters and enhancers, respectively, and both at insulators. H3K4me1 remains at enhancers of cell type-specific genes and TFs binding motifs, which regulate cell type-specific gene expression during prometaphase. This indicates that histone methylations act as a widespread epigenetic memory of regulatory information previously active in the mother cells. Limited H3K27ac remains associated with mitotic chromatin for the accurate transmission of transcription programs and early expression of cell type-specific genes. Loss of H3K27ac in prometaphase is recovered in anaphase/telophase preferentially at promoters and insulators. This recovery of H3K27ac by anaphase/telophase is required for gene reactivation and is particularly re-localized at the TAD boundaries. When cells enter cytokinesis, most of the genes are transcribed. Long-range chromatin interactions gradually increase from cytokinesis, and are complete between 90-120 min G1. In addition to H3K27ac, CTCF lost in prometaphase is recruited in anaphase/telophase at the TAD boundaries, which may be involved in the reformation of TADs in the daughter cells. Overall, the genome is orderly reformed in which histone methylations are retained throughout mitosis, followed by histone acetylation and CTCF in

anaphase/telophase, transcription in cytokinesis, then long-range interactions in 90 min G1 (Fig. 7).

Consistent with previous reports using different approaches such as quantitative mass spectrometry (Javasky et al. 2018, Ginno et al. 2018, Zhiteneva et al. 2017), our ChIP-seq analysis reveals the global retention of H3K4me3 and H3K4me1, but reduction in H3K27ac during prometaphase. Our spike-in normalized ChIP-seq allows us to study quantitative and spatial changes in histone modifications during the mitosis-G1 transition. This retention of histone modifications has been suggested to function as a bookmark of the transcriptional program during mitosis. Notably, we observed that widespread histone methylations on mitotic chromatin bookmark *cis*-REs. First, H3K4me3 bookmarks promoters of genes during prometaphase. 98 % of promoters retain H3K4me3 during prometaphase (Fig. 2A) and mitotic H3K4me3 binding has positive correlations with gene expression (Fig. 4D). However, harboring H3K4me3 does not seem to facilitate rapid transcriptional reactivation because the Pearson correlation between H3K4me3 signals and gene expression is not particularly high in early expressing genes such as 0 min or 35 min genes, compared to late expressing genes such as 90 min, 120 min, or 180 min genes (Supplemental Fig. S4C). Second, H3K4me1 bookmarks enhancers of cell type-specific genes during prometaphase. Cell type-specific genes tend to contain H3K4me1 during prometaphase and to be expressed early in the mitosis-G1 transition (Fig. 3A,B,4H). This may associate with TFs binding such as AP1 family TFs (Long 2011), RUNX2 (Ducy et al. 1997, Komori et al. 1997, Otto et al. 1997), TEADs (Kegelman et al. 2018), or FOXO1 (Rached et al. 2010, Teixeira et al. 2010) which are known to have a crucial role in bone formation or

homeostasis. Genome-wide approach remains to be examined to reveal whether these TFs occupy with H3K4me1 during mitosis at cell type-specific enhancers. Lastly, H3K4me3 and H3K4me1 bookmark insulators during prometaphase (Fig. 6G,H). Although active histone marks have been well investigated to be enriched at TAD boundaries, the distribution of mitotic histone marks at TADs boundaries has not. Altogether, these data indicate that mitotic H3K4me3 and H3K4me1 contribute to the faithful establishment of the transcriptional program, epigenetic landscapes, and chromatin architecture across mitosis. Similar to these active histone methylation marks, repressive histone methylation marks, including H3K9me2, H3K9me3, and H3K27me3, are globally maintained during mitosis (Wang and Higgins 2013). A recent study shows that H3K9me2 ensures the inheritance of spatial position at the nuclear periphery throughout mitosis (Poleshko et al. 2019). Thus, these suggest that repressive histone methylation marks likewise would have a role in epigenetic memory of transcriptionally silent genes as well as spatial organization of genome throughout mitosis.

In our ChIP-seq analysis, H3K27ac substantially increases in the number of binding sites and binding signal on anaphase/telophase chromatin (Fig.1B,E). First, this increase may have a role in transcriptional reactivation. A recent study shows that H3K27ac signals during mitotic exit correlate with increased transcriptional activity in early G1 at both promoters and enhancers by measuring Pol II binding in erythroblasts (Hsiung et al. 2016). Our analysis combined with EU-RNA-seq, and with the use of spike-in normalization, reveals that H3K27ac in anaphase/telophase, deposited only at promoters but not at enhancers, is also the most predictive histone mark for

transcriptional reactivation among the three active histone marks tested in this study (Fig. 4D). Enhancer-promoter loops were lost in mitosis and not formed until cytokinesis at 60 min (Fig. 6D), which may explain why we did not observe any positive correlations with transcriptional activation at AE regions. Furthermore, A-485-treated H3K27ac inhibition confirmed that H3K27ac recovery has a mitotic bookmarking function. Surprisingly, transcriptional activation was perturbed for about 50% of dysregulated genes by inhibiting H3K27ac recovery (Fig. 5B), indicating that H3K27ac is required for post-transcriptional activation. In addition to transcription, as H3K27ac is enriched at the TAD boundaries in interphase chromatin (Dixon et al. 2012), we tested whether the increase of H3K27ac in anaphase/telophase has a role in the formation of TADs. We found a significant number of new H3K27ac binding sites in anaphase/telophase, which are only present in anaphase/telophase (Fig. 1B). Combined with Hi-C data, we surprisingly found that this anaphase/telophase specific H3K27ac binding was particularly enriched at the TAD boundaries and was even higher than interphase specific peaks (Fig. 6J), suggesting anaphase/telophase specific function of H3K27ac at insulators. In the future, it would be interesting to determine the functional role of H3K27ac in the reformation of long-range interactions after mitosis and whether it serves to recruit architectural proteins CTCF or cohesin complex or/and provide a bookmark for domain boundaries or A-A and B-B compartments. Taken together, the increase of H3K27ac in anaphase/telophase seems to influence promoters-driven transcriptional reactivation and TAD reformation.

BRD4 is a histone acetyltransferase (HAT) that acetylates histones H3 and H4 such as H3K14ac, H3K27ac, H3K122ac, and H4K16ac (Devaiah et al. 2016,

Filippakopoulos et al. 2012). It binds AEs and controls the activation of cell type-specific genes in various cell systems (Lee et al. 2017, Najafova et al. 2017, Wu, Kamikawa and Donohoe 2018). Prior studies have shown that BRD4 is partially retained on mitotic chromatin and its overexpression accelerates the transcriptional activation in early G1 (Zhao et al. 2011, Dey et al. 2009), suggesting its function as a transcriptional bookmark on mitotic chromatin. Recently, a genome-wide approach reveals that BRD4 widely occupies mitotic chromatin at H3K27ac sites. However, neither transcription activation nor H3K27ac mitotic binding were perturbed by mitotic specific inhibition of BRD4 following JQ treatment (Behera et al. 2019). This suggests that BRD4 is dispensable for either transcriptional reactivation or H3K27ac retention during mitosis, but BRD4 may still be involved in some other regulatory function. Another recent study shows that BRD4 is indispensable for osteoblast-lineage specification during differentiation. ChIP-seq reveals the high co-occupancy of BRD4 with other TFs such as C/EBPb, TEAD1, FOSL2, and JUND at putative osteoblast-specific enhancers in human fetal osteoblasts cells, hFOB (Najafova et al. 2017). We observed that a subset of BRD4 and c-Jun associated with mitotic chromatin using immunofluorescence analysis in U2OS cells (data not shown). Although the colocalization of two TFs and genome-wide spatial information needs to be explored, these observations suggest that mitotic BRD4 may recruit TFs at cell type-specific enhancers and play a role in epigenetic memory of cell type-specific transcriptional program.

Recently, a genome-wide RNA pulse-labeling study showed that some genes are actively transcribed in prometaphase arrested cells, and described waves of gene reactivation during mitotic exit (Palozola et al. 2017). Using the same approach, we

were able to observe mitotically expressed genes, as well as the hierarchy of gene activation from prometaphase to G1 phase (Fig. 4). However, we also made a set of different observations. First, while our study reveals that the largest number of genes are first activated at 60 min (cytokinesis/early G1), the other study shows it at 80 min (metaphase-anaphase), which is earlier in the cell cycle than our observation. This conflicting result can be explained by the use of different synchronization protocols. Although both studies utilize thymidine-nocodazole block to arrest prometaphase cells, the efficiency of cell cycle synchronization can be affected by incubation time and concentration of chemicals. Long incubation or high concentration of chemicals can prevent the ability of cells exiting mitosis and re-entering the next G1 phase, and therefore can delay cells released from mitotic arrest and lead to a wide range of heterogeneous cell populations (Zieve et al. 1980). Thus, we used less nocodazole for shorter incubation time and enabled to efficiently enrich homogenous cell populations at each time point. Second, our analysis reveals that the largest number of cell type-specific genes are expressed at 60 min (cytokinesis/early G1) in a similar trend with general EU-labelled gene expression, yet the other study shows that most are expressed at 300 min (early G1), which is later than when the largest number of EU-labelled genes are first activated at 80 min. This difference may simply result from low coverage of cell type-specific genes: 113 bone specific-genes in our study and 149 liver-specific genes in their study. However, both studies are in agreement regarding the timing of activation of cell type-specific genes at early G1. Activation of cell type-specific gene expression requires appropriate cell type-specific TFs, which are mostly recruited by cytokinesis, and enhancer-mediated loops, which start to be formed after cytokinesis.

Overall, in spite of a few different observations, we were able to find genes actively transcribed throughout mitosis to G1.

Multiple studies show that CTCF remains associated with mitotic chromosomes using imaging and western blot analyses (Burke et al. 2005, Liu et al. 2017), which provide suggestive mitotic bookmarking function at insulator elements, given its essential role in TAD formation. Our ChIP-seq analysis, however, shows that CTCF binding sites are almost entirely lost during prometaphase. Dissociation of CTCF from mitotic chromatin was also observed using imaging and chromatin fractionation approaches. Phosphorylation of CTCF may explain this dissociation. *In vitro* assay shows that CTCF becomes highly phosphorylated during mitosis and this phosphorylation of CTCF impairs its DNA binding activity (Sekiya et al. 2017). A recent study using a different genomic technique, CUT&RUN, which can be performed on unfixed cells, unlike ChIP-seq, reveals the loss of CTCF binding in prometaphase as well (Oomen et al. 2019). Thus, it seems unlikely our observation is due to technical artifacts such as formaldehyde-induced fixation. Interestingly, the majority of loss of CTCF binding during prometaphase is regained by anaphase/telophase, earlier than TAD formation, and CTCF relocalizes at the TAD boundaries. Similarly, cohesin almost completely dissociates during prometaphase and rapidly reassociates as cells exit mitosis (Cai et al. 2018, Abramo et al. 2019). The loop extrusion model underlies TAD formation through cohesin-mediated loop extrusion, which is stalled at TAD boundaries due to CTCF binding (Fudenberg et al. 2016, Sanborn et al. 2015). Thus, loss of TADs during prometaphase seems to be due to loss of CTCF and cohesin and TAD

reformation seems to be mediated by CTCF and cohesin recruitment at the boundaries during anaphase/telophase.

1.5 Materials and methods

Cell culture and cell cycle synchronization

U2OS osteosarcoma cells were cultured in DMEM (Gibco) and 10% FBS. To obtain mitotic cells, U2OS cells were treated with filter-sterilized 2.5 mM thymidine (Sigma) for 30 h, washed, and released into thymidine-free fresh medium. After 10 h release from S phase arrest, the cells were incubated with 20 ng/ml nocodazole (Sigma) for 4 h. To enrich for mitotic cells, rounded floating cells were collected with shake-off. To release the cells from arrest, mitotic cells were washed three times with PBS to remove nocodazole and then incubated in fresh medium in suspension culture.

RPE1 hTERT immortalized cells were cultured in DMEM-F12 (Gibco) and 10% FBS. RPE1 cells were synchronized in S phase by double thymidine block with 2 mM thymidine for 14 h, release into fresh media for 10 h, and 2 mM thymidine for 14 h. After 6 h release from thymidine block, cells were synchronized in prometaphase using 20 ng/ml nocodazole for 4 h cells. The mitotic cells were then collected by mitotic shake-off. Anaphase/telophase enriched cells were collected after 35 min incubation in the nocodazole-free medium.

10uM A-485 (Tocris) was used to inhibit H3K27ac levels.

Immunofluorescence

Cells were grown on glass coverslips and fixed with 4% paraformaldehyde in PBS for 5 min at RT. Fixed cells were permeabilized with cold PBS containing 0.5% Triton X-100 for 5 min. Cells were blocked with 1% BSA in PBS for 1h at RT and incubated in primary antibody in blocking buffer overnight at 4°C, followed by secondary

antibody for 1 h at RT. Cells were then briefly stained with 1 ug/ml Hoechst 33342 (H-1399, Molecular Probes) in PBS and mounted in Vectashield (Vector Laboratories). Images were acquired in a Zeiss LSM710 confocal microscope. Images were analyzed and prepared for presentation in Photoshop.

Isolation of nuclear and cytoplasmic fractions

Cells were resuspended in hypotonic buffer (5 mM Pipes pH 8, 85 mM KCl, 0.5% NP-40, and protease inhibitor) on ice for 10 min, followed by centrifugation at 500*g* for 10 min at 4°C. The supernatant containing the cytoplasmic fraction was transferred and saved. The pellet was resuspended in lysis buffer (50 mM Hepes pH 7.9, 5 mM $MgCl_2$, 0.2% Triton X-100, 20% glycerol, 300 mM NaCl, and protease inhibitor) on ice for 30 min, followed by centrifugation at 12,000*g* for 20 min at 4°C. The supernatant was collected as the nuclear fraction.

Histone isolation and western blotting

For histone extraction, the protocol is adapted from previous work (Shechter et al. 2007). Briefly, following nuclei isolation, soluble histones were extracted with 0.2 M HCl, followed by TCA/acetone precipitation. For western blot analysis, protein samples were resolved in SDS-PAGE gels and transferred to PVDF membranes (Millipore). Membranes were blocked with 5% milk in TBST (0.25% Tween 20, 20 mM Tris, pH 8.0, and 137 mM NaCl) and incubated with primary antibody overnight at 4°C. After 3 x 5 min washes in TBST, HRP-conjugated secondary antibody was added for 1 h at RT.

Membranes were visualized by SuperSignal West Pico or Femto (Thermo Fisher Scientific) reagent.

Antibodies

The following antibodies were purchased from the indicated commercial sources: anti-H3K4me3 (ab8580, Abcam), anti-H3K4me1 (ab8895, Abcam), anti-H3K27ac (ab4729, Abcam), anti-CTCF (61311, Active Motif), anti-Spike-in (61686, Active Motif), anti-α-Tubulin (T5168, Sigma), anti-Histone H3 (4499, Cell Signaling,), and anti-H3S10p (3377, Cell Signaling).

ChIP-seq

Cells (5×10^6) were cross-linked with 1% formaldehyde for 10 min, and ChIP-seq was performed as previously described (Toyama et al. 2019). Spike-in was carried out according to vendor protocols (Active Motif). Briefly, 50 ng of Spike-in chromatin (53083, Active Motif) was added to 25 µg of U2OS or RPE1 chromatin to incubate with 2 µg Spike-in antibody together with 5 µg of anti-H3K4me3, anti-H3K4me1, anti-H3K27ac, or anti-CTCF antibodies. DNA libraries were generated using the Kapa Hyper Prep Kit for Illumina Platforms (Kapa biosystems). Libraries were sequenced in a NextSeq 500 system (Illumina). See Supplemental Material for detailed information about data analysis, including alignment, normalization, peak calling, *cis*-REs identification, motif analysis, and Pearson correlation coefficient test.

Spike-in control sequences and EU-RNA-seq

Biotinylated spike-in controls and samples for EU-RNA-seq were prepared as previously described (Palozola et al. 2017). Briefly, U2OS cells were pulse-labeled with 0.5 mM EU for 35 min at 37°C. Total RNA was harvested using Trizol (Ambion) and purified using miRNeasy (Qiagen). Click reaction was performed to conjugate biotin to the EU-labelled RNA using Click-iT Nascent RNA Capture Kit (Invitrogen). Two biotinylated spike-in control RNAs were added to 1.5 ug of each biotinylated sample (0.36 ng of control #1 and 0.036 ng of control #2). Biotin-EU-RNAs, including spike-in controls, were pulled down with streptavidin-coated magnetic beads. For validation of biotin-RNA spike-in controls, cDNA was generated using the SuperScript VILO cDNA synthesis kit (Invitrogen) followed by qPCR. For sequencing, cDNA libraries were generated using the Ovation Human FFPE RNA-Seq Multiplex System. Multiplexed pair-end sequencing was performed on a NextSeq 500 instrument (Illumina). See Supplemental Material for detailed information about data analysis, including alignment, normalization, identification of hierarchy of gene expression, and GO enrichment analysis.

Hi-C

Hi-C was performed using the *in situ* method as previously described (Rao et al. 2014). Briefly, U2OS cells (2×10^6) were cross-linked with formaldehyde. Chromatin was digested with a restriction enzyme MboI (NEB), biotinylated with biotin-ATP (Life Technologies), and then ligated with T4 DNA ligase (NEB). DNA was purified and sheared with Covaris LE220 instrument (Covaris). Biotinylated DNA interactions were pulled down with Dynabeads MyOne Streptavin T1 Beads (Life Technologies) and

sequenced in a NovaSeq 6000 sequencing system (Illumina). See Supplemental Material for detailed information about data analysis.

ChIP-seq Analysis

Raw read quality was checked using FastQC and contamination was checked with FastqScreen and BLAST. Reads were mapped to an hg19 (human) and dm6 (fly spike-in) combined genome using the STAR aligner version 2.5.3b (Dobin et al. 2013). Mapping was carried out using default parameters (up to 10 mismatches per read, and up to 9 multi-mapping locations per read). The genome index was constructed using the gene annotation supplied with the hg19 and dm6 Illumina iGenomes (iGenomes online. Illumina. 2015. http://support.illumina.com/sequencing/sequencing_software/igenome.html) collection and sjdbOverhang value of 100. After mapping, fly reads were quantified separately and used to determined spike-in normalization factors for all samples assuming a constant amount of spike-in added. Final normalization factors(f) were calculated by renormalizing each cell cycle phase(p) to the interphase(I) within each replicate(r) for each antibody(a):

$$f_{p,r,a}=(|human_{p,r,a}|+|fly_{p,r,a}|)|fly_{p=I,r,a}|/|fly_{p,r,a}|(|human_{p=I,r,a}|+|fly_{p=I,r,a}|)$$

Peaks were identified using HOMER (Heinz et al., 2010), using default parameters and input condition as background reference. Normalized read counts for peaks were calculated using the fragments per kilobase per million mapped reads

(FPKM) normalization multiplied by the spike-in factors. Low coverage peaks were filtered out (average log2 normalized read counts < 3 across all phases for H3K27ac, H3K4me3, and H3K4me1, and average log2 normalized read counts < 1 across all phases for CTCF, due to lower quality ChIP for CTCF). Then peaks were defined as present in a phase if the average normalized expression in that phase was at least the ¾ the maximum normalized read count across all 3 phases. Peak overlap across cell cycle phases was calculated using HOMER mergePeaks routines with a maximum distance for merging of 1000 bp.

Genomic Element Analysis

Phase-specific genomic elements were defined according to the presence of H3K27ac, H3K4me1, and H3K4me3 normalized peaks in each phase and their proximity to the transcription start sites (TSS) of annotated RefSeq genes. Promoters (Pr) were defined as any regions containing H3K4me3 within 1kb of the TSS of known genes. Primed enhancers (PE) were defined as regions containing only H3K4me1 peaks at a distance of more than 1kb away from the TSS of known genes. Active enhancers (AE) were defined as regions containing both H3K4me1 and H3K27ac peaks at a distance of more than 1kb away from the TSS of known genes. HOMER mergePeaks was used to find all combinations of overlaps between peaks in each phase and HOMER annotatePeaks was used to determine the distance to the nearest TSS.

To calculate the distribution of normalized read coverage around the center of genomic elements (Pr, AE, PE), HOMER annotatePeaks was used with a window size

of +/- 3kb and a bin size of 100 bp. Spike-in normalization factors were applied and the average read coverage of replicates was shown as a histogram.

The set of promoters and enhancers maintained during prometaphase and those lost in prometaphase, then regained in anaphase/telophase, was determined with HOMER mergePeaks applied to the elements directly. The known motif enrichment analysis was carried out using HOMER findMotifsGenome.pl with -size given.

EU-RNA Analysis

Raw read quality was checked using FastQC and contamination was checked with FastqScreen and BLAST. Reads were mapped to an hg19 (human) using the STAR aligner version 2.5.3b (Dobin et al. 2013). FPKM (fragments per kilobase per million mapped reads) gene expression was quantified across the entire gene with HOMER analyzeRepeats. In addition, reads mapping to spike-in sequences were used to calculate the normalization slope based on the expected concentrations of the spike-ins as was done previously (Palozola et al. 2017). Expression values were further log2 transformed, averaged across replicates, and NoEU control expression values were subtracted from EU values at each time point. Next, time point-specific genes were identified as genes whose expression exceeds 50% of the average expression across all times (excluding asynchronous) and continues to exceed 50% for the duration of the time course. Asynchronous genes were defined as those that were not time point specific and whose values were at least twice as high in the asynchronous time point compared to any of the other time points. Heatmaps were generated using R libraries

gplots (heatmap.2 function), or plot.matrix (plot function) with scaling across conditions. An absolute log2fold change of 1 was used to determine genes up or down with A-485.

To correlate EU expression with the ChIP-seq results, we used the merged peaks from the replicates of each ChIP antibody and cell-cycle phase to quantify the EU read counts at each time point averaged across both replicates and normalized for peak size. These values were then correlated to the average ChIP read counts for that antibody and cell-cycle phase normalized to the peak size. Gene Ontology functional enrichment analysis was performed using DAVID (Dennis et al. 2003).

Hi-C data analysis

Sequencing reads generated from samples of eight time points with two replicates were subjected to alignment and processing as previously described (Dixon et al. 2018), and contact matrices were constructed and normalized by matrix balancing. We have performed standard identification of features in Hi-C datasets, including compartments (Lieberman-Aiden et al. 2009), TADs (Dixon et al. 2012), loops (Rao et al. 2014) and insulation scores (Crane et al. 2015). Annotated TADs of 360 minutes samples were normalized by size and divided into 20 bins for ChIP-seq peak mapping for all time points. Local minimums were identified for insulation vectors of all samples for plotting.

Accession numbers

The Gene Expression Omnibus accession number for the ChIP-seq, EU-RNA-seq, and Hi-C data reported in this study is GSE141139.

1.6 Acknowledgments

Chapter 1, in full, has been submitted for publication as it may appear in *Genes Development*. Hyeseon Kang, Maxim N. Shokhirev, Zhichao Xu, Sahaana Chandran, Jesse R. Dixon, Martin W. Hetzer. “Dynamic regulation of histone modifications and long-range chromosomal interactions during post-mitotic transcriptional reactivation.” The author of this dissertation was the primary investigator and author of this paper.

Figure S1.1 Retention of histone modifications on mitotic chromatin. (A) Synchronization was monitored by microscopy using both Hoechst and α-Tubulin staining. The number of U2OS cells was counted in the left panel: mitotic contamination in asynchronous cells (left), mitotic index in mitotic arrest cells (middle), and mitotic release from prometaphase for indicated time (right). The number of cells released from mitotic arrest was also counted in RPE1 cells (right panel). (B) Immunofluorescence images show the presence of histone modifications on mitotic chromatin. U2OS and RPE1 were stained for α-Tubulin (green) and either H3K4me3, H3K27ac, or H3K4me1 (red). Images were taken at mitotic cells naturally occurred. Scale bars, 10 μm. (C) Western blot analysis shows an abundance of H3K4me3, H3K4me1, and H3K27ac in histone extracts from interphase (Int), prometaphase (Pro), and anaphase/telophase (Ana/Tel) enriched cells. Histone H3 was used as the loading control. H3pser10 was used as the mitotic marker. (D) Venn diagram showing the number of promoters, AEs, and PEs in each cell cycle phase. Regulatory elements were defined as indicated in U2OS (left panel) and RPE1 (right panel) cells. (E) Histogram showing ChIP-seq reads of H3K4me3, H3K27ac, and H3K4me1 relative to TSS during interphase (orange), prometaphase (gray), and anaphase/telophase (green) in U2OS (upper panel) and RPE1 (bottom panel) cells.

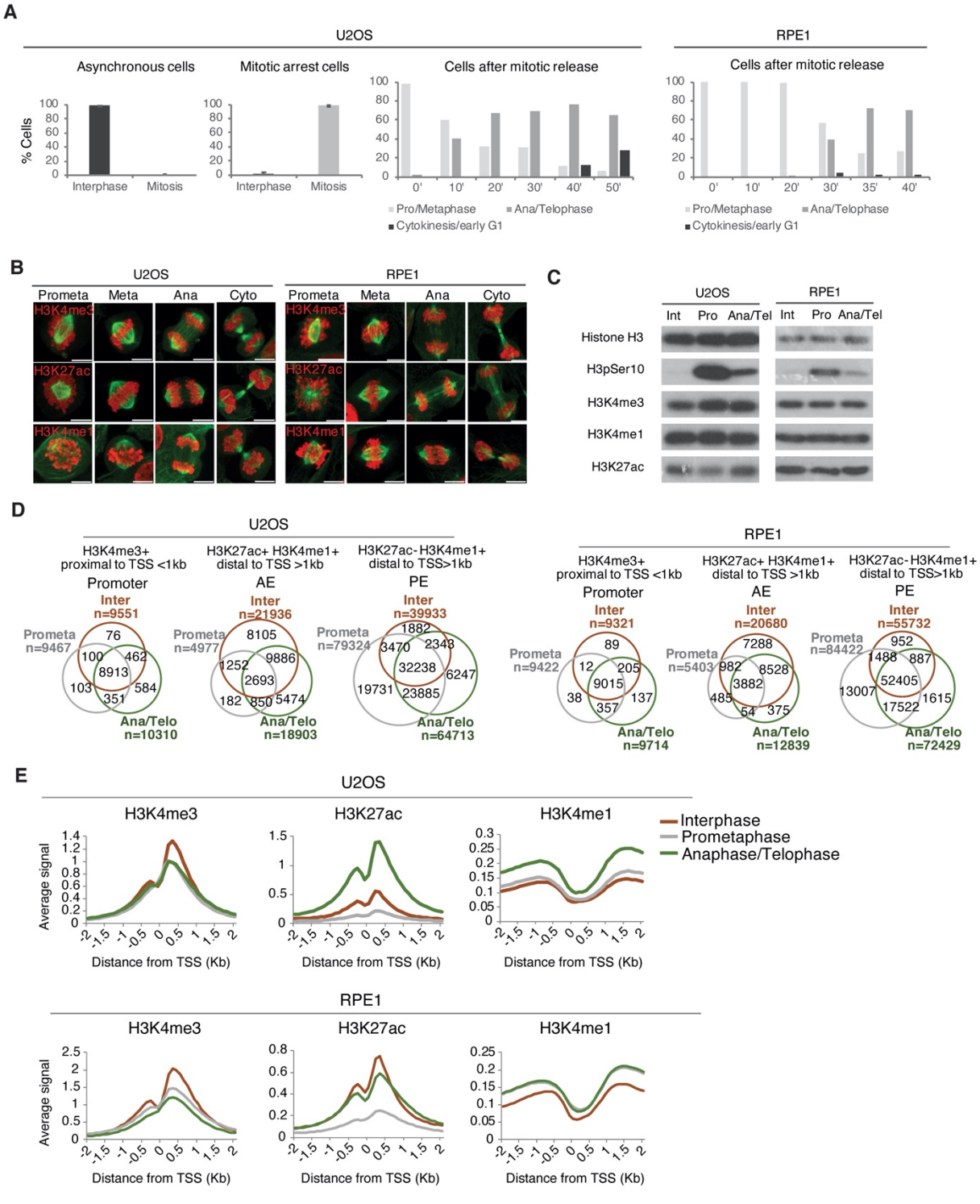
A
U2OS
RPE1
Asynchronous cells
Mitotic arrest cells
Cells after mitotic release
Cells after mitotic release
% Cells
Interphase
Mitosis
Pro/Metaphase
Ana/Telophase
Cytokinesis/early G1
B
U2OS
RPE1
Prometa
Meta
Ana
Cyto
H3K4me3
H3K27ac
H3K4me1
C
U2OS
RPE1
Int
Pro
Ana/Tel
Histone H3
H3pSer10
H3K4me3
H3K4me1
H3K27ac
D
U2OS
RPE1
H3K4me3+ proximal to TSS <1kb
Promoter
H3K27ac+ H3K4me1+ distal to TSS >1kb
AE
H3K27ac- H3K4me1+ distal to TSS>1kb
PE
Inter
Prometa
Ana/Telo
n=9551
n=9467
n=10310
n=21936
n=4977
n=18903
n=39933
n=79324
n=64713
n=9321
n=9422
n=9714
n=20680
n=5403
n=12839
n=55732
n=84422
n=72429
E
U2OS
RPE1
H3K4me3
H3K27ac
H3K4me1
Average signal
Distance from TSS (Kb)
Interphase
Prometaphase
Anaphase/Telophase

Figure S1.2 Histone methylations bookmark promoters and enhancers in the absence of H3K27ac during prometaphase in RPE1 cells. (A) Quantification of interphase promoters that are also detected in prometaphase or in anaphase/telophase. Promoters harboring both H3K27ac and H3K4me3 are shown in blue and H3K4me3 only in light blue. Promoters not containing any histone modification are shown in the lightest blue color. (B) ChIP-seq tracks at the promoter of the SMC3 gene for H3K4me3, H3K27ac, and H3K4me1 during interphase, prometaphase, and anaphase/telophase. (C) Quantification of interphase AEs that are also detected in prometaphase or in anaphase/telophase. AEs harboring both H3K27ac and H3K4me1 are shown in orange and H3K4me1 only in gray. AEs not containing any histone modification are shown in light orange. (D) ChIP-seq tracks at AE of BRINP3 gene for H3K4me3, H3K27ac, and H3K4me1 during interphase, prometaphase, and anaphase/telophase. (E) Quantification of interphase PEs that are also detected in prometaphase or in anaphase/telophase. PEs harboring H3K4me1 are shown in gray. PEs not containing any histone modification are shown in light gray. (F) ChIP-seq tracks at PE of EMP1 gene for H3K4me3, H3K27ac, and H3K4me1 during interphase, prometaphase, and anaphase/telophase. Peaks are highlighted by brown boxes. Abbreviations: interphase (Inter), prometaphase (Prometa), anaphase/telophase (Ana/telo), histone modification (HM).

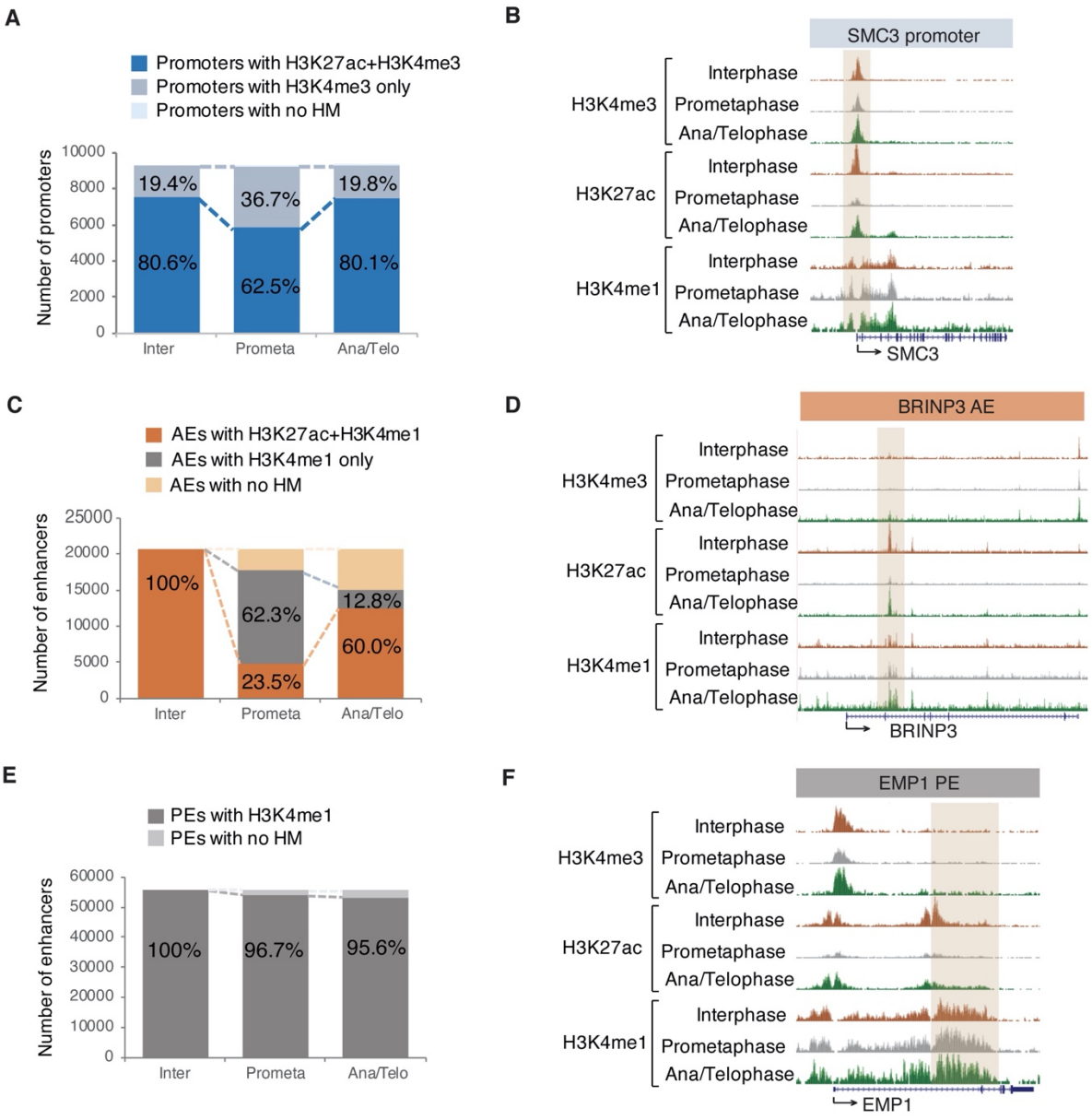
A
Promoters with H3K27ac+H3K4me3
Promoters with H3K4me3 only
Promoters with no HM
Number of promoters
10000
8000
6000
4000
2000
0
19.4%
80.6%
36.7%
62.5%
19.8%
80.1%
Inter
Prometa
Ana/Telo
B
SMC3 promoter
H3K4me3
H3K27ac
H3K4me1
Interphase
Prometaphase
Ana/Telophase
SMC3
C
AEs with H3K27ac+H3K4me1
AEs with H3K4me1 only
AEs with no HM
Number of enhancers
25000
20000
15000
10000
5000
0
100%
62.3%
23.5%
12.8%
60.0%
Inter
Prometa
Ana/Telo
D
BRINP3 AE
H3K4me3
H3K27ac
H3K4me1
Interphase
Prometaphase
Ana/Telophase
BRINP3
E
PEs with H3K4me1
PEs with no HM
Number of enhancers
60000
50000
40000
30000
20000
10000
0
100%
96.7%
95.6%
Inter
Prometa
Ana/Telo
F
EMP1 PE
H3K4me3
H3K27ac
H3K4me1
Interphase
Prometaphase
Ana/Telophase
EMP1

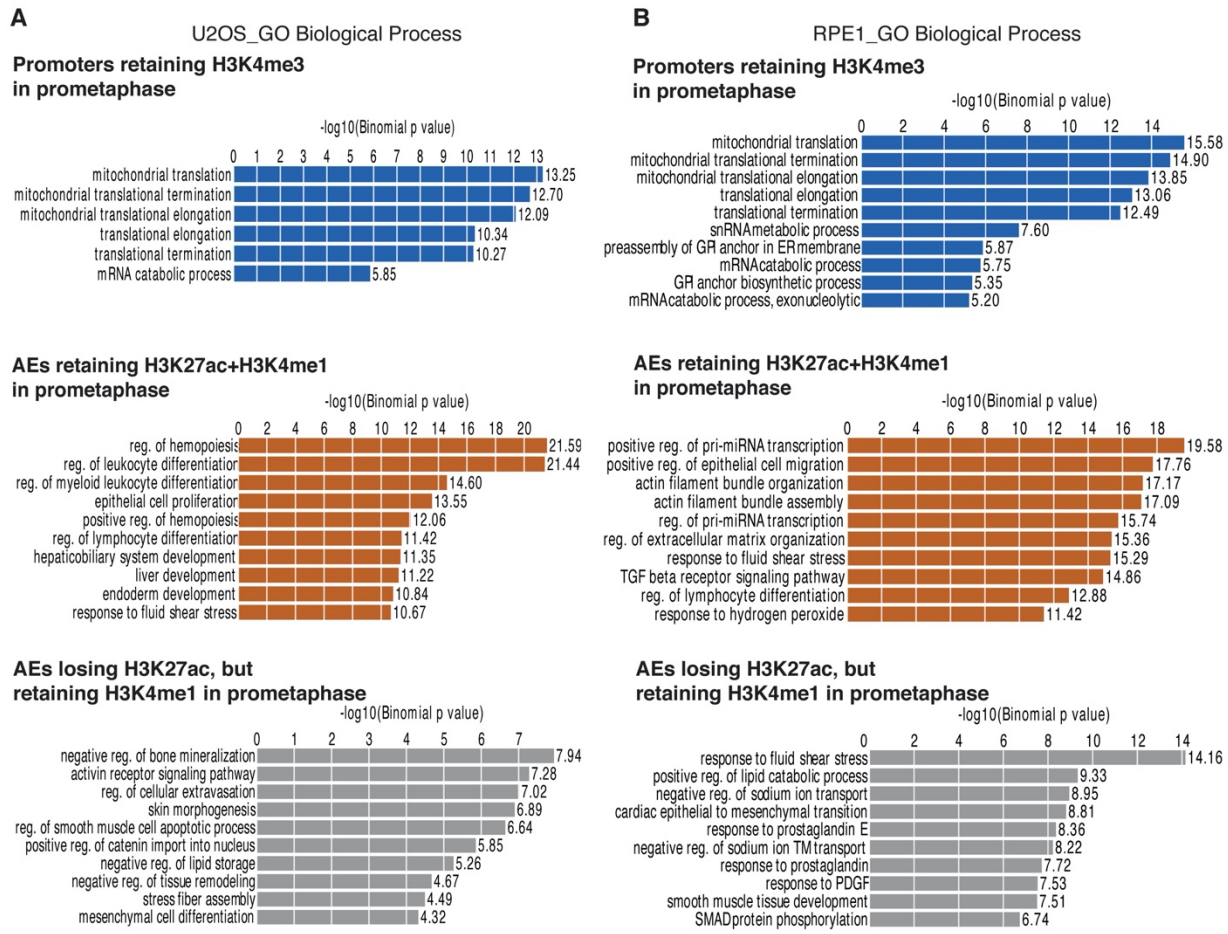

Figure S1.3 H3K4me1 remains at enhancers of cell type-specific genes during prometaphase in U2OS and RPE1. (A, B) Top 10 Gene Ontology (GO) annotations enriched in promoters retaining H3K4me3 (blue), AEs retaining both H3K27ac and H3K4me1 (orange) and AEs losing H3K27ac, but retaining H3K4me1 (gray) during prometaphase in U2OS (A, left panel) and RPE1 (B, right panel).

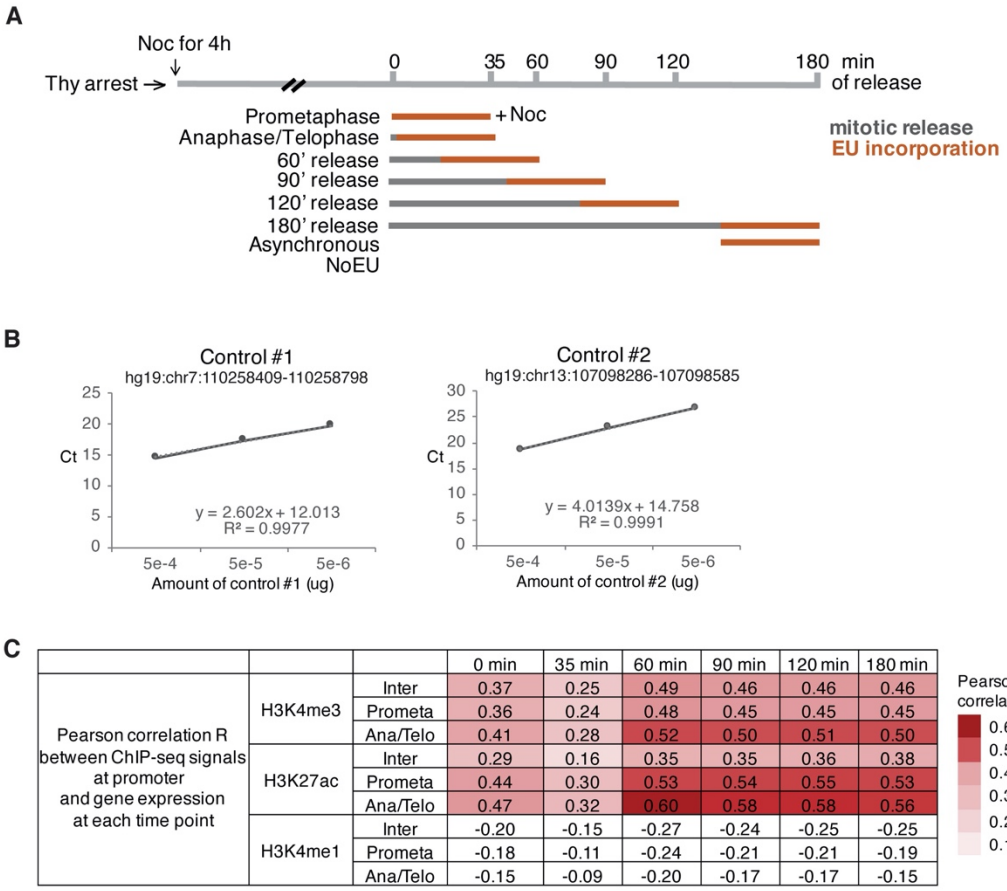

			0 min	35 min	60 min	90 min	120 min	180 min
Pearson correlation R between ChIP-seq signals at promoter and gene expression at each time point	H3K4me3	Inter	0.37	0.25	0.49	0.46	0.46	0.46
		Prometa	0.36	0.24	0.48	0.45	0.45	0.45
		Ana/Telo	0.41	0.28	0.52	0.50	0.51	0.50
	H3K27ac	Inter	0.29	0.16	0.35	0.35	0.36	0.38
		Prometa	0.44	0.30	0.53	0.54	0.55	0.53
		Ana/Telo	0.47	0.32	0.60	0.58	0.58	0.56
	H3K4me1	Inter	-0.20	-0.15	-0.27	-0.24	-0.25	-0.25
		Prometa	-0.18	-0.11	-0.24	-0.21	-0.21	-0.19
		Ana/Telo	-0.15	-0.09	-0.20	-0.17	-0.17	-0.15

Figure S1.4 EU-RNA-seq reveals nascent RNA during mitosis-G1. (A) Schematic of EU-RNA-seq strategy illustrating pulse-labeling during mitosis-G1. (B) Validation of spike-in controls by RT-qPCR. The indicated amount of control #1 or control #2 was added at 1.5 ug of asynchronous biotin-EU-RNA and pulled down with streptavidin-coated magnetic beads. Ct values of control #1 or control #2 show the control sequences are pulled down proportionally on streptavidin-coated magnetic beads in the presence of total asynchronous RNA. (C) Pearson correlation coefficient (R) was determined between the transcriptional level at each time point and the ChIP-seq reads of H3K4me3, H3K27ac, and H3K4me1 in interphase (Inter), prometaphase (Prometa), and anaphase/telophase (Ana/Telo) at the promoter. Positive correlations are shown in red color (R > 0).

Figure S1.5 Inhibition of mitotic H3K27ac and H3K27ac recovery by A-485 alters gene expression pattern. (A) Western blot analysis shows A-485 treatment during mitosis inhibits H3K27ac levels in histone extracts from prometaphase (Prometa) (left panel). H3K27ac levels in cytokinesis (Cytoki) and 24h release cells after wash out A-485 from mitotic arrest (middle panel). A-485 treatment upon releasing cells from mitotic arrest inhibits H3K27ac levels in cytokinesis (Cytoki) and 3h G1 cells (right panel). U2OS cells were treated with 1h of 10μM A-485 or EtOH as a control. Histone H3 was used as the loading control. (B) Heatmaps of Pearson correlations between replicates of the same conditions. (C) Heatmap demonstrating the differential gene expression pattern between control (EtOH) and A-485 treatment in each cell cycle phase.

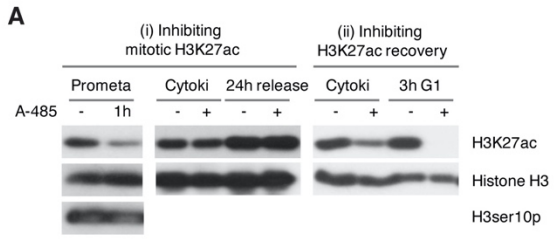
A
(i) Inhibiting mitotic H3K27ac
(ii) Inhibiting H3K27ac recovery
Prometa
Cytoki
24h release
Cytoki
3h G1
A-485
- 1h - + - + - + - +
H3K27ac
Histone H3
H3ser10p

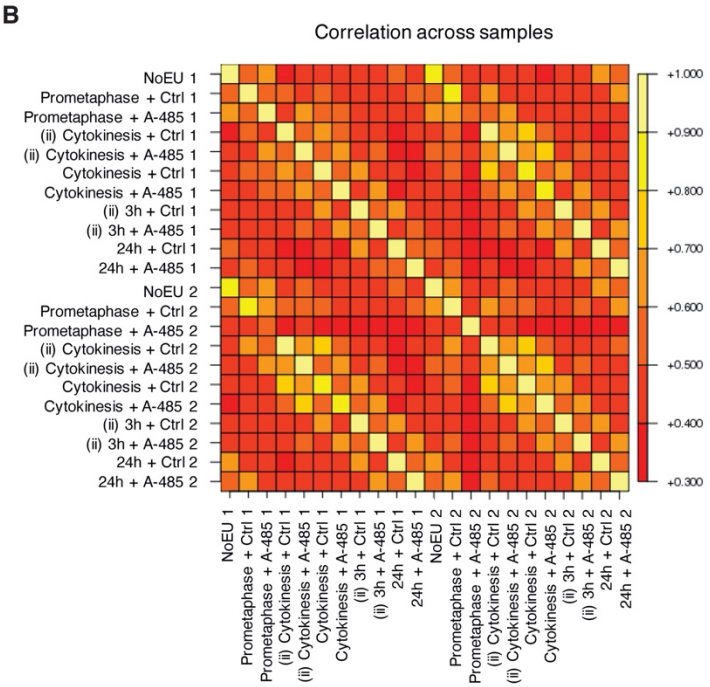
B
Correlation across samples
NoEU 1
Prometaphase + Ctrl 1
Prometaphase + A-485 1
(ii) Cytokinesis + Ctrl 1
(ii) Cytokinesis + A-485 1
Cytokinesis + Ctrl 1
Cytokinesis + A-485 1
(ii) 3h + Ctrl 1
(ii) 3h + A-485 1
24h + Ctrl 1
24h + A-485 1
NoEU 2
Prometaphase + Ctrl 2
Prometaphase + A-485 2
(ii) Cytokinesis + Ctrl 2
(ii) Cytokinesis + A-485 2
Cytokinesis + Ctrl 2
Cytokinesis + A-485 2
(ii) 3h + Ctrl 2
(ii) 3h + A-485 2
24h + Ctrl 2
24h + A-485 2
+1.000
+0.900
+0.800
+0.700
+0.600
+0.500
+0.400
+0.300

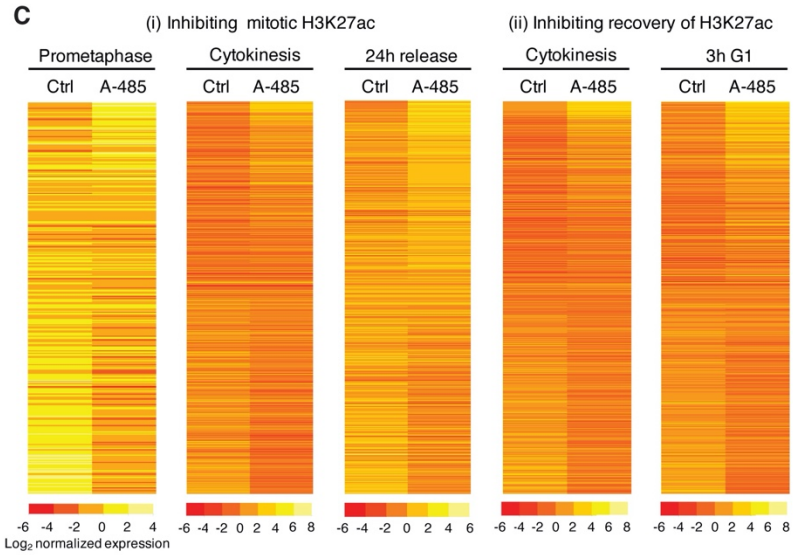
C
(i) Inhibiting mitotic H3K27ac
(ii) Inhibiting recovery of H3K27ac
Prometaphase
Cytokinesis
24h release
Cytokinesis
3h G1
Ctrl A-485
-6 -4 -2 0 2 4
-6 -4 -2 0 2 4 6 8
-6 -4 -2 0 2 4 6
-6 -4 -2 0 2 4 6 8
-6 -4 -2 0 2 4 6 8
Log2 normalized expression

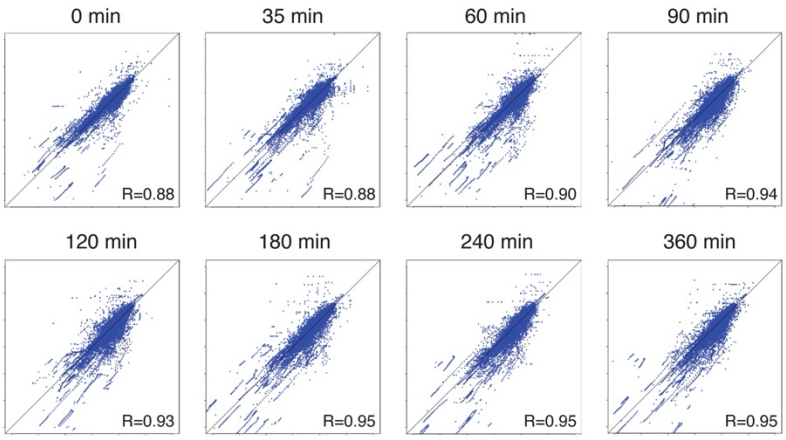

Figure S1.6 Hi-C analysis during mitosis-G1. Pearson correlation of compartment eigen vector between two replicates at each time point and 1 Mb bin size.

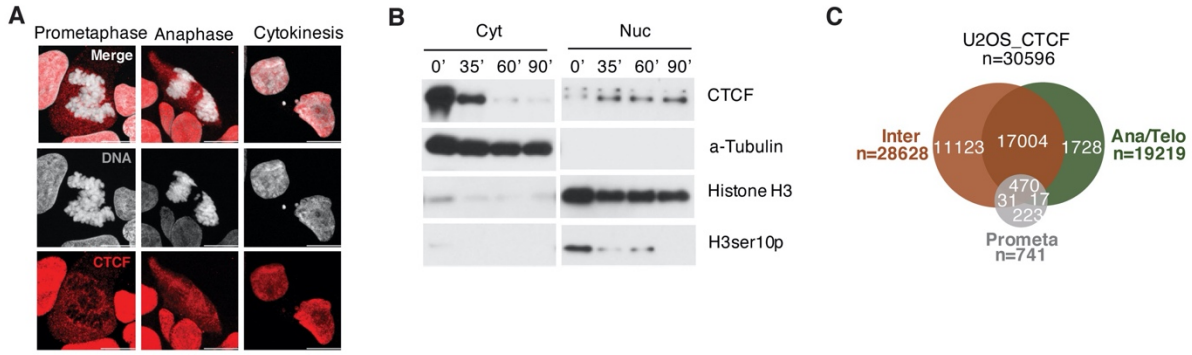

Figure S1.7 Global level change of CTCF during mitosis. (A) Immunofluorescence analysis of CTCF in mitotic phases. U2OS cells were stained for Hoechst (gray) and CTCF (red). CTCF was largely dispersed to the cytoplasm during prometaphase. (B) Western blot showing CTCF levels in nuclear or cytoplasmic fractions isolated from U2OS cell lysates after thymidine-nocodazole mitotic arrest or nocodazole washout. α-Tubulin and Histone H3 were used as the loading control in the cytoplasmic or nuclear fraction, respectively. H3ser10p was used as the mitotic marker. (C) Venn diagram showing the number of CTCF binding sites in interphase (Inter), prometaphase (Prometa), and anaphase/telophase (Ana/Telo) in U2OS cells, with n representing the number of observed CTCF peaks in each cell cycle phase.

Chapter 2. Dynamic regulation of genome at the nuclear periphery

2.1 Abstract

Nucleoporins (Nups) interact with super-enhancers (SEs) to the nuclear periphery in multiple cell types. However, the molecular mechanisms that underlie Nup-SEs interactions at the nuclear periphery remains unknown. Here, we identified an unexpected link between NPC and architecture protein CTCF for regulating key SE-associated genes. Our super-resolution microscopy showed that CTCF is localized at the edge of the nucleus with the NPCs. Our genomic analysis revealed that the depletion of Nup153 or Tpr influenced CTCF binding preferentially at SEs. Interestingly, Nup-mediated CTCF binding also regulated key cell identity gene expression. These data suggest that NPCs may serve as structural anchors for the SE elements by providing a scaffold for interaction with architecture proteins like CTCF to control SE-associated cell identity genes.

2.2 Introduction

The nucleus is separated by the nuclear envelope (NE), a double membrane bilayer, the outer nuclear membrane (ONM) and the inner nuclear membrane (INM). NE associates with genome structure and function, which composed of two major components, the nuclear lamina and the nuclear pore complexes (NPCs). The nuclear lamina is a layer of filamentous proteins, the nuclear lamins, underlining the INM. NPC is composed of several copies of ~30 different subunits, called nucleoporins (Nups) and multiple NPCs perforate NE. High-resolution microscopy shows that heterochromatin is

clustered underneath the nuclear lamina, except the NPCs (Capelson and Hetzer 2009, Solovei, Thanisch and Feodorova 2016). Besides, Hi-C analyses indicate that B-compartment is preferentially localized at the nuclear periphery, while A-compartment in the nuclear interior (Stevens et al. 2017, Bonev and Cavalli 2016). Heterochromatin and nuclear lamina have been proposed to drive genome organization (Falk et al. 2019) . However, despite the high occupancy in the genome, the NPCs are studied to a lesser extent regarding in genome organization and gene regulation.

Several studies suggest that NPC-genome contacts at the nuclear periphery may have a function in the structural organization of the genome. Components of the NPC, such as nuclear basket protein, Nup2, which is homologous to human NUP153, and Tpr act as a chromatin insulator in both yeast and fly cells (Ishii et al. 2002, Kalverda et al. 2010). In human, Tpr contributes to the formation of heterochromatin exclusion zones beneath NPCs (Krull et al. 2010). In metazoans, Nup98 mediates enhancer-promoter looping and facilitate transcriptional memory of developmentally regulated genes upon ecdysone activation. This inducible gene activation promotes the interaction of Nup98 with several chromatin architectural proteins, including CTCF (Pascual-Garcia et al. 2017). In addition, Nup153 has shown to interact with architectural proteins, CTCF, SMC1A, and SMC3 in mouse extraembryonic endoderm stem cells (Sachani et al. 2018). These studies suggest that the NPC may have a function in higher-order chromatin organization by providing a scaffold for architecture proteins or acting as architecture proteins like CTCF. However, we still know little about whether the NPC directly impacts the formation or maintenance of chromatin structure and how the NPC mediates chromatin interactions at the nuclear periphery. If the NPC requires

architecture proteins such as CTCF to modulate genome organization, they should tightly colocalize, which never has been shown previously and needs to be uncovered as all of the previous studies show their interactions by immunoprecipitation.

NPC associated genomic regions regulate gene expression at the nuclear periphery. NPC components like Nup153 regulate gene expression in *Drosophila melanogaster* and mouse cells without having a significant impact on global transport or nuclear compartmentalization (Vaquerizas et al. 2010, Jacinto, Benner and Hetzer 2015). In human cells, Nup153 and Nup93 interact with SEs in several cell types (Ibarra et al. 2016). SEs are clusters of enhancers that are occupied by the high density of master transcription factors and drive high levels of transcription of genes involved in cell-type identity. These Nup-associated SEs localize to the nuclear periphery, and the depletion of Nup153 and Nup93 dysregulated the expression of SE-associated cell identity genes. Nevertheless, we have little understanding of the molecular mechanisms that underlie Nup-mediated SEs at the nuclear periphery.

To address these questions, we investigate the molecular mechanisms that control Nup-associated SEs-driven gene expression. Our studies enabled us to identify CTCF as a mediator for regulating NPC–genome interactions. Interestingly, super-resolution microscopy showed that CTCF associates with NPCs at the nuclear periphery. Ablation of NPC components disrupted SE interactions with CTCF and RNA polymerase II and transcription of SE-associated cell identity genes. Altogether, these results suggest that NPCs control cell identity genes by interacting with CTCF at the SE-associated gene.

2.3 Results

2.3.1 NPC components interact with CTCF at the nuclear periphery.

Nucleoporins interact with SEs to the nuclear periphery (Ibarra et al. 2016). However, the molecular player that mediates Nup-SE interactions at the periphery remains unknown. SEs are occupied by high concentration of enhancer-associated factors, including transcription factors, Mediators, and coactivators, and RNA polymerase II (Pol II) (Hnisz et al. 2013, Lovén et al. 2013). A subset of SEs contains a hierarchical structure, mediated by CTCF and cohesion (Huang et al. 2018). We thus examined the interaction between these factors associated with SEs and components of the NPCs, such as the nuclear basket member Nup153, using *in situ* proximity ligation assay (PLA), which can detect two proteins in close proximity within 40nm. Most PLA signals between Nup153 and CTCF, Med1, and Pol II were seen at the edge of the nucleus, which was determined by DAPI staining (Fig. 1A). Such PLA signals were diminished upon Nup153 depletion (Fig. 1B), suggesting that the detected signals are specific to the presence of Nup153. We also noticed that Nup153 interacted with other SE components, BRD4 and p300, as well as one of the cohesin complex, SMC3 (Data not shown). In addition, another nuclear basket protein Tpr was located adjacent to these factors (Data not shown). To confirm this colocalization, direct Stochastic Optical Reconstruction Microscopy (dSTORM) super-resolution microscopy was further examined. dSTORM image showed that Nup153 was localized at every single nuclear pore and preferentially at the nuclear periphery, suggesting that Nup153 staining represents NPC. Med1 was localized all over the nucleus, but a subset of Med1 was co-localized with NPC (Fig. 1C). In addition, the super-resolution image of CTCF exhibited

a localization all over the nucleus as well. Surprisingly, however, a subset of CTCF was tightly co-localized with NPC at almost every nuclear pore (Fig. 1D). This suggests that coactivators and architecture proteins may involve in mediating NPC-SE interactions.

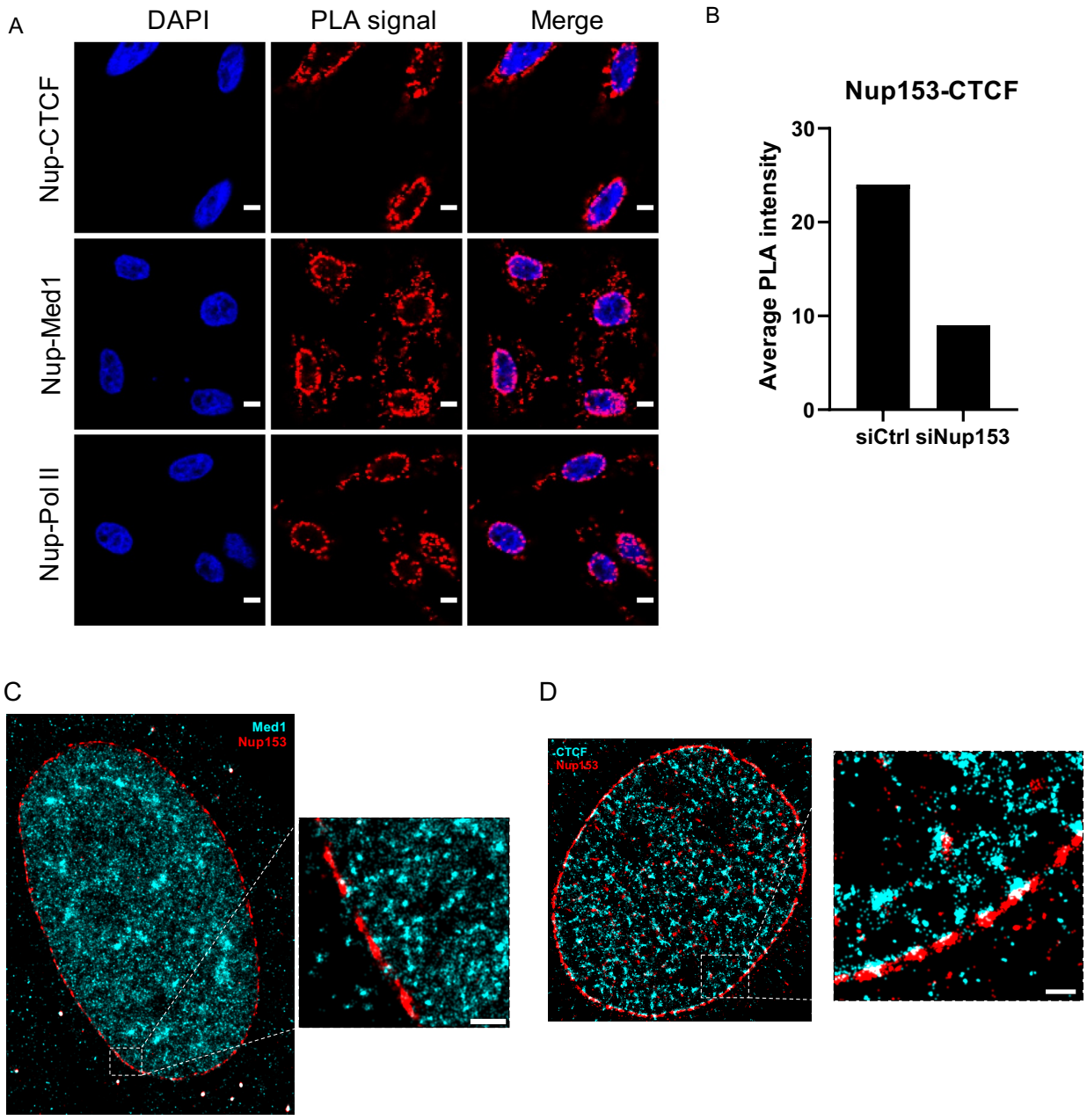

Figure 2.1 CTCF interacts with NPC at the nuclear periphery. (A) U2OS cells were fixed and stained with antibodies against Nups and CTCF/ Med1/ Pol II, combined with secondary PLA probes. The interaction events are visible as red dots. Nuclei were stained with DAPI (blue). Scale bars, 1 μm. (B) graph shows the average number of PLA signals per cell. Nup153 KD exhibits a noticeable decrease in interaction between Nup153 and CTCF. (C-D) Tow-color dSTORM images of Nup153 and Med1 (C) or CTCF (D) in a cell. Nup153 shown in red, Med1 and CTCF shown in cyan. Scale bars, 0.5 μm.

2.3.2 NPC components influence CTCF binding.

To gain insights into CTCF-NPC interactions, we transiently transfected IMR90 cells with siRNA against Nup153 and Tpr, and asked whether depletion of NPC components influences CTCF binding. We first performed CUT&RUN for CTCF in Nup153 or Tpr KD cells, and sought for differential CTCF binding sites compared with control KD. We identified 4,767 CTCF differential binding sites that were either down-(2,424 sites) or up-(2,343 sites) regulated in Nup153 KD cells. Similarly, Tpr KD altered 4,182 CTCF binding sites (1,032 down- and 3,150 up-regulated sites) (Fig. 2A). We next examined whether depletion of Nups alters the genomic distribution of differential CTCF binding sites. In control cells, CTCF was distributed at introns (37%), intergenic regions (41%), and promoters (15%). In contrast, in both Nup153 and Tpr KD cells, down-regulated CTCF binding sties exhibited a higher accumulation of CTCF binding at intron (46% and 43%) and intergenic sites (47% and 45%), whereas a lower CTCF binding at promoters (3% and 4%) (Fig. 2B). These results suggest that NPC may impact genome-wide patterns of CTCF binding.

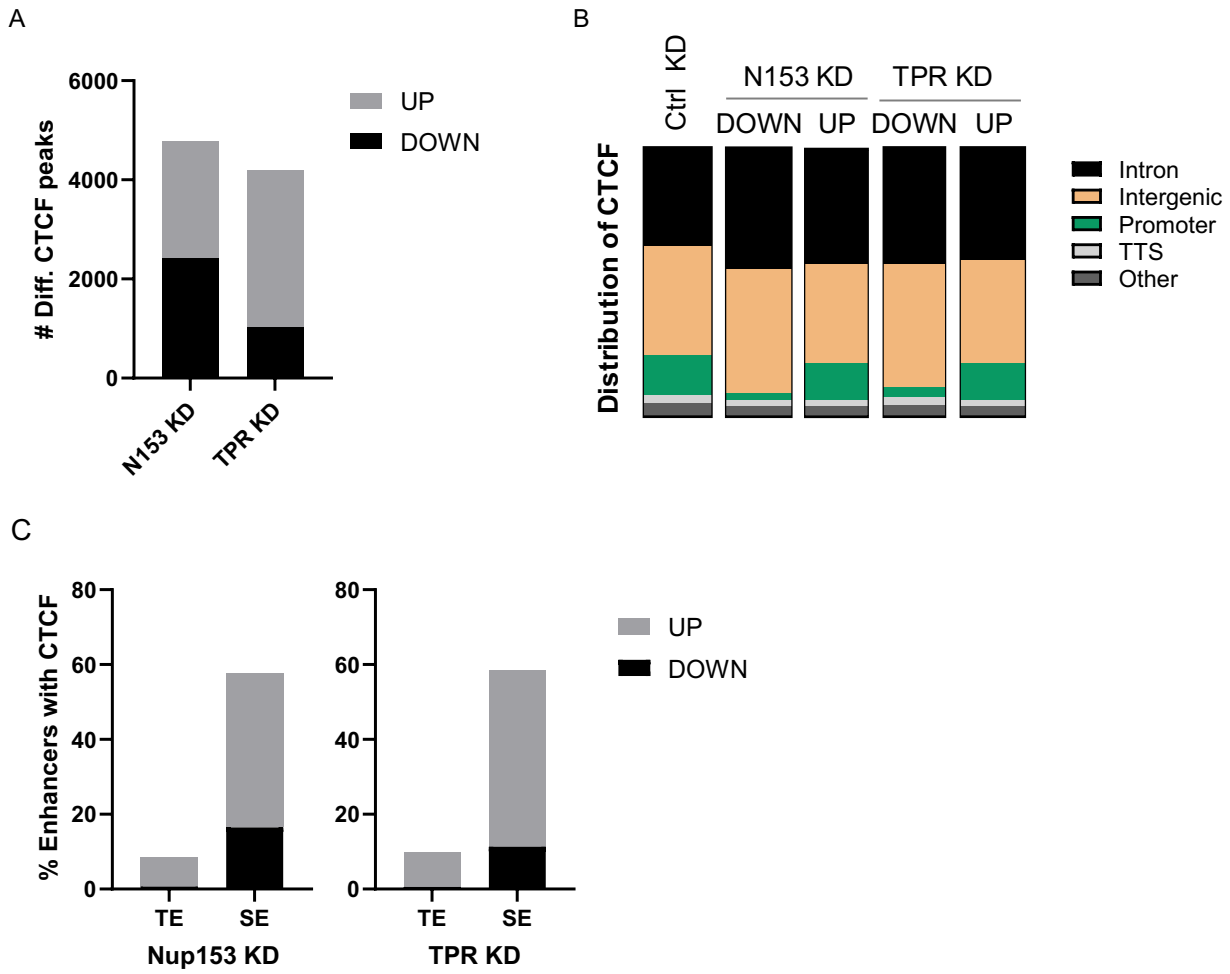

Figure 2.2 NPC components influence CTCF binding. (A) Differential binding sites of CTCF were compared in control and Nup153 and Tpr deficient IMR90 cells. Up-regulated binding sites were shown in gray. Down-regulated binding sites were shown in black. (B) Distribution of CTCF binding peaks relative to genomic elements in control siRNA, Nup153 KD, and Tpr KD. (C) % of enhancers associated with Nup-mediated CTCF binding in typical enhancer (TE) and super-enhancer (SE). Up-regulated binding sites were shown in gray. Down-regulated binding sites were shown in black.

2.3.3 NPC components mediate CTCF binding preferentially at SEs.

Given the colocalization of CTCF with NPC (Fig. 1), we explored the potential role of CTCF in NPC-genome contacts at the nuclear periphery. We hypothesized that NPC components may bring CTCF to SE regions at the nuclear periphery to regulate SE-associated genes. To test this idea, we first determined whether Nup-mediated CTCF binding occurs preferentially at SEs, compared to typical enhancers (TEs). We collected 8,803 TEs and 618 SEs defined by H3K27ac (Hnisz et al. 2013) and compared the number of TEs and SEs interacting with Nup-mediated CTCF binding. Strikingly, Nup-mediated CTCF binding exhibited a higher enrichment in SEs, compared to TEs. In Nup153 KD cells, 16.5% and 41.1% of SEs were associated with down- and up-regulated CTCF binding, while 0.6% and 7.9% of TEs were associated with down- and up-regulated CTCF binding. In addition, Tpr-mediated CTCF binding sites were also enriched in SEs; about 60% of SEs interacted with Tpr-mediated differential CTCF binding sites (11.3% and 47.1% of down- and up-regulated CTCF binding), while only 10% of TEs associated (0.5% and 9.3% of down- and up-regulated CTCF binding) (Fig. 2C). These results indicate that Nup-mediated CTCF is preferentially binding to SEs and may play a role in regulating SE-associated genes.

2.3.4 Nucleoporins control cell identity genes by mediating CTCF binding at SE-associated genes.

Along with other coactivators and Med1, Pol II is efficiently recruited to SEs and initiates transcription (Lovén et al. 2013, Hnisz et al. 2013). We therefore determined whether Pol II-SE association is dependent on nucleoporins. We performed CUT&RUN for Pol II in Nup153 and Tpr deficient IMR90 cells. The absence of Nup153 and Tpr resulted in a decrease in Pol II binding sites; 1,637 and 732 Pol II binding sites were down-regulated in Nup153 KD and Tpr KD, respectively (Fig. 3A). The genomic distribution of Pol II binding was altered in the absence of Nup153 and Tpr (Fig. 3B). In control cells, 40% of Nup-mediated Pol II binding sites were deposited at introns, 27% at intergenic sites, and 27% at promoters. In contrast, Nup153 KD altered the distribution of Pol II binding across the genome, less binding at introns (22.6%) and intergenic sites (16.3%), whereas more binding at promoters (53.3%). Tpr KD showed a similar, but even more dramatic change; 13% at introns, 8.7% at intergenic sites, and 66.8% at promoters. Furthermore, we compared Nup-mediated Pol II binding at TEs versus SEs. We found that Nup153-mediated Pol II binding sites were predominantly enriched in SEs (45.5%, 281/618). On the other hand, only 3.6% TEs (317/8,803) were associated with Nup153-mediated Pol II. Likewise, we observed an enrichment of Tpr-mediated Pol II binding in SEs (16.6%, 103 /618), compared to TEs (0.8% 71/8,803). Both knockdown of Nups exhibited the same impact on Pol II binding, but we noticed that Nup153-mediated Pol II showed more pronounced enrichment in SEs (Fig. 3C). Collectively, as it has been suggested, these data indicate that NPC components, especially Nup153, mediate the Pol II association with SEs.

In order to determine whether Nup-mediated CTCF binding impact SE associated gene expression, we performed RNA-seq in Nup153 KD. Consistent with previous report (Ibarra et al. 2016), knockdown of Nup153 altered transcriptional activity in IMR90 cells (false discovery rate [FDR] < 0.05 and fold change >4; 1,101 down- and 1,503 up-regulated genes). Among these dysregulated genes by the absence of Nup153, we found that 541 differential regulated genes (221 down- and 320 up-regulated) by Nup153-mediated CTCF binding (Fig. 4A). GO analysis revealed that these 541 differential regulated genes were predominantly linked to key genes involved in vascular endothelial regulation (NRP2, FLT1), hematopoietic progenitor cell differentiation (INHBA, PTPRQ), and lung development (LOX, FGF1) (Fig. 4B). In addition, Myc, FOXL1, and TBX2 genes, which were previously identified as super-enhancer driven genes (Ibarra et al. 2016), showed decreases in Pol II and CTCF binding in Nup153 KD and Tpr KD cells (Fig. 4C). Thus, our finding supports the idea that Nup153-mediated CTCF involves in regulating SE-associated cell identity genes.

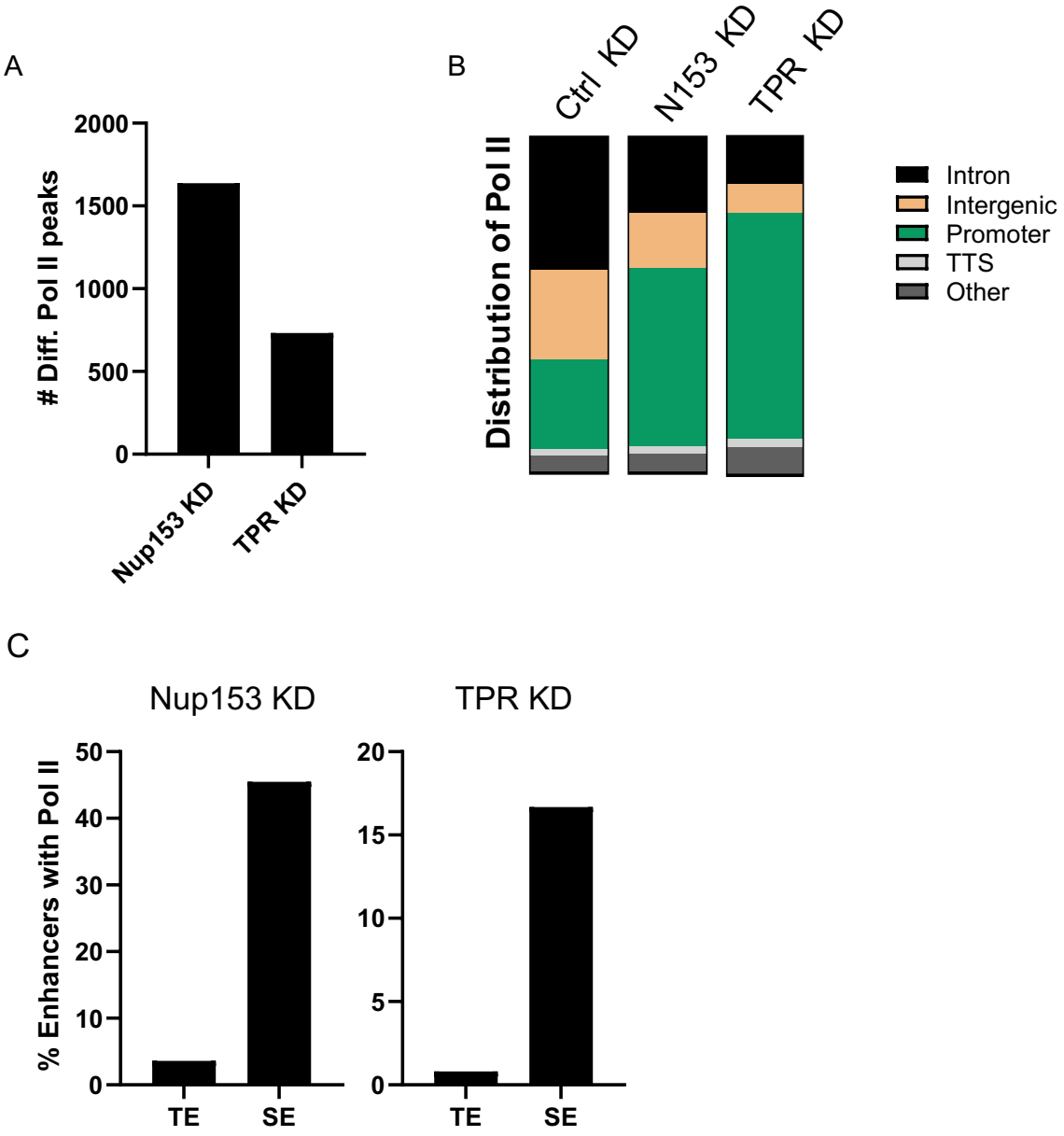

Figure 2.3 NPC components influence Pol II binding. (A) Down-regulated Pol II binding sites in Nup153 and Tpr deficient IMR90 cells. Up-regulated binding sites were shown in gray. Down-regulated binding sites were shown in black. (B) Distribution of Pol II binding peaks relative to genomic elements in control siRNA, Nup153 KD, and Tpr KD. (C) % of enhancers associated with Nup-mediated Pol II binding in typical enhancer (TE) and super-enhancer (SE).

A

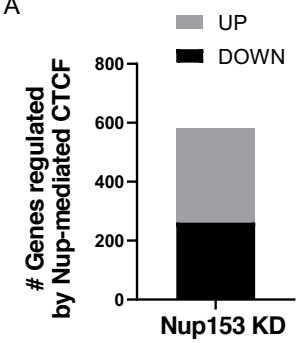

B

GO terms	Rank	Genes
Angiogenesis	1	NRXN3, COL8A1
Positive regulation of endothelial cell migration	4	NRP2, SPARC
Vascular endothelial growth factor signaling pathway	5	FLT1
Positive regulation of cell proliferation	6	CSNK2A3, ESM1
Hematopoietic progenitor cell differentiation	8	INHBA, PTPRQ
Lung development	9	LOX, FGF1

C

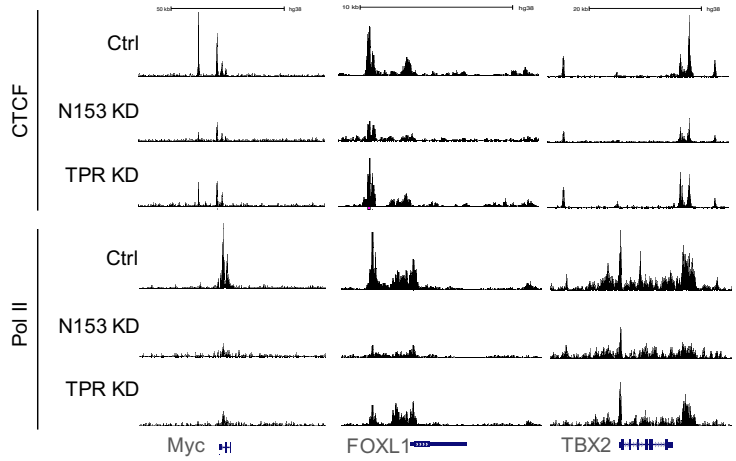

Figure 2.4 NPC-mediated CTCF binding regulates SE-associated genes. (A) The graph shows the overlaps of RNA-seq and CTCF CUT&RUN upon Nup153 KD. 320 Up-regulated bound genes were shown in gray. 221 Down-regulated bound genes were shown in black. (B) Gene ontology (GO) terms analysis of 221 down-regulated CTCF bound genes in Nup153 KD. (C) Representative genome browser view of SE-associated genes, Myc, FOXL1, and TBX2 with CTCF and Pol II binding in control KD, Nup153 KD, and Tpr KD.

2.4 Discussion

Together, our results identified an unexpected link between NPC and CTCF for regulating key SE-associated genes. Surprisingly, our super-resolution microscopy revealed the localization of CTCF and Med1 at the NPCs. CTCF and Med1 localized all over the nucleus, but NPC-CTCF interaction mainly took place at the edge of the nucleus, suggesting the impact of CTCF on Nup-genome interactions is limited at the NPC, rather than within the nucleoplasm. The depletion of Nup153 or Tpr influenced CTCF binding genome-wide, but more pronounced at SEs than TEs. Interestingly, our RNA-seq analysis revealed that Nup-mediated CTCF binding regulated key cell identity gene expression. Knockdown of Nup153 or Tpr altered another SE component Pol II binding at SEs. These data suggest that NPCs provide the scaffold for interaction between CTCF and SEs at the nuclear periphery to control key SE-associated genes.

It remains unanswered whether CTCF is truly the key player to bring all the factors to SEs at the NPCs. All these components were localized very close to NPC, and nucleoporins impact not only CTCF but also other factors such as Pol II. However, the localization of CTCF was right at the NPC, much closer than Med1. Thus, we argue that CTCF serves as a mediator for binding other factors to SEs at the NPC. We are currently working on how NPCs impact genome architecture at SEs using Hi-C. If NPC components play a direct role in the formation or maintenance of SEs, we expect to see defects in long-range SE interactions upon knockdown of nucleoporins. Furthermore, we are planning to ensure the effect of nucleoporins on bringing CTCF to the nuclear periphery using super-resolution microscopy. If nucleoporins require CTCF binding, the depletion of nucleoporins will fail CTCF localization at the nuclear periphery.

2.5 Materials and Methods

Cell culture

U2OS cells were cultured in DMEM (Gibco) and 10% FBS. IMR90 cells were cultured in DMEM and 20% FBS supplemented with nonessential amino acids (Gibco) and low oxygen conditions (3%).

siRNA transfections

siRNAs against human Nup153 and Tpr were designed according to previous studies (McCloskey, Ibarra and Hetzer 2018, Ibarra et al. 2016). siRNA mediated gene silencing was performed using the following oligos (Invitrogen): control (Luc; 5'-UAUGCAGUUGCUCUCCAGC-3'), Nup153 (5'-ACAUUUGGUAGAGUCUGCCUU-3') and Tpr (5′-UUUAACUGAAGUUCACCCU-3′) and delivered using siLenFect (Bio-Rad).

In situ proximity ligation assay

Proximity ligation assay was performed using the Duolink Proximity ligation assay kit (Sigma). To analyze the interaction between NPC components and SE components, we used the following antibodies: Nup153 (906201, BioLegend), CTCF (61311, Active Motif), Med1 (A300-793A, Bethyl Labs), and Pol II (ab5131, abcam).

Super-resolution microscopy

U2OS cells were seeded in a Sticky-Slide 8-well system (80827, ibidi) 24 h prior to imaging at a density of ~25,000 cells/well. Cells were pre-fixed in 2.4% PFA for 20 sec, washed in PBS for 2 min, permeabilized in 0.4% Triton-X for 3 min, and washed in

PBS for 2 min. Cells were then fixed in 2.4% PFA for 30 min followed by quenching in 50 mM ammonium chloride. After washing in PBS three times for 5 min each, 5% BSA was added for 1 h for blocking, then primary antibody for overnight. Next day, secondary antibody was added for 1 h, then 2.4% PFA for 5 min for post-fixation.

For super-resolution imaging, freshly made imaging buffer (cysteamine hydrochloride, glucose, glucose oxidase, catalase, NaOH pH 7.5 in PBS) was added and dSTORM imaging was taken by oxford nanoimaging station with 100x oil immersion objective (1.4NA) and HILO excitation to visualize a plane of nuclei. The fluorophore (Alexa 647 or Alexa 488) was activated with 640 nm, 488 nm, 405 nm lasers followed by the acquisition of 20,000 frame movies were with 30 msec exposure time.

CUT&RUN

CUT&RUN was performed according to the published protocol (Skene and Henikoff 2017). In brief, siRNA treated IMR90 cells were washed at room temperature in wash buffer (20 mM HEPES pH 7.5, 150 mM NaCl, 0.5 mM spermidine). After adding Concanavalin A-coated magnetic beads for 10 min with rotation, beads were resuspended in antibody buffer (2 mM EDTA and digitonin), and antibodies (1:100) were incubated at room temperature for 10 min with rotation. Antibodies used were CTCF 61311, Active Motif) and Pol II (ab5131, abcam). Beads were washed in digitonin buffer to remove unbound antibody. Nuclei were incubated with protein A-MNase (700 ng/ml) for 10 min with rotation, then washed in digitonin buffer to remove unbound protein A-MNase. 2mM $CaCl_2$ were mixed, then 2x stop buffer (340 mM NaCl, 20 mM EDTA pH8, 4 mM EGTA, 0.05% digitonin, 50 µg/ml glycogen, and 2pg/ml spike-in DNA) were

added. DNA fragments were released from the insoluble nuclear chromatin, extracted, and purified. The Kapa HyperPrep kit (Roche) was used for library preparation.

RNA-seq

RNA-seq was performed according to the previous study (Ibarra et al. 2016). Briefly, total RNA was isolated from control and Nup153/Tpr KD IMR90 cells using Trizol (Ambion) and purified using the RNAeasy kit (Qiagen). Then, 1.5ug of total RNA was converted into RNA-seq libraries using the Illumina Tru-Seq Stranded RNA kit (Illumina).

2.6 Acknowledgement

Chapter 2, in part, is being prepared for submission for publication. Swati Tyagi, Hyeseon Kang, Martin W. Hetzer. “Nucleoporins regulate super-enhancer-associated genes through mediating CTCF.” The author of this dissertation was the co-primary investigator with Swati Tyagi and will submit as the co-first author of this paper.

CONCLUSION

Genome regulation during the mitosis-G1 phase transition

The aim of Chapter 1 was to determine the molecular mechanisms by which cells maintain the defined transcriptional programs, transcriptional regulatory elements, and spatial chromatin interactions over multiple cell cycles. This question was investigated using ChIP-seq, EU-RNA-seq, and Hi-C on synchronized cells at different stages after mitosis using the thymidine-nocodazole synchronization method. A number of studies have tackled the question of how the genome is faithfully reorganized after mitosis in different aspects. Our study, however, provides a valuable perspective in addition to previous studies. Each study utilizes different experimental designs and conditions. Thus, making a direct comparison between different studies causes confusion due to the inconsistent cell cycle stage represented at a given time point. Here, we provide three aspects at the same time, which enables us to properly compare the temporal relationship of one another.

Our ChIP-seq analysis improves our understanding of where histone modifications are distributed at *cis*-REs during the mitosis-G1 phase transition and whether they have a functional role in post-mitotic transcription. We show that during mitosis, H3K4me3 and H3K4me1 stably bind to promoters and enhancers, respectively. H3K4me3 remains at promoters of housekeeping genes, involved in mRNA and protein metabolism, while H3K4me1 remains at enhancers of cell type-specific genes, associated with cell differentiation and development. H3K27ac also remains at limited enhancers and promoters during prometaphase, which impacts mitotically active gene

expression. The inhibition of mitotic H3K27ac impairs the early activation of cell type-specific genes as well as genes linked to fundamental cellular processes. Given that there are no chromosomal interactions observed in mitotic cells, this mitotically active transcription seems to be driven by the promoters. In addition, the recovery of H3K27ac in anaphase/telophase is required for post-mitotic transcriptional activation. This indicates that histone modifications are crucial factors to mediate transcriptional memory in the daughter cells.

We also provide evidence that histone modifications contribute to long-range chromatin interactions. We hypothesized that a subset of CTCF remains at the TAD boundaries during mitosis and plays a role in TAD reformation. However, most of the CTCF binding has gone during prometaphase. Although mitotic CTCF is depleted at the boundaries, H3K4me3 and H3K4me1 remain associated at the TAD boundaries during prometaphase, suggesting H3K4me3 and H3K4me1 may bookmark insulators and dictate where TADs need to be formed after mitosis. H3K27ac is absent at the TAD boundaries during prometaphase. However, insulators regain H3K27ac as well as CTCF in anaphase/telophase. These results suggest that an increase in H3K27ac binding in anaphase/telophase may have a role in recruiting CTCF or reforming TAD boundaries. Anaphase/telophase is an exciting and critical time window when genomes start to decondensed for gene activation in order to understand the complexity of the transcription network following mitosis. However, it has been challenging to collect anaphase/telophase enriched cell population because of its short retention in the cell cycle. Our optimized cell synchronization protocol enables us to get the relatively pure population of anaphase/telophase enriched cells. To the best of our knowledge, we

show for the first time the dynamics of *cis*-REs, the distribution of histone marks, and CTCF at the TAD boundaries during anaphase/telophase, which gives us insights into the chromatin landscape when cells exit mitosis.

Regulation of post-mitotic transcription has remained obscure relative to interphase transcription. Combined with *cis*-REs activity, nascent transcription profiles, and chromatin interactions, our study shed light on a long-standing question about temporal order between histone modification, chromatin structure, and transcription during the mitosis-G1 phase transition. These results indicate that genome is reorganized in a sequential order in which H3K4me3 and H3K4me1 occur first in prometaphase, H3K27ac and CTCF in anaphase/telophase, the majority of transcription in cytokinesis, and long-range chromatin interactions in 90' G1. Since histone modification binding comes first, we conclude that the histone modification landscape may bookmark the transcriptional program and insulators during mitosis for faithful transmission of genome structure and function. Nevertheless, several interesting questions about the regulation of post-mitotic transcription and the formation of long-range interactions following mitosis need to be answered to understand how the genome is appropriately re-established after cell division.

It is well established that the spatial organization of the genome has an important role in the regulation of gene expression. Although chromatin structure seems to be unnecessary for post-mitotic transcription based on its late formation time, some TAD and DNA loop interactions were detected after 35 min at low levels. Thus, we cannot rule out that limited early formed chromatin interactions (35 min, 60 min) may influence on late expressed genes (90 min, 120 min). Conversely, the transcription machinery has

been suggested to contribute to genome organization. The TSS of protein-coding genes are enriched at the TAD boundaries in mouse (Dixon et al. 2012, Matthews and Waxman 2018). Furthermore, treatment with triptolide and flavopiridol to inhibit Pol II initiation and elongation, respectively, resulted in modestly reduced TAD border strength in *D. melanogaster* (Li et al. 2015, Rowley et al. 2017). Since transcription is reactivated earlier than long-range interactions, it is possible that mitotic transcription may involve in activating long-range interactions, which needs to be further examined. However, it would be technically changeling to inhibit mitotic transcription without interfering centromeric transcription, which is required for proper chromosome segregation (Liu et al. 2015).

Overall, our work fills a gap in the field by providing the whole picture that the genome is reorganized in a sequential order. Spatial and temporal regulation of epigenetic modifications and 3D genome architecture give us better insights into how transcription networks are accurately reestablished after cell division.

Dynamic regulation of genome at the nuclear periphery

In Chapter 2, we aimed to provide a mechanistic understanding of how NPC components mediate SE interactions at the nuclear periphery. Our super-resolution microscopy and genome analyses enabled us to detect CTCF-SE interactions at the NPCs, suggesting a new function of CTCF in NPC-mediated chromatin structure and gene regulation. CTCF has been suggested to organize the hierarchical structure of a subset of SE (Huang et al. 2018). However, the role of CTCF at the nuclear periphery in controlling SE-associated genes has not been shown before. In the viewpoint of the

NPC, the interaction with CTCF is an exciting finding as well because this suggests that the NPC may contribute to higher-order chromatin architecture through mediating architecture proteins or act as architecture proteins like CTCF. Interestingly, the NPC has been recently shown to interact with CTCF and the cohesin complex, SMC1 and SMC3 (Pascual-Garcia et al. 2017, Sachani et al. 2018), supporting our speculation.

In the near future, it will be a great interest to determine the molecular mechanisms by which CTCF mediates regulation of SE interactions at the NPC. First, why do NPC components need CTCF interaction at the nuclear periphery? Most nucleoporins do not contain recognizable domains for directly binding DNA or chromatin. Transcription factors (Toda et al. 2017, Raices et al. 2017) and chromatin-modifying complexes (Jacinto et al. 2015) binding to nucleoporins have been suggested to mediate the interaction of nucleoporins with DNA. Therefore, it seems likely CTCF may serve as intermediate between nucleoporins and genome. Another question to be addressed is whether CTCF brings SEs to the NPCs. To answer this question, it is inevitable to test the functional role of CTCF at the nuclear periphery upon CTCF depletion. The way to investigate the NPC-specific function of CTCF would be the use of a nucleoporin mutant, which depletes the CTCF binding domain. We can then take advantage of super-resolution microscopy and examine whether the depletion of CTCF at the NPC would take away SE components, such as Med1, BRD4, and Pol II, from the NPC.

It also remains unknown how NPC components associate with SE. Recently, coactivators, including MED1 and BRD4, have been shown to form condensates at SEs (Sabari et al. 2018). Treatment with 1,6-hexanediol that perturb condensates disrupt

MED1 and BRD4 nuclear bodies as well as lose genomic interactions of MED1, BRD4, and Pol II at SEs. Condensate formation can be predicted by intrinsically disordered regions (IDRs) of proteins. Interestingly, nucleoporins contain intrinsically disordered FG repeat domains and form phase-separated liquid-like condensates (Celetti et al. 2020). These suggest that NPC-SE association could be formed through condensation and phase separation, which needs to be explored further. In addition, genomic analysis upon 1,6-hexanediol will help us understand the potential role of NPC in forming phase separation at SEs.

Regulation of gene expression at the NPC is one of the long-standing questions to be addressed in the field. Further uncovering mechanistic details of NPC-genome interactions at the nuclear periphery will provide exciting improvements in a deeper understanding of how the genome structure affects its function.

REFERENCES

Abramo, K., A. L. Valton, S. V. Venev, H. Ozadam, A. N. Fox & J. Dekker (2019) A chromosome folding intermediate at the condensin-to-cohesin transition during telophase. *Nat Cell Biol*.

Amendola, M. & B. van Steensel (2014) Mechanisms and dynamics of nuclear lamina-genome interactions. *Curr Opin Cell Biol,* 28**,** 61-8.

Amendola, M. & B. van Steensel (2015) Nuclear lamins are not required for lamina-associated domain organization in mouse embryonic stem cells. *EMBO Rep,* 16**,** 610-7.

Behera, V., A. J. Stonestrom, N. Hamagami, C. C. Hsiung, C. A. Keller, B. Giardine, S. Sidoli, Z. F. Yuan, N. V. Bhanu, M. T. Werner, H. Wang, B. A. Garcia, R. C. Hardison & G. A. Blobel (2019) Interrogating Histone Acetylation and BRD4 as Mitotic Bookmarks of Transcription. *Cell Rep,* 27**,** 400-415.e5.

Bonev, B. & G. Cavalli (2016) Organization and function of the 3D genome. *Nat Rev Genet,* 17**,** 772.

Bozec, A., L. Bakiri, M. Jimenez, T. Schinke, M. Amling & E. F. Wagner (2010) Fra-2/AP-1 controls bone formation by regulating osteoblast differentiation and collagen production. *J Cell Biol,* 190**,** 1093-106.

Buchwalter, A., J. M. Kaneshiro & M. W. Hetzer (2019) Coaching from the sidelines: the nuclear periphery in genome regulation. *Nat Rev Genet,* 20**,** 39-50.

Burke, B. & J. Ellenberg (2002) Remodelling the walls of the nucleus. *Nat Rev Mol Cell Biol,* 3**,** 487-97.

Burke, L. J., R. Zhang, M. Bartkuhn, V. K. Tiwari, G. Tavoosidana, S. Kurukuti, C. Weth, J. Leers, N. Galjart, R. Ohlsson & R. Renkawitz (2005) CTCF binding and higher order chromatin structure of the H19 locus are maintained in mitotic chromatin. *EMBO J,* 24**,** 3291-300.

Cai, Y., M. J. Hossain, J. K. Hériché, A. Z. Politi, N. Walther, B. Koch, M. Wachsmuth, B. Nijmeijer, M. Kueblbeck, M. Martinic-Kavur, R. Ladurner, S. Alexander, J. M. Peters & J. Ellenberg (2018) Experimental and computational framework for a dynamic protein atlas of human cell division. *Nature,* 561**,** 411-415.

Calo, E. & J. Wysocka (2013) Modification of enhancer chromatin: what, how, and why? *Mol Cell,* 49**,** 825-37.

Capelson, M. & M. W. Hetzer (2009) The role of nuclear pores in gene regulation, development and disease. *EMBO Rep,* 10**,** 697-705.

Caravaca, J. M., G. Donahue, J. S. Becker, X. He, C. Vinson & K. S. Zaret (2013) Bookmarking by specific and nonspecific binding of FoxA1 pioneer factor to mitotic chromosomes. *Genes Dev,* 27**,** 251-60.

Celetti, G., G. Paci, J. Caria, V. VanDelinder, G. Bachand & E. A. Lemke (2020) The liquid state of FG-nucleoporins mimics permeability barrier properties of nuclear pore complexes. *J Cell Biol,* 219.

Chapurlat, R. D. & C. B. Confavreux (2016) Novel biological markers of bone: from bone metabolism to bone physiology. *Rheumatology (Oxford),* 55**,** 1714-25.

Crane, E., Q. Bian, R. P. McCord, B. R. Lajoie, B. S. Wheeler, E. J. Ralston, S. Uzawa, J. Dekker & B. J. Meyer (2015) Condensin-driven remodelling of X chromosome topology during dosage compensation. *Nature,* 523**,** 240-4.

Creyghton, M. P., A. W. Cheng, G. G. Welstead, T. Kooistra, B. W. Carey, E. J. Steine, J. Hanna, M. A. Lodato, G. M. Frampton, P. A. Sharp, L. A. Boyer, R. A. Young & R. Jaenisch (2010) Histone H3K27ac separates active from poised enhancers and predicts developmental state. *Proc Natl Acad Sci U S A,* 107**,** 21931-6.

D'Angelo, M. A., D. J. Anderson, E. Richard & M. W. Hetzer (2006) Nuclear pores form de novo from both sides of the nuclear envelope. *Science,* 312**,** 440-3.

D'Angelo, M. A. & M. W. Hetzer (2008) Structure, dynamics and function of nuclear pore complexes. *Trends Cell Biol,* 18**,** 456-66.

de Castro, I. J., E. Gokhan & P. Vagnarelli (2016) Resetting a functional G1 nucleus after mitosis. *Chromosoma,* 125**,** 607-19.

Deluz, C., E. T. Friman, D. Strebinger, A. Benke, M. Raccaud, A. Callegari, M. Leleu, S. Manley & D. M. Suter (2016) A role for mitotic bookmarking of SOX2 in pluripotency and differentiation. *Genes Dev,* 30**,** 2538-2550.

Dennis, G., B. T. Sherman, D. A. Hosack, J. Yang, W. Gao, H. C. Lane & R. A. Lempicki (2003) DAVID: Database for Annotation, Visualization, and Integrated Discovery. *Genome Biol,* 4**,** P3.

Devaiah, B. N., C. Case-Borden, A. Gegonne, C. H. Hsu, Q. Chen, D. Meerzaman, A. Dey, K. Ozato & D. S. Singer (2016) BRD4 is a histone acetyltransferase that evicts nucleosomes from chromatin. *Nat Struct Mol Biol,* 23**,** 540-8.

Dey, A., A. Nishiyama, T. Karpova, J. McNally & K. Ozato (2009) Brd4 marks select genes on mitotic chromatin and directs postmitotic transcription. *Mol Biol Cell,* 20**,** 4899-909.

Dileep, V., F. Ay, J. Sima, D. L. Vera, W. S. Noble & D. M. Gilbert (2015) Topologically associating domains and their long-range contacts are established during early G1 coincident with the establishment of the replication-timing program. *Genome Res,* 25**,** 1104-13.

Dixon, J. R., S. Selvaraj, F. Yue, A. Kim, Y. Li, Y. Shen, M. Hu, J. S. Liu & B. Ren (2012) Topological domains in mammalian genomes identified by analysis of chromatin interactions. *Nature,* 485**,** 376-80.

Dixon, J. R., J. Xu, V. Dileep, Y. Zhan, F. Song, V. T. Le, G. G. Yardımcı, A. Chakraborty, D. V. Bann, Y. Wang, R. Clark, L. Zhang, H. Yang, T. Liu, S. Iyyanki, L. An, C. Pool, T. Sasaki, J. C. Rivera-Mulia, H. Ozadam, B. R. Lajoie, R. Kaul, M. Buckley, K. Lee, M. Diegel, D. Pezic, C. Ernst, S. Hadjur, D. T. Odom, J. A. Stamatoyannopoulos, J. R. Broach, R. C. Hardison, F. Ay, W. S. Noble, J. Dekker, D. M. Gilbert & F. Yue (2018) Integrative detection and analysis of structural variation in cancer genomes. *Nat Genet,* 50**,** 1388-1398.

Dobin, A., C. A. Davis, F. Schlesinger, J. Drenkow, C. Zaleski, S. Jha, P. Batut, M. Chaisson & T. R. Gingeras (2013) STAR: ultrafast universal RNA-seq aligner. *Bioinformatics,* 29**,** 15-21.

Ducy, P., R. Zhang, V. Geoffroy, A. L. Ridall & G. Karsenty (1997) Osf2/Cbfa1: a transcriptional activator of osteoblast differentiation. *Cell,* 89**,** 747-54.

Dultz, E., E. Zanin, C. Wurzenberger, M. Braun, G. Rabut, L. Sironi & J. Ellenberg (2008) Systematic kinetic analysis of mitotic dis- and reassembly of the nuclear pore in living cells. *J Cell Biol,* 180**,** 857-65.

Egan, B., C. C. Yuan, M. L. Craske, P. Labhart, G. D. Guler, D. Arnott, T. M. Maile, J. Busby, C. Henry, T. K. Kelly, C. A. Tindell, S. Jhunjhunwala, F. Zhao, C. Hatton, B. M. Bryant, M. Classon & P. Trojer (2016) An Alternative Approach to ChIP-Seq Normalization Enables Detection of Genome-Wide Changes in Histone H3 Lysine 27 Trimethylation upon EZH2 Inhibition. *PLoS One,* 11**,** e0166438.

Ellenberg, J., E. D. Siggia, J. E. Moreira, C. L. Smith, J. F. Presley, H. J. Worman & J. Lippincott-Schwartz (1997) Nuclear membrane dynamics and reassembly in living cells: targeting of an inner nuclear membrane protein in interphase and mitosis. *J Cell Biol,* 138**,** 1193-206.

Falk, M., Y. Feodorova, N. Naumova, M. Imakaev, B. R. Lajoie, H. Leonhardt, B. Joffe, J. Dekker, G. Fudenberg, I. Solovei & L. A. Mirny (2019) Heterochromatin drives compartmentalization of inverted and conventional nuclei. *Nature,* 570**,** 395-399.

Festuccia, N., A. Dubois, S. Vandormael-Pournin, E. Gallego Tejeda, A. Mouren, S. Bessonnard, F. Mueller, C. Proux, M. Cohen-Tannoudji & P. Navarro (2016) Mitotic binding of Esrrb marks key regulatory regions of the pluripotency network. *Nat Cell Biol,* 18**,** 1139-1148.

Filippakopoulos, P., S. Picaud, M. Mangos, T. Keates, J. P. Lambert, D. Barsyte-Lovejoy, I. Felletar, R. Volkmer, S. Müller, T. Pawson, A. C. Gingras, C. H. Arrowsmith & S. Knapp (2012) Histone recognition and large-scale structural analysis of the human bromodomain family. *Cell,* 149**,** 214-31.

Fudenberg, G., M. Imakaev, C. Lu, A. Goloborodko, N. Abdennur & L. A. Mirny (2016) Formation of Chromosomal Domains by Loop Extrusion. *Cell Rep,* 15**,** 2038-49.

Gibcus, J. H., K. Samejima, A. Goloborodko, I. Samejima, N. Naumova, J. Nuebler, M. T. Kanemaki, L. Xie, J. R. Paulson, W. C. Earnshaw, L. A. Mirny & J. Dekker (2018) A pathway for mitotic chromosome formation. *Science,* 359.

Ginno, P. A., L. Burger, J. Seebacher, V. Iesmantavicius & D. Schübeler (2018) Cell cycle-resolved chromatin proteomics reveals the extent of mitotic preservation of the genomic regulatory landscape. *Nat Commun,* 9**,** 4048.

Gottesfeld, J. M. & D. J. Forbes (1997) Mitotic repression of the transcriptional machinery. *Trends Biochem Sci,* 22**,** 197-202.

GR, K. & C. SH. 2007. *Genes and proteins involved in the regulation of osteogenesis*. Topics in Tissue Engineering.

Heintzman, N. D., G. C. Hon, R. D. Hawkins, P. Kheradpour, A. Stark, L. F. Harp, Z. Ye, L. K. Lee, R. K. Stuart, C. W. Ching, K. A. Ching, J. E. Antosiewicz-Bourget, H. Liu, X. Zhang, R. D. Green, V. V. Lobanenkov, R. Stewart, J. A. Thomson, G. E. Crawford, M. Kellis & B. Ren (2009) Histone modifications at human enhancers reflect global cell-type-specific gene expression. *Nature,* 459**,** 108-12.

Heintzman, N. D., R. K. Stuart, G. Hon, Y. Fu, C. W. Ching, R. D. Hawkins, L. O. Barrera, S. Van Calcar, C. Qu, K. A. Ching, W. Wang, Z. Weng, R. D. Green, G. E. Crawford & B. Ren (2007) Distinct and predictive chromatin signatures of transcriptional promoters and enhancers in the human genome. *Nat Genet,* 39**,** 311-8.

Hnisz, D., B. J. Abraham, T. I. Lee, A. Lau, V. Saint-André, A. A. Sigova, H. A. Hoke & R. A. Young (2013) Super-enhancers in the control of cell identity and disease. *Cell,* 155**,** 934-47.

Hsiung, C. C., C. R. Bartman, P. Huang, P. Ginart, A. J. Stonestrom, C. A. Keller, C. Face, K. S. Jahn, P. Evans, L. Sankaranarayanan, B. Giardine, R. C. Hardison,

A. Raj & G. A. Blobel (2016) A hyperactive transcriptional state marks genome reactivation at the mitosis-G1 transition. *Genes Dev,* 30**,** 1423-39.

Hsiung, C. C., C. S. Morrissey, M. Udugama, C. L. Frank, C. A. Keller, S. Baek, B. Giardine, G. E. Crawford, M. H. Sung, R. C. Hardison & G. A. Blobel (2015) Genome accessibility is widely preserved and locally modulated during mitosis. *Genome Res,* 25**,** 213-25.

Huang, J., K. Li, W. Cai, X. Liu, Y. Zhang, S. H. Orkin, J. Xu & G. C. Yuan (2018) Dissecting super-enhancer hierarchy based on chromatin interactions. *Nat Commun,* 9**,** 943.

Ibarra, A., C. Benner, S. Tyagi, J. Cool & M. W. Hetzer (2016) Nucleoporin-mediated regulation of cell identity genes. *Genes Dev,* 30**,** 2253-2258.

Ishii, K., G. Arib, C. Lin, G. Van Houwe & U. K. Laemmli (2002) Chromatin boundaries in budding yeast: the nuclear pore connection. *Cell,* 109**,** 551-62.

Jacinto, F. V., C. Benner & M. W. Hetzer (2015) The nucleoporin Nup153 regulates embryonic stem cell pluripotency through gene silencing. *Genes Dev,* 29**,** 1224-38.

Javasky, E., I. Shamir, S. Gandhi, S. Egri, O. Sandler, S. B. Rothbart, N. Kaplan, J. D. Jaffe, A. Goren & I. Simon (2018) Study of mitotic chromatin supports a model of bookmarking by histone modifications and reveals nucleosome deposition patterns. *Genome Res,* 28**,** 1455-1466.

Jochum, W., J. P. David, C. Elliott, A. Wutz, H. Plenk, K. Matsuo & E. F. Wagner (2000) Increased bone formation and osteosclerosis in mice overexpressing the transcription factor Fra-1. *Nat Med,* 6**,** 980-4.

Kadauke, S., M. I. Udugama, J. M. Pawlicki, J. C. Achtman, D. P. Jain, Y. Cheng, R. C. Hardison & G. A. Blobel (2012) Tissue-specific mitotic bookmarking by hematopoietic transcription factor GATA1. *Cell,* 150**,** 725-37.

Kadota, S., J. Ou, Y. Shi, J. T. Lee, J. Sun & E. Yildirim (2020) Nucleoporin 153 links nuclear pore complex to chromatin architecture by mediating CTCF and cohesin binding. *Nat Commun,* 11**,** 2606.

Kalverda, B., H. Pickersgill, V. V. Shloma & M. Fornerod (2010) Nucleoporins directly stimulate expression of developmental and cell-cycle genes inside the nucleoplasm. *Cell,* 140**,** 360-71.

Kegelman, C. D., D. E. Mason, J. H. Dawahare, D. J. Horan, G. D. Vigil, S. S. Howard, A. G. Robling, T. M. Bellido & J. D. Boerckel (2018) Skeletal cell YAP and TAZ combinatorially promote bone development. *FASEB J,* 32**,** 2706-2721.

Kind, J., L. Pagie, H. Ortabozkoyun, S. Boyle, S. S. de Vries, H. Janssen, M. Amendola, L. D. Nolen, W. A. Bickmore & B. van Steensel (2013) Single-cell dynamics of genome-nuclear lamina interactions. *Cell,* 153**,** 178-92.

Kirkham, G. R. & S. H. Cartmell. 2007. *Genes and proteins involved in the regulation of osteogenesis*. Topics in Tissue Engeneering.

Komori, T. (2005) Regulation of skeletal development by the Runx family of transcription factors. *J Cell Biochem,* 95**,** 445-53.

Komori, T., H. Yagi, S. Nomura, A. Yamaguchi, K. Sasaki, K. Deguchi, Y. Shimizu, R. T. Bronson, Y. H. Gao, M. Inada, M. Sato, R. Okamoto, Y. Kitamura, S. Yoshiki & T. Kishimoto (1997) Targeted disruption of Cbfa1 results in a complete lack of bone formation owing to maturational arrest of osteoblasts. *Cell,* 89**,** 755-64.

Kouskouti, A. & I. Talianidis (2005) Histone modifications defining active genes persist after transcriptional and mitotic inactivation. *EMBO J,* 24**,** 347-57.

Krull, S., J. Dörries, B. Boysen, S. Reidenbach, L. Magnius, H. Norder, J. Thyberg & V. C. Cordes (2010) Protein Tpr is required for establishing nuclear pore-associated zones of heterochromatin exclusion. *EMBO J,* 29**,** 1659-73.

Kveiborg, M., G. Sabatakos, R. Chiusaroli, M. Wu, W. M. Philbrick, W. C. Horne & R. Baron (2004) DeltaFosB induces osteosclerosis and decreases adipogenesis by two independent cell-autonomous mechanisms. *Mol Cell Biol,* 24**,** 2820-30.

Lasko, L. M., C. G. Jakob, R. P. Edalji, W. Qiu, D. Montgomery, E. L. Digiammarino, T. M. Hansen, R. M. Risi, R. Frey, V. Manaves, B. Shaw, M. Algire, P. Hessler, L. T. Lam, T. Uziel, E. Faivre, D. Ferguson, F. G. Buchanan, R. L. Martin, M. Torrent, G. G. Chiang, K. Karukurichi, J. W. Langston, B. T. Weinert, C. Choudhary, P. de Vries, J. H. Van Drie, D. McElligott, E. Kesicki, R. Marmorstein, C. Sun, P. A. Cole, S. H. Rosenberg, M. R. Michaelides, A. Lai & K. D. Bromberg (2017) Discovery of a selective catalytic p300/CBP inhibitor that targets lineage-specific tumours. *Nature,* 550**,** 128-132.

Lee, J. E., Y. K. Park, S. Park, Y. Jang, N. Waring, A. Dey, K. Ozato, B. Lai, W. Peng & K. Ge (2017) Brd4 binds to active enhancers to control cell identity gene induction in adipogenesis and myogenesis. *Nat Commun,* 8**,** 2217.

Li, L., X. Lyu, C. Hou, N. Takenaka, H. Q. Nguyen, C. T. Ong, C. Cubeñas-Potts, M. Hu, E. P. Lei, G. Bosco, Z. S. Qin & V. G. Corces (2015) Widespread rearrangement of 3D chromatin organization underlies polycomb-mediated stress-induced silencing. *Mol Cell,* 58**,** 216-31.

Liang, K., A. R. Woodfin, B. D. Slaughter, J. R. Unruh, A. C. Box, R. A. Rickels, X. Gao, J. S. Haug, S. L. Jaspersen & A. Shilatifard (2015) Mitotic Transcriptional

Activation: Clearance of Actively Engaged Pol II via Transcriptional Elongation Control in Mitosis. *Mol Cell,* 60**,** 435-45.

Lieberman-Aiden, E., N. L. van Berkum, L. Williams, M. Imakaev, T. Ragoczy, A. Telling, I. Amit, B. R. Lajoie, P. J. Sabo, M. O. Dorschner, R. Sandstrom, B. Bernstein, M. A. Bender, M. Groudine, A. Gnirke, J. Stamatoyannopoulos, L. A. Mirny, E. S. Lander & J. Dekker (2009) Comprehensive mapping of long-range interactions reveals folding principles of the human genome. *Science,* 326**,** 289-93.

Liu, H., Q. Qu, R. Warrington, A. Rice, N. Cheng & H. Yu (2015) Mitotic Transcription Installs Sgo1 at Centromeres to Coordinate Chromosome Segregation. *Mol Cell,* 59**,** 426-36.

Liu, X., X. Yu, D. J. Zack, H. Zhu & J. Qian (2008) TiGER: a database for tissue-specific gene expression and regulation. *BMC Bioinformatics,* 9**,** 271.

Liu, Y., B. Pelham-Webb, D. C. Di Giammartino, J. Li, D. Kim, K. Kita, N. Saiz, V. Garg, A. Doane, P. Giannakakou, A. K. Hadjantonakis, O. Elemento & E. Apostolou (2017) Widespread Mitotic Bookmarking by Histone Marks and Transcription Factors in Pluripotent Stem Cells. *Cell Rep,* 19**,** 1283-1293.

Lochs, S. J. A., S. Kefalopoulou & J. Kind (2019) Lamina Associated Domains and Gene Regulation in Development and Cancer. *Cells,* 8.

Long, F. (2011) Building strong bones: molecular regulation of the osteoblast lineage. *Nat Rev Mol Cell Biol,* 13**,** 27-38.

Lovén, J., H. A. Hoke, C. Y. Lin, A. Lau, D. A. Orlando, C. R. Vakoc, J. E. Bradner, T. I. Lee & R. A. Young (2013) Selective inhibition of tumor oncogenes by disruption of super-enhancers. *Cell,* 153**,** 320-34.

Martínez-Balbás, M. A., A. Dey, S. K. Rabindran, K. Ozato & C. Wu (1995) Displacement of sequence-specific transcription factors from mitotic chromatin. *Cell,* 83**,** 29-38.

Matthews, B. J. & D. J. Waxman (2018) Computational prediction of CTCF/cohesin-based intra-TAD loops that insulate chromatin contacts and gene expression in mouse liver. *Elife,* 7.

McCloskey, A., A. Ibarra & M. W. Hetzer (2018) Tpr regulates the total number of nuclear pore complexes per cell nucleus. *Genes Dev,* 32**,** 1321-1331.

McLean, C. Y., D. Bristor, M. Hiller, S. L. Clarke, B. T. Schaar, C. B. Lowe, A. M. Wenger & G. Bejerano (2010) GREAT improves functional interpretation of cis-regulatory regions. *Nat Biotechnol,* 28**,** 495-501.

Muramoto, T., I. Müller, G. Thomas, A. Melvin & J. R. Chubb (2010) Methylation of H3K4 Is required for inheritance of active transcriptional states. *Curr Biol,* 20**,** 397-406.

Nagano, T., Y. Lubling, C. Várnai, C. Dudley, W. Leung, Y. Baran, N. Mendelson Cohen, S. Wingett, P. Fraser & A. Tanay (2017) Cell-cycle dynamics of chromosomal organization at single-cell resolution. *Nature,* 547**,** 61-67.

Najafova, Z., R. Tirado-Magallanes, M. Subramaniam, T. Hossan, G. Schmidt, S. Nagarajan, S. J. Baumgart, V. K. Mishra, U. Bedi, E. Hesse, S. Knapp, J. R. Hawse & S. A. Johnsen (2017) BRD4 localization to lineage-specific enhancers is associated with a distinct transcription factor repertoire. *Nucleic Acids Res,* 45**,** 127-141.

Naumova, N., M. Imakaev, G. Fudenberg, Y. Zhan, B. R. Lajoie, L. A. Mirny & J. Dekker (2013) Organization of the mitotic chromosome. *Science,* 342**,** 948-53.

Nora, E. P., A. Goloborodko, A. L. Valton, J. H. Gibcus, A. Uebersohn, N. Abdennur, J. Dekker, L. A. Mirny & B. G. Bruneau (2017) Targeted Degradation of CTCF Decouples Local Insulation of Chromosome Domains from Genomic Compartmentalization. *Cell,* 169**,** 930-944.e22.

Nora, E. P., B. R. Lajoie, E. G. Schulz, L. Giorgetti, I. Okamoto, N. Servant, T. Piolot, N. L. van Berkum, J. Meisig, J. Sedat, J. Gribnau, E. Barillot, N. Blüthgen, J. Dekker & E. Heard (2012) Spatial partitioning of the regulatory landscape of the X-inactivation centre. *Nature,* 485**,** 381-5.

Oomen, M. E., A. S. Hansen, Y. Liu, X. Darzacq & J. Dekker (2019) CTCF sites display cell cycle-dependent dynamics in factor binding and nucleosome positioning. *Genome Res,* 29**,** 236-249.

Orlando, D. A., M. W. Chen, V. E. Brown, S. Solanki, Y. J. Choi, E. R. Olson, C. C. Fritz, J. E. Bradner & M. G. Guenther (2014) Quantitative ChIP-Seq normalization reveals global modulation of the epigenome. *Cell Rep,* 9**,** 1163-70.

Otto, F., A. P. Thornell, T. Crompton, A. Denzel, K. C. Gilmour, I. R. Rosewell, G. W. Stamp, R. S. Beddington, S. Mundlos, B. R. Olsen, P. B. Selby & M. J. Owen (1997) Cbfa1, a candidate gene for cleidocranial dysplasia syndrome, is essential for osteoblast differentiation and bone development. *Cell,* 89**,** 765-71.

Palozola, K. C., G. Donahue, H. Liu, G. R. Grant, J. S. Becker, A. Cote, H. Yu, A. Raj & K. S. Zaret (2017) Mitotic transcription and waves of gene reactivation during mitotic exit. *Science,* 358**,** 119-122.

Pascual-Garcia, P., B. Debo, J. R. Aleman, J. A. Talamas, Y. Lan, N. H. Nguyen, K. J. Won & M. Capelson (2017) Metazoan Nuclear Pores Provide a Scaffold for

Poised Genes and Mediate Induced Enhancer-Promoter Contacts. *Mol Cell,* 66**,** 63-76.e6.

Peric-Hupkes, D., W. Meuleman, L. Pagie, S. W. Bruggeman, I. Solovei, W. Brugman, S. Gräf, P. Flicek, R. M. Kerkhoven, M. van Lohuizen, M. Reinders, L. Wessels & B. van Steensel (2010) Molecular maps of the reorganization of genome-nuclear lamina interactions during differentiation. *Mol Cell,* 38**,** 603-13.

Poleshko, A., P. P. Shah, M. Gupta, A. Babu, M. P. Morley, L. J. Manderfield, J. L. Ifkovits, D. Calderon, H. Aghajanian, J. E. Sierra-Pagán, Z. Sun, Q. Wang, L. Li, N. C. Dubois, E. E. Morrisey, M. A. Lazar, C. L. Smith, J. A. Epstein & R. Jain (2017) Genome-Nuclear Lamina Interactions Regulate Cardiac Stem Cell Lineage Restriction. *Cell,* 171**,** 573-587.e14.

Poleshko, A., C. L. Smith, S. C. Nguyen, P. Sivaramakrishnan, K. G. Wong, J. I. Murray, M. Lakadamyali, E. F. Joyce, R. Jain & J. A. Epstein (2019) H3K9me2 orchestrates inheritance of spatial positioning of peripheral heterochromatin through mitosis. *Elife,* 8.

Prasanth, K. V., P. A. Sacco-Bubulya, S. G. Prasanth & D. L. Spector (2003) Sequential entry of components of the gene expression machinery into daughter nuclei. *Mol Biol Cell,* 14**,** 1043-57.

Prescott, D. M. & M. A. Bender (1962) Synthesis of RNA and protein during mitosis in mammalian tissue culture cells. *Exp Cell Res,* 26**,** 260-8.

Rached, M. T., A. Kode, L. Xu, Y. Yoshikawa, J. H. Paik, R. A. Depinho & S. Kousteni (2010) FoxO1 is a positive regulator of bone formation by favoring protein synthesis and resistance to oxidative stress in osteoblasts. *Cell Metab,* 11**,** 147-60.

Raices, M., L. Bukata, S. Sakuma, J. Borlido, L. S. Hernandez, D. O. Hart & M. A. D'Angelo (2017) Nuclear Pores Regulate Muscle Development and Maintenance by Assembling a Localized Mef2C Complex. *Dev Cell,* 41**,** 540-554.e7.

Rao, S. S., M. H. Huntley, N. C. Durand, E. K. Stamenova, I. D. Bochkov, J. T. Robinson, A. L. Sanborn, I. Machol, A. D. Omer, E. S. Lander & E. L. Aiden (2014) A 3D map of the human genome at kilobase resolution reveals principles of chromatin looping. *Cell,* 159**,** 1665-80.

Rowley, M. J., M. H. Nichols, X. Lyu, M. Ando-Kuri, I. S. M. Rivera, K. Hermetz, P. Wang, Y. Ruan & V. G. Corces (2017) Evolutionarily Conserved Principles Predict 3D Chromatin Organization. *Mol Cell,* 67**,** 837-852.e7.

Rutkovskiy, A., K. O. Stensløkken & I. J. Vaage (2016) Osteoblast Differentiation at a Glance. *Med Sci Monit Basic Res,* 22**,** 95-106.

Sabari, B. R., A. Dall'Agnese, A. Boija, I. A. Klein, E. L. Coffey, K. Shrinivas, B. J. Abraham, N. M. Hannett, A. V. Zamudio, J. C. Manteiga, C. H. Li, Y. E. Guo, D. S. Day, J. Schuijers, E. Vasile, S. Malik, D. Hnisz, T. I. Lee, I. I. Cisse, R. G. Roeder, P. A. Sharp, A. K. Chakraborty & R. A. Young (2018) Coactivator condensation at super-enhancers links phase separation and gene control. *Science,* 361.

Sabatakos, G., N. A. Sims, J. Chen, K. Aoki, M. B. Kelz, M. Amling, Y. Bouali, K. Mukhopadhyay, K. Ford, E. J. Nestler & R. Baron (2000) Overexpression of DeltaFosB transcription factor(s) increases bone formation and inhibits adipogenesis. *Nat Med,* 6**,** 985-90.

Sachani, S. S., L. S. Landschoot, L. Zhang, C. R. White, W. A. MacDonald, M. C. Golding & M. R. W. Mann (2018) Nucleoporin 107, 62 and 153 mediate Kcnq1ot1 imprinted domain regulation in extraembryonic endoderm stem cells. *Nat Commun,* 9**,** 2795.

Sanborn, A. L., S. S. Rao, S. C. Huang, N. C. Durand, M. H. Huntley, A. I. Jewett, I. D. Bochkov, D. Chinnappan, A. Cutkosky, J. Li, K. P. Geeting, A. Gnirke, A. Melnikov, D. McKenna, E. K. Stamenova, E. S. Lander & E. L. Aiden (2015) Chromatin extrusion explains key features of loop and domain formation in wild-type and engineered genomes. *Proc Natl Acad Sci U S A,* 112**,** E6456-65.

Sekiya, T., K. Murano, K. Kato, A. Kawaguchi & K. Nagata (2017) Mitotic phosphorylation of CCCTC-binding factor (CTCF) reduces its DNA binding activity. *FEBS Open Bio,* 7**,** 397-404.

Shechter, D., H. L. Dormann, C. D. Allis & S. B. Hake (2007) Extraction, purification and analysis of histones. *Nat Protoc,* 2**,** 1445-57.

Skene, P. J. & S. Henikoff (2017) An efficient targeted nuclease strategy for high-resolution mapping of DNA binding sites. *Elife,* 6.

Solovei, I., K. Thanisch & Y. Feodorova (2016) How to rule the nucleus: divide et impera. *Curr Opin Cell Biol,* 40**,** 47-59.

Stevens, T. J., D. Lando, S. Basu, L. P. Atkinson, Y. Cao, S. F. Lee, M. Leeb, K. J. Wohlfahrt, W. Boucher, A. O'Shaughnessy-Kirwan, J. Cramard, A. J. Faure, M. Ralser, E. Blanco, L. Morey, M. Sansó, M. G. S. Palayret, B. Lehner, L. Di Croce, A. Wutz, B. Hendrich, D. Klenerman & E. D. Laue (2017) 3D structures of individual mammalian genomes studied by single-cell Hi-C. *Nature,* 544**,** 59-64.

Teixeira, C. C., Y. Liu, L. M. Thant, J. Pang, G. Palmer & M. Alikhani (2010) Foxo1, a novel regulator of osteoblast differentiation and skeletogenesis. *J Biol Chem,* 285**,** 31055-65.

Teves, S. S., L. An, A. S. Hansen, L. Xie, X. Darzacq & R. Tjian (2016) A dynamic mode of mitotic bookmarking by transcription factors. *Elife,* 5.

Toda, T., J. Y. Hsu, S. B. Linker, L. Hu, S. T. Schafer, J. Mertens, F. V. Jacinto, M. W. Hetzer & F. H. Gage (2017) Nup153 Interacts with Sox2 to Enable Bimodal Gene Regulation and Maintenance of Neural Progenitor Cells. *Cell Stem Cell,* 21**,** 618-634.e7.

Toyama, B. H., R. Arrojo E Drigo, V. Lev-Ram, R. Ramachandra, T. J. Deerinck, C. Lechene, M. H. Ellisman & M. W. Hetzer (2019) Visualization of long-lived proteins reveals age mosaicism within nuclei of postmitotic cells. *J Cell Biol,* 218**,** 433-444.

Vagnarelli, P. (2013) Chromatin reorganization through mitosis. *Adv Protein Chem Struct Biol,* 90**,** 179-224.

Valls, E., S. Sánchez-Molina & M. A. Martínez-Balbás (2005) Role of histone modifications in marking and activating genes through mitosis. *J Biol Chem,* 280**,** 42592-600.

Vaquerizas, J. M., R. Suyama, J. Kind, K. Miura, N. M. Luscombe & A. Akhtar (2010) Nuclear pore proteins nup153 and megator define transcriptionally active regions in the Drosophila genome. *PLoS Genet,* 6**,** e1000846.

Vietri Rudan, M., C. Barrington, S. Henderson, C. Ernst, D. T. Odom, A. Tanay & S. Hadjur (2015) Comparative Hi-C reveals that CTCF underlies evolution of chromosomal domain architecture. *Cell Rep,* 10**,** 1297-309.

Walter, J., L. Schermelleh, M. Cremer, S. Tashiro & T. Cremer (2003) Chromosome order in HeLa cells changes during mitosis and early G1, but is stably maintained during subsequent interphase stages. *J Cell Biol,* 160**,** 685-97.

Wandke, C. & U. Kutay (2013) Enclosing chromatin: reassembly of the nucleus after open mitosis. *Cell,* 152**,** 1222-5.

Wang, F. & J. M. Higgins (2013) Histone modifications and mitosis: countermarks, landmarks, and bookmarks. *Trends Cell Biol,* 23**,** 175-84.

Wu, T., Y. F. Kamikawa & M. E. Donohoe (2018) Brd4's Bromodomains Mediate Histone H3 Acetylation and Chromatin Remodeling in Pluripotent Cells through P300 and Brg1. *Cell Rep,* 25**,** 1756-1771.

Young, D. W., M. Q. Hassan, X. Q. Yang, M. Galindo, A. Javed, S. K. Zaidi, P. Furcinitti, D. Lapointe, M. Montecino, J. B. Lian, J. L. Stein, A. J. van Wijnen & G. S. Stein (2007) Mitotic retention of gene expression patterns by the cell fate-determining transcription factor Runx2. *Proc Natl Acad Sci U S A,* 104**,** 3189-94.

Zhang, Z., Y. Zhang, H. Xiao, X. Liang, D. Sun & S. Peng (2012) A gene expression profile of the developing human retinal pigment epithelium. *Mol Vis,* 18**,** 2961-75.

Zhao, R., T. Nakamura, Y. Fu, Z. Lazar & D. L. Spector (2011) Gene bookmarking accelerates the kinetics of post-mitotic transcriptional re-activation. *Nat Cell Biol,* 13**,** 1295-304.

Zhiteneva, A., J. J. Bonfiglio, A. Makarov, T. Colby, P. Vagnarelli, E. C. Schirmer, I. Matic & W. C. Earnshaw (2017) Mitotic post-translational modifications of histones promote chromatin compaction. *Open Biol,* 7.

Zieve, G. W., D. Turnbull, J. M. Mullins & J. R. McIntosh (1980) Production of large numbers of mitotic mammalian cells by use of the reversible microtubule inhibitor nocodazole. Nocodazole accumulated mitotic cells. *Exp Cell Res,* 126**,** 397-405.